U.S.N.A.--- Trident Scholar Report; no. 303 (2003)

Investigation of Tellurium-130 Nuclear Structure using Inelastic Neutron Scattering

by

Midshipman Tyler Hale Churchill, Class of 2003
United States Naval Academy
Annapolis, MD

Certification of Advisor Approval

Professor Jeffrey R. Vanhoy
Department of Physics

Acceptance for the Trident Scholar Committee

Professor Joyce E. Shade
Deputy Director of Research & Scholarship

REPORT DOCUMENTATION PAGE

Form Approved OMB No. 0704-0188

Public reporting burder for this collection of information is estibated to average 1 hour per response, including the time for reviewing instructions, searching existing data sources, gathering and maintaining the data needed, and completing and reviewing this collection of information. Send comments regarding this burden estimate or any other aspect of this collection of information, including suggestions for reducing this burder to Department of Defense, Washington Headquarters Services, Directorate for Information Operations and Reports (0704-0188), 1215 Jefferson Davis Highway, Suite 1204, Arlington, VA 22202-4302. Respondents should be aware that notwithstanding any other provision of law, no person shall be subject to any penalty for failing to comply with a collection of information if it does not display a currently valid OMB control number. PLEASE DO NOT RETURN YOUR FORM TO THE ABOVE ADDRESS.

1. REPORT DATE (DD-MM-YYYY)	2. REPORT TYPE	3. DATES COVERED (FROM - TO)
07-05-2003		00-00-2003 to 00-00-2003

4. TITLE AND SUBTITLE
Investigation of Tellurium-130 nuclear structure using inelastic neutron scattering
Unclassified

5a. CONTRACT NUMBER
5b. GRANT NUMBER
5c. PROGRAM ELEMENT NUMBER

6. AUTHOR(S)
,
,
,
,
,

5d. PROJECT NUMBER
5e. TASK NUMBER
5f. WORK UNIT NUMBER

7. PERFORMING ORGANIZATION NAME AND ADDRESS
U.S. Naval Academy
Trident
Annapolis, M 21402

8. PERFORMING ORGANIZATION REPORT NUMBER

9. SPONSORING/MONITORING AGENCY NAME AND ADDRESS
,

10. SPONSOR/MONITOR'S ACRONYM(S)
11. SPONSOR/MONITOR'S REPORT NUMBER(S)

12. DISTRIBUTION/AVAILABILITY STATEMENT
A
00-00- 0
,

13. SUPPLEMENTARY NOTES

14. ABSTRACT
The purpose of nuclear structure research is to understand the features of the nuclear force that determine the various ways a nucleus can behave upon excitation. Theoretical model calculations are compared to experimental data in order to understand which models better predict different nuclear properties.

15. SUBJECT TERMS

16. SECURITY CLASSIFICATION OF:			17. LIMITATION OF ABSTRACT	18. NUMBER OF PAGES	19. NAME OF RESPONSIBLE PERSON
a. REPORT	b. ABSTRACT	c. THIS PAGE	Public Release	120	Rike, Jack jrike@dtic.mil
Unclassified	Unclassified	Unclassified			19b. TELEPHONE NUMBER International Area Code Area Code Telephone Number DSN

REPORT DOCUMENTATION PAGE

Form Approved
OMB No. 074-0188

Public reporting burden for this collection of information is estimated to average 1 hour per response, including g the time for reviewing instructions, searching existing data sources, gathering and maintaining the data needed, and completing and reviewing the collection of information. Send comments regarding this burden estimate or any other aspect of the collection of information, including suggestions for reducing this burden to Washington Headquarters Services, Directorate for Information Operations and Reports, 1215 Jefferson Davis Highway, Suite 1204, Arlington, VA 22202-4302, and to the Office of Management and Budget, Paperwork Reduction Project (0704-0188), Washington, DC 20503.

1. AGENCY USE ONLY (Leave blank)	2. REPORT DATE	3. REPORT TYPE AND DATE COVERED
	7 May 2003	

4. TITLE AND SUBTITLE
Investigation of Tellurium-130 nuclear structure using inelastic neutron scattering

5. FUNDING NUMBERS

6. AUTHOR(S)
Churchill, Tyler Hale, |d1981-

7. PERFORMING ORGANIZATION NAME(S) AND ADDRESS(ES)		8. PERFORMING ORGANIZATION REPORT NUMBER

9. SPONSORING/MONITORING AGENCY NAME(S) AND ADDRESS(ES)		10. SPONSORING/MONITORING AGENCY REPORT NUMBER
US Naval Academy Annapolis, MD 21402		Trident Scholar project report no. 303 (2003)

11. SUPPLEMENTARY NOTES

12a. DISTRIBUTION/AVAILABILITY STATEMENT	12b. DISTRIBUTION CODE
This document has been approved for public release; its distribution is UNLIMITED.	

13. ABSTRACT: The purpose of nuclear structure research is to understand the features of the nuclear force that determine the various ways a nucleus can behave upon excitation. Theoretical model calculations are compared to experimental data in order to understand which models better predict different nuclear properties. The tellurium-130 nucleus has two valence protons with respect to a closed proton shell and several different types of nuclear structure behavior are thought to be active. Experimental data were collected at the University of Kentucky Nuclear Structure Laboratory using a technique called inelastic neutron scattering. By scattering neutrons off of ^{130}Te, the nucleus was excited, and the resulting de-excitation gamma rays recorded as ^{130}Te excited states relaxed. Through analytical techniques, the energy level scheme has been constructed, and spectroscopic information such as lifetimes, level spins, and branching ratios has been obtained. The behavior of the ^{130}Te nucleus was examined from the viewpoints of the General Collective Model and the Particle-Core Vibration Model. The General Collective Model was found to be inadequate. The Particle-Core Vibration Model shows promise, but the best technique to improve the understanding of the observed level scheme and properties may still have to await the availability of large-scale Shell Model calculations.

14. SUBJECT TERMS:	15. NUMBER OF PAGES
Nuclear structure, Tellurium-130, Nuclear spectroscopy	118
	16. PRICE CODE

17. SECURITY CLASSIFICATION OF REPORT	18. SECURITY CLASSIFICATION OF THIS PAGE	19. SECURITY CLASSIFICATION OF ABSTRACT	20. LIMITATION OF ABSTRACT

Abstract

The purpose of nuclear structure research is to understand the features of the nuclear force that determine the various ways a nucleus can behave upon excitation. Theoretical model calculations are compared to experimental data in order to understand which models better predict different nuclear properties. The tellurium-130 nucleus has two valence protons with respect to a closed proton shell and several different types of nuclear structure behavior are thought to be active.

Experimental data were collected at the University of Kentucky Nuclear Structure Laboratory using a technique called inelastic neutron scattering. By scattering neutrons off of ^{130}Te, the nucleus was excited, and the resulting de-excitation gamma rays recorded as ^{130}Te excited states relaxed. Through analytical techniques, the energy level scheme has been constructed, and spectroscopic information such as lifetimes, level spins, and branching ratios has been obtained. The behavior of the ^{130}Te nucleus was examined from the viewpoints of the General Collective Model and the Particle-Core Vibration Model. The General Collective Model was found to be inadequate. The Particle-Core Vibration Model shows promise, but the best technique to improve the understanding of the observed level scheme and properties may still have to await the availability of large-scale Shell Model calculations.

Keywords: Nuclear Structure, Tellurium-130, Nuclear Spectroscopy

Acknowledgments

I would like to thank my project advisor, Professor Jeff Vanhoy for his exceptional guidance, assistance, and advice, without which my work would have been impossible. I would also like to thank Dr. Shade and the Trident Scholar Committee. Also, gratitude is extended to Professor Sally Hicks at the University of Dallas, and Professor Steven Yates, Professor Marcus McEllistrem, Shelly Lesher, and Harvey Baber at the University of Kentucky for their assistance while at the accelerator lab and help in analysis. This work supported in part by the National Science Foundation Grants PHY-0139504, PHY-9901508, and by the U.S. Naval Academy Midshipmen Research Fund.

Table of Contents

Page

I. INTRODUCTION

A. A Nuclear Primer

Many people have taken introductory chemistry courses and have some basic knowledge of the atom and molecular structure. Few have taken nuclear physics courses. This section introduces the reader to the world of nuclear physics through analogy with atomic physics.

The atom can be considered a collection of electrons orbiting in a force field created by a miniscule point-like central object, the nucleus. The positively charged nucleus attracts the negatively charged electrons through the "fundamental" electromagnetic force. Because the electrons are "bound" to the atom, the system is quantized and the electrons are found only with specific energies corresponding to specific orbits. If energy is put into the system, electrons can be "excited" to higher orbits with higher energies. In the hydrogen atom, where there is only one electron, photons are emitted (called infrared, optical, and ultraviolet photons) as the excited electron falls back down to lower states.

In a multi-electron atom, many electrons can be involved in the excitations. The whole system again can only exist with specific energies in the "ground state" or in other specific "excited states." Specifying the electronic configuration of the system in an excited state becomes much more complicated, and uncovering the underlying structure of an excited state from experimental observations can be quite a chore in the multi-electron atom. One must perform a model calculation with computer codes and compare its predictions with measured quantities.

If one zooms in on the nucleus of an atom, one will find that it is not a point object, but instead a rather large blob of nucleons (protons and neutrons), with a radius of ~6 femtometers for tellurium-130 (^{130}Te). Each nucleon moves in the attractive force field created by all the other nucleons through residual effects of the "fundamental" "strong" force. Much like in the atomic system, because the nucleon is confined to a region of space, the nuclear system is quantized and the nucleons occupy specific orbits. If energy is put into the system, the nucleons can be excited to higher orbits. When nucleons fall back down to their ground states, photons (called gamma (γ) rays) are emitted. In nuclei with high atomic numbers, many nucleons are involved in the excitations. Still, according to quantum mechanics, the system can only exist in certain "excited states." Specifying the nucleon configuration of the system in a specific excited state becomes extremely complicated, and uncovering the underlying structure of an excited state from experimental observations can be quite difficult. Again, one must perform a model calculation with computer codes and compare its predictions with measured quantities.

In this project, we excite the tellurium-130 nucleus by striking it with a fast moving neutron. We measure the emitted de-excitation gamma rays and determine each excited state's excitation energy, total angular momentum (a.k.a. spin), and lifetime. We use several different model calculations in an attempt to uncover the underlying nuclear structure.

We complete the introduction with a slightly more detailed introduction to the project. A description of the accelerator and experimental setup is provided in Section II. Section III presents the specific measurements performed and the analysis techniques that allow one to extract the spectroscopic information from the data. Section IV contains experiment results and detailed arguments that were used in deciding the properties of each excited state. The discussion and model interpretations are presented in section V. Finally, we summarize the results.

B. Nuclear Structure

The role of modern nuclear physics is to understand how the interactions of dozens and dozens of neutrons and protons determine the behavior of the atomic nucleus. Just as the van der Waals forces between molecules are the result of residual electromagnetic interactions, the "nuclear force" is simply the result of residual long-range quark interactions. As the nucleus is a complicated system of many objects, many models have been developed to try to understand and predict its behavior, and this research continues to develop the existing models and improve them.

For the purposes of the Introduction, we consider three classifications of nuclear models: the independent-particle models, the collective models, and a combination of these, called hybrid models.

The independent-particle models [Kr88] are nearly identical to the quantum mechanical treatment of atomic (electron) structure. Nucleons (neutrons and protons) occupy discrete orbitals, and may jump to a higher orbital if they absorb energy or return to a lower orbital by releasing energy via gamma rays. Independent-particle models seek to explain how the individual excited states are constructed from nucleons occupying the particular orbitals and how the combinations of orbitals determine the properties (energy, angular momentum, and lifetime) of the excited states. However, a full calculation is not possible in the case of the nucleus because a) there are hundreds of particles involved and b) the interactions between neighboring nucleons are very strong. All independent-particle models have a theoretical structure somewhat like that of the larger atoms in that several "valence" nucleons are said to orbit a stable inner core.

The collective models [Kr88] describe the nucleus as a fluid of neutrons and protons. These models seek to describe oscillations of the fluid in terms of the normal modes of oscillation in a liquid drop. Each vibration mode has a definite energy associated with it, and this gives rise to a sequence of excited states. Rotational excitations also occur when the fluid acquires some deformation and thus is able to spin like a top. Again the models seek to explain the properties (energy, angular momentum, and lifetime) of these states by choosing an appropriate potential energy function.

The independent-particle models are not fit to describe situations where large numbers (greater than three or four) of nucleons are involved and the collective models are not fit to describe situations where only a few valence nucleons are involved. Hybrid models [Kr88] seek to

combine features of both. The valence nucleons are considered to orbit a core that can undergo vibrations and rotations.

Tellurium was chosen for this and previous experiments because it has a wide range of abundant stable isotopes. Very little is known about the tellurium-130 isotope nucleus [Fi98, BNL02, Ki02]. Although it is naturally abundant, it is not well studied, likely because it is not accessible by as many reactions as other nuclei. The tellurium nuclei have two valence protons with respect to the Z = 50 (atomic number, number of protons) closed shell and a range of neutron numbers. Three different models of structure are thought to be active in these nuclei: collective, two valence particle, and particle-hole excitations known as intruders. Because there are seven stable Te nuclei each with an even number of neutrons and an even number of protons ("even-even nuclei"), one can study the evolution of these excitation modes over a wide range in neutron number, allowing for good quantitative analysis of the nuclei.

The ultimate goal in nuclear structure research is to understand the features of the nuclear force that determine the balance between the various collective- and particle- like behaviors. This is done through comparing the nuclear models to data taken from experiments and seeing which models work better under which circumstances. For this Trident project, data have been taken using the inelastic neutron scattering process on ^{130}Te and recording the gamma rays that are emitted from the resulting excited nucleus. Through various analytical techniques, a scheme of the excited state energy levels has been constructed complete with information on energies, lifetimes, spins, parities, and decay branching ratios. This scheme was then compared with model calculations to see how the different models describe the ^{130}Te nucleus. Emphasis centers on understanding the interplay between particle and collective features and on the aspects of the nuclear forces and shell model orbitals that determine the relative importance of each model. Often level energies are more important for evaluating whether a model has sufficient built-in complexity than distinguishing between physical descriptions, and selection rules, lifetimes, and transition rate information are crucial to revealing the amplitudes of particle and collective components in the wave functions. Results from these ^{130}Te studies will be combined with previous information on the other lighter tellurium nuclei ^{120}Te [Va01, Va02], ^{122}Te [Co], ^{124}Te [Et97, Wa98], ^{126}Te [Ta99, Ta01], and ^{128}Te [Ch97a, Ch97b] to eventually study the evolution of these structures across an isotopic chain.

II. EQUIPMENT AND EXPERIMENTAL PROCEDURES

Inelastic neutron scattering (INS; n,n'γ) is an excellent method to obtain spectroscopic information for nuclear excited states. Using neutron collisions to excite nuclei is non-selective in the states that can be excited, as only the neutron energy and the angular momentum limit the possible states that can be activated. The high quality (n,n'γ) facility at the University of Kentucky undergoes continuous improvement (www.pa.uky.edu/~marcus/nukes.html). Recent upgrades have made operation much more stable and user-friendly. Special detector shielding and gating techniques are available to eliminate the large neutron backgrounds present in neutron scattering experiments.

The accelerator at the University of Kentucky is a 7 MV single-ended Van de Graaff with a pulsing/bunching system located inside the high-voltage dome. Proton beams emerging from the radio frequency source are pulsed by sweeping across a chopping aperture. This 10-20 ns wide chopped pulse immediately passes through a klystron buncher that reduces the pulse width to 1 ns on target. The repetition rate of the pulsed beam is 1.875 MHz. Protons are accelerated and impinge on a gas cell at the end of the beamline containing tritium at atmospheric pressure to produce a secondary beam of neutrons with the $p + {}^{3}H \rightarrow n + {}^{3}He$ reaction. Typical proton beam currents are 2nA or $\sim 10^{19}$ particles/second. The neutron production rate is approximately 10^{3} particles/second.

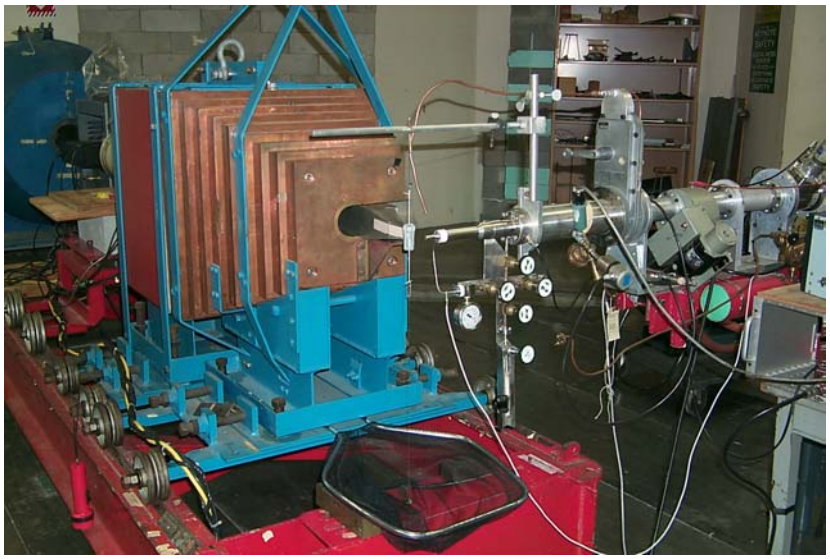

Figure 1. View at the end of the beamline. Protons arrive through the pipe to the right and strike the tritium cell at the end of the beampipe. The ^{130}Te sample is in the small vertical cylinder in the center. Layers of square copper plates shield the γ-ray detector from stray neutrons and γ rays.

The sample of interest (^{130}Te) is hung in the emerging spray of neutrons that exits the gas cell. For our experiments, a ~50 g metallic sample of >99% enriched ^{130}Te was borrowed from the Materials Research Collection housed at Oak Ridge National Lab. The University of Kentucky Nuclear Lab and University of Dallas were responsible for arranging the sample loan and sample rental. Since we were identifying gamma-ray transitions for the first time, it was crucial to have

a sample of high purity.

The standard detector arrangement employs a single ">50% efficiency" high-purity Germanium (HPGe) detector and an anti-Compton shield. The Compton shield consists of a Bismuth Germinate (BGO) crystal with six photomultiplier tubes (PMTs) which surrounds the HPGe. Many gamma rays do not deposit their full energy into the Germanium crystal, but instead bounce out and are detected by the surrounding BGO detector. If gamma rays are detected in the BGO and HPGe at the same time (in the time-resolution of the detection system), then they are assumed to be the same gamma ray, only scattered. Therefore the data corresponding to that gamma ray event is meaningless and not recorded. The detector is mounted inside graded copper, lithium-loaded paraffin, and lead shielding and rests with its cryostat and electronics on a detector carriage which may be rotated through scattering angles up to 150 degrees. A spectrum from the HPGe detector is shown in Fig. 2.

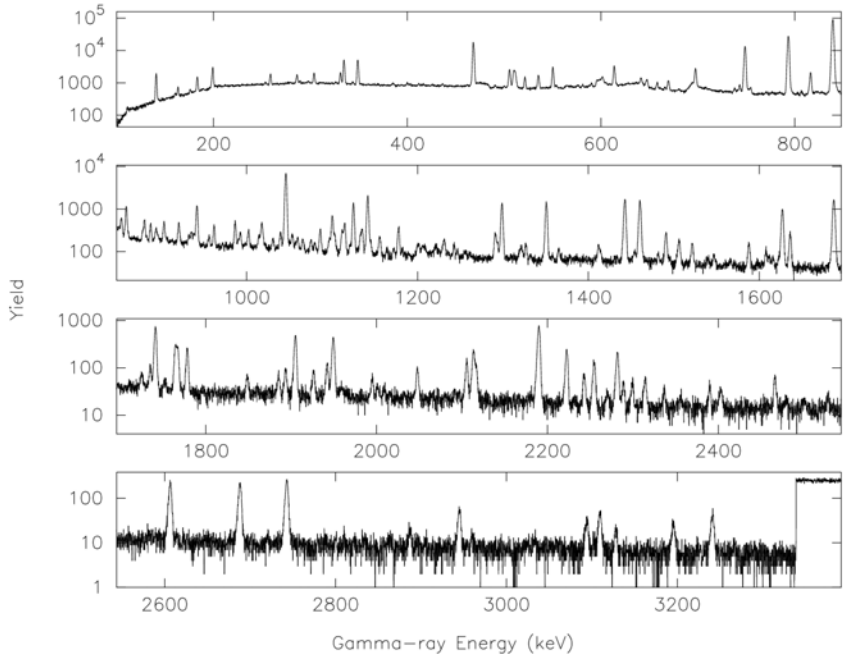

Figure 2. A gamma-ray spectrum obtained with the high-purity Germanium detector – this is one of the excitation function data files from the ^{130}Te(n,n'γ) data runs in June. Approximately 150 lines are present in each detector spectrum.

Data is recorded by use of a Pentium PC based – Computer Automated Measurement and Control (CAMAC) data acquisition system. The system allows both online-sorting and event-mode storage. Pulses from the HPGe are shaped and amplified before they reach the analog-to-digital converter (ADC). Based on the recorded energy of the gamma ray captured in the crystal, one count will be placed somewhere in a 16384-channel histogram. The channel number-gamma ray energy relationship was calibrated using a radioactive radium-226 source for known gamma ray transition energies. The detector efficiency (probability that a γ ray of a given energy stops

in the detector) was also calculated using the known transitions in the ^{226}Ra source. Sufficient beam time was assured since this experiment is consistent with the mainstream experimental effort of the nuclear structure group. With the exception of several typical problems with the accelerator, we obtained two good weeks of beam time during the summer.

The available technical support in the physics and chemistry departments at the University of Kentucky is excellent. Services include a full-time accelerator engineer and part-time assistant. Fully staffed electronics, machine, and glass blowing shops are available free of labor charges. The accelerator is operated by the users.

Excitation function measurements were done in mid June 2002. While in Kentucky, "accelerator watch" was stood by the researchers. This duty included paying attention to machine operation, saving data periodically, and checking levels and gauges while analyzing gathered data. Angular distribution measurements were done during the first week of August 2002. At this time, work began on the excitation function analysis. Advisors Jeffrey Vanhoy, USNA, and Sally Hicks, University of Dallas, coordinated the use of the accelerator and acquisition system.

Gamma-gamma coincidence measurements done on natural tellurium by Brian Champine, USNA '98 in 1997 were used to help place some of the gamma rays. The measurement involves setting up multiple detectors around the target in close proximity. When two or more gamma rays are detected in close temporal proximity, they are recorded. This can show which gamma rays are part of the same decay chain. The resulting data helped to confirm several suspicions about the level schemes while making placements from examination of the excitation functions.

III. ANALYSIS

A. Peak-stripping Codes

After the data have been taken, the process of analysis begins. The choice of analysis method is important because some methods are better equipped to extract accurate and precise data than others under various circumstances. The analysis package needs to be able to read the format from the University of Kentucky data collection system, plot histograms of yield vs. ADC channel number, calibrate the channel number/γ-ray energy relation using known radioactive sources, fit appropriately-shaped peaks to the histograms, and precisely predict the shape characteristics of these peaks.

While taking data, it is a good idea to analyze what you have in order to determine if there is something wrong with the accelerator or acquisition system. Several programs were used initially to plot data "on the fly" because of their familiarity and therefore ease of use. These programs, HYPERMET[Ph76] and PKS[Wa88], are Windows-based programs which utilize a user-created input file and the data file to fit peaks specified by the user. A program called SIMPLEFIT was also used to integrate the area of the histograms given user-defined backgrounds and peak limits. PKS finds its own backgrounds and looks for peaks based on user-defined window limits and approximations of peak centroids. PKS treats Gaussian-shaped peaks on a linear or quadratic background. Developed originally at the Naval Research Laboratory, HYPERMET is the most sophisticated analysis program due to its ability to model peak shapes but does not have an extensive graphical interface and program control features. For the excitation function data analysis, a program package commonly used at the University of Kentucky was chosen. The package is a set of Linux-based programs that center on the data stripping program "FITPIC"[UF96] (see Fig. 3).

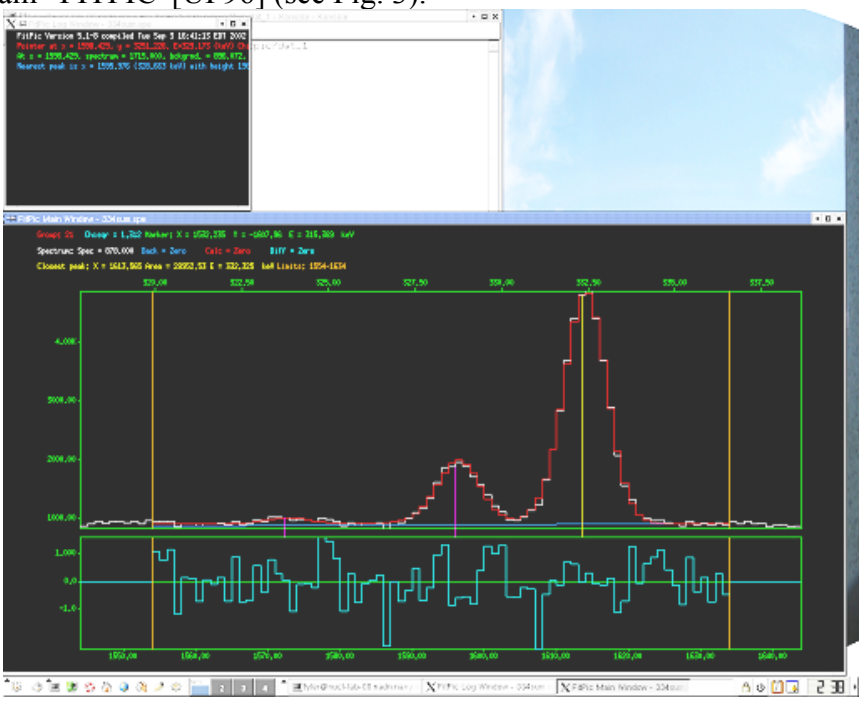

Figure 3. A screen shot of the program Fitpic run in Linux.

FITPIC has relatively good capabilities when it comes to fitting the peak shapes produced by the γ-ray detectors, but the reason it was chosen above the others is because its graphical control is far superior to that of PKS or HYPERMET. This makes the program easier to learn and master, as well as cuts down on the amount of time spent writing input files, running the program, printing results, interpreting difficulties, re-writing the input file, and repeating the process, as all of this can be done at the same time when using FITPIC. Another advantage of using FITPIC, with its graphical control, is that you can visually examine, interpolate, and change multiple parameters of the peak shape to deal with variations among different detectors and analog to digital converters. The satellite programs used with FITPIC manage detector efficiency and ADC nonlinearity corrections, as well as plot the data in a form necessary for proper analysis.

For the angular distribution and lifetime data analysis, the Windows-based program PKS was used. After using FITPIC initially for angular data stripping, it was found that it did not have the ability to maintain reliable centroids as accurately as necessary for these analyses. After peak areas and centroids were extracted, spreadsheets and numerous small FORTRAN codes were used to further reduce the data. Angular data-related properties (lifetimes, branching ratios, mixing ratios, etc.) were extracted using the reduced data and programs dedicated to these individual tasks.

B. Excitation Functions

The most logical first measurement is to generate the set of excitation functions. An excitation function is the yield of each gamma ray as a function of neutron bombarding energy. These measurements were done in the middle of June 2002. To get the set of neutron energies, the accelerator was run at each energy for about eight hours at a time, and the beam energy was increased by approximately 90 keV each time. This was done from beam energies of 1.89 to 3.34 MeV, recording gamma rays with the detector at a constant 90 degrees to the beamline. Each gamma ray that is produced for a given neutron energy has a yield that is extracted from the area of its peak in the gamma ray spectrum. When the yields are plotted against neutron energy, the minimum neutron energy required to produce that gamma ray, the "threshold," becomes evident. Three ^{130}Te gamma ray excitation functions are shown in Fig. 4, measured in beam energy steps of ~90 keV, enabling a γ-ray's production threshold to be identified to <0.1 MeV.

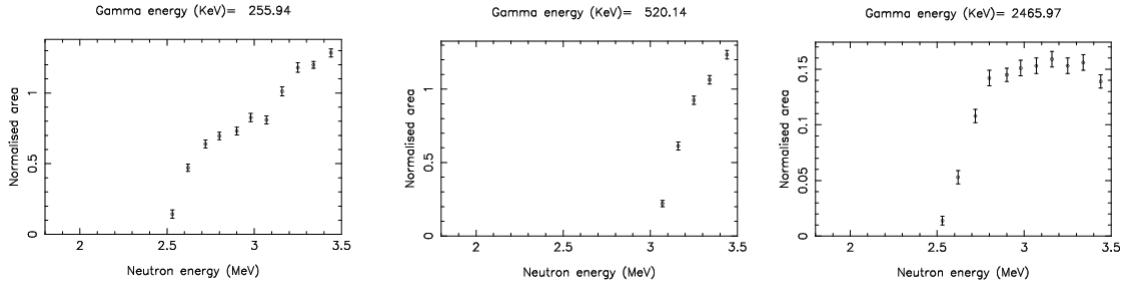

Figure 4. A selection of excitation functions from the ^{130}Te(n,n'γ) experiment.

Thresholds are determined by extrapolating the yield plots down to zero yield, and seeing where the excitation function intersects the neutron energy axis. This is the energy of the bombarding neutrons, and therefore approximately the energy of the γ-ray's emitting excited state. From the excited state level energies obtained through analysis of the excitation functions, unidentified gamma rays can be added/subtracted to/from these level energies to discover new energy levels. For example, the gamma ray with energy 2403 keV was added to the energy of the known first excited state, 839 keV, to get a new level at 3242 keV, which coincides with the apparent threshold of the 2403-keV gamma ray.

Excitation function measurements contribute in two ways to the level scheme. First, knowing the threshold energies, level placements are made for all the apparent transitions. Second, the shape of the excitation function is sensitive to both the spin and branching ratios of the parent state, and therefore different γ-rays with the same excitation function shape and threshold can be identified as coming out of the same state. This helps by aiding in placing gamma rays whose excitation functions look the same. The complete set of excitation functions is given in Appendix A.

C. Angular Distributions

The second series of measurements, taken at the beginning of August 2002, are angular distributions. Angular distributions are measured by taking spectral data at a series of detector angles with respect to the beamline at a fixed incident neutron energy. From the angular distribution, two pieces of experimental information were extracted for each peak: the yield of each individual γ-ray peak versus detection angle, and the centroid energy of each peak versus detector angle.

The angular variation of an individual γ-ray's yield (Fig. 5) will tell how many units of angular momenta were carried away from the nucleus by the gamma-ray photon. This information can be used to extract the total angular momentum (or "spin") of the emitting level [Sh66]. The complete set of angular distributions is available in Appendices B and C.

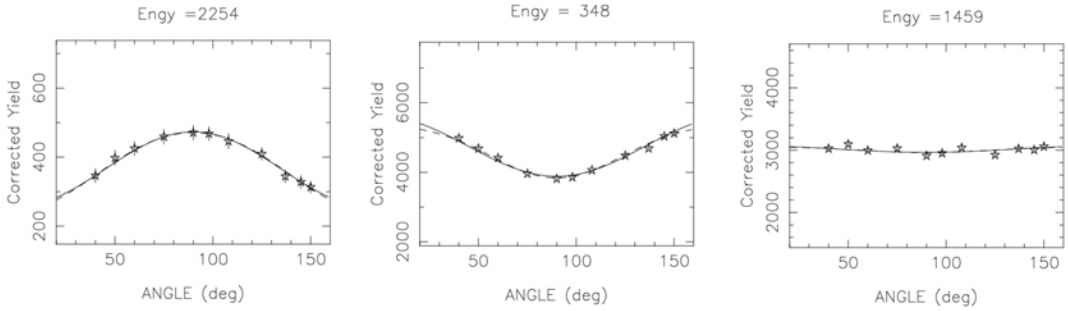

Figure 5. Sample angular distributions from a ^{130}Te(n,n'γ) experiment.
The line is a fit to a Legendre polynomial expansion.

Level spins and γ-ray mixing ratios are determined by comparing measured γ-ray angular distributions to model calculations. Angular distributions are fit to a Legendre polynomial expansion generated with the compound nucleus code CINDY [Sh66]. The chi-squared values

of the fits of Legendre polynomials to the angular distribution data are plotted against the arctangent of the "mixing ratio," or how much of each type and multipolarity (E1, M1, or E2) is present in a measured gamma-ray transition. The multipolarity is how much angular momentum is carried away from the nucleus by the detected gamma ray. The type of transition is either electric or magnetic and the multipolarities considered are 1 and 2 [Li01]. (The arctangent function is used since the mixing ratio can go from negative infinity to positive infinity.) Picking the best fit (point at which chi-squared is minimized) from these plots will give possible spins of the source excited states as well as the mixing ratios. Shown in Fig. 6 is the chi-squared plot of the CINDY comparisons for the 793-keV gamma ray.

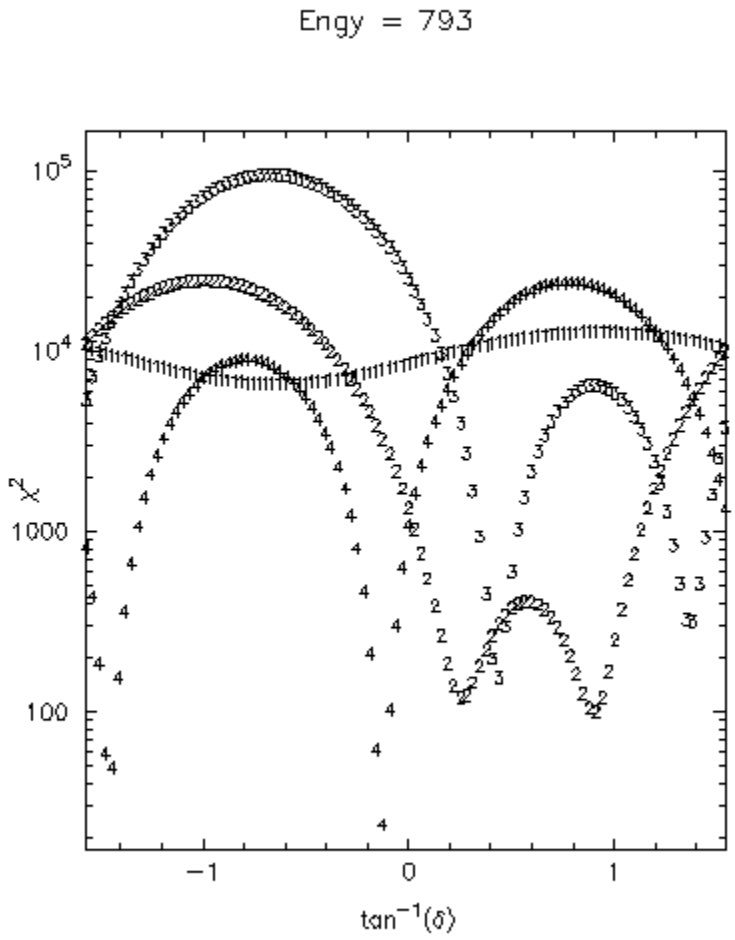

Figure 6. The value of chi-squared for fits of CINDY model angular distributions corresponding to source state spins of 1, 2, 3, and 4 plotted versus the tangent of the mixing ratio.

Upon inspection of the figure, one can see that the value of chi-squared is minimized for the initial level which produces the 793-keV gamma ray having a spin of 4, and the arctangent of the gamma-ray's mixing ratio is near –0.15. The mixing ratio is the ratio of the transition amplitudes of the multipolarities. Mathematically, it is defined as

$$\delta=<|L+1|>/<L> \qquad [1]$$

Where <L> is the reduced transmission amplitude for multipolarity L.

An excited state may decay to one of several lower-lying levels. The branching ratio (BR) indicates what fraction of time a particular decay branch occurs. Branching ratios were determined by comparing the angle-integrated yields of all the gamma rays from the same excited state. Branching ratios of low energy gamma rays must be corrected for a process known as internal conversion. In internal conversion, the excitation energy is transferred to the atomic electrons rather than being released in the form of a gamma ray. This process is generally negligible for transitions greater than a few hundred keV. Internal conversion coefficients were calculated from the National Nuclear Data Center at the Brookhaven National Lab website [BNL03].

D. Lifetimes

The angular variation of an individual γ-ray's energy can be used to discover the lifetime of the emitting level. Lifetimes were extracted with the Doppler-shift attenuation method (DSAM) [Wi75, Be94]. Although there are other techniques for determining lifetimes, DSAM offers a good approximation for lifetimes between one femtosecond and one picosecond. Some states in ^{130}Te are known to have lifetimes longer than one picosecond, outside the bound of precise measurement for DSAM. These lifetimes will be obtained from literature. The tellurium nucleus recoils when it is struck by the incident neutron, and the excited residual nucleus emits a γ-ray as it slows down in the target material. As with the classical Doppler shift, the apparent frequency of the photon is greater in front of the moving source than behind it (see Fig. 7). The complete set of Doppler shifts is available in Appendices D and E.

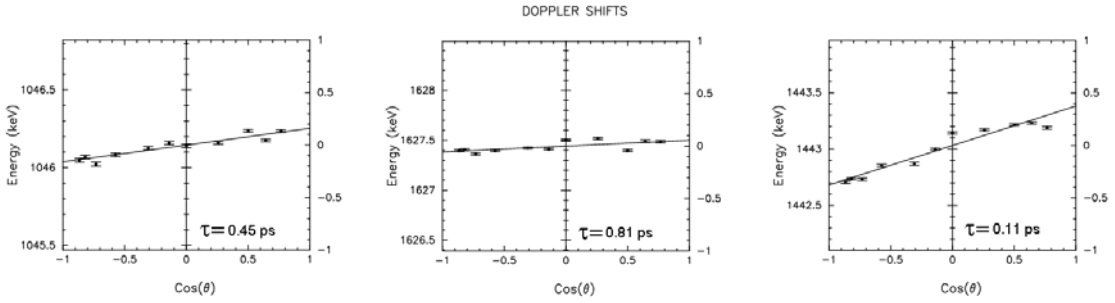

Figure 7. Doppler-shift data for three transitions in ^{130}Te. The experimental value of the Doppler-shift attenuation factor F is determined from the slope of the best fit line.

At the recoil velocities in these experiments, the energy centroid varies with the angular dependence indicated in the following equation:

$$E_\gamma(\theta)=E_\gamma^0 [\ 1 + F\beta \cos(\theta)\ ] . \qquad [2]$$

The product Fβ can be thought of as the average velocity at which the excited nucleus emits the

gamma ray. The symbol β is the initial velocity of the recoiling nucleus (relative to the speed of light), E_γ^0 is the true γ-ray energy, and F is the attenuation factor which takes into account the slowing down of the recoiling nucleus. The nucleus will slow down in the material due to energy loss in the electron cloud and collisions with other nuclei in the sample. The ratio of the speed of the average recoiling nucleus to the speed of light for the 3.3 MeV data set was calculated to be $\beta = 0.00064$. The attenuation factor F carries the dependence on the level lifetime. We use the formalism of Winterbon [Wi75] to relate the observed attenuation factors to lifetimes as it produces more reliable results for a greater variety of target compounds. If the slope is steep, then F is large, the nucleus decays relatively soon after it has been struck, and the lifetime is short. If the slope is flat, then F is small, the nucleus has slowed down significantly before decaying, and the state lifetime is long. States with lifetimes of a few fs to 1 ps can be determined for the ^{130}Te nuclei using the beam energies available at Kentucky. Figure 8 shows the relationship between the attenuation factor, F, and the lifetime, τ.

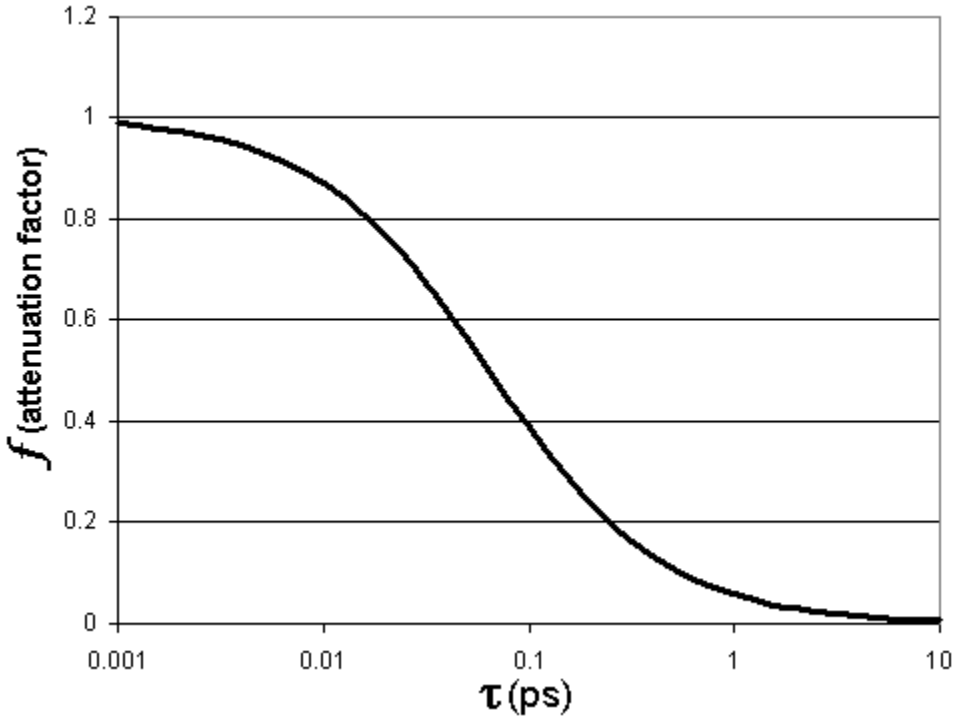

Figure 8. The Winterbon curve relates the measured attenuation factor and the source state's lifetime.

Much effort has been placed on improving the DSAM method at Kentucky during the past 10 years. This effort has focused on reducing and monitoring peak shifts (changes in the building line voltage, HVAC fluctuations, and amplifier gain drift) in the γ-ray spectrum and improving the understanding of stopping powers of ions recoiling in a variety of target compositions. Gain shifts have been greatly reduced by special power isolation and special cabling for detectors and spectroscopy amplifiers. Close track is kept of even minute gain shifts by calibrating detectors using radioactive ^{56}Co, ^{152}Eu, and ^{226}Ra sources before and after measurements at each detector angle.

E. Level Scheme Discussion

Once the values for lifetimes, spins, energies, and ratios were determined, the results were compiled into a single spreadsheet for transition rate calculations and comparative analysis. In this section the experiment findings are expounded upon. Presented first are several discussions of gamma rays that caused some difficulty in placement. Following are the discussions of the level scheme, including the level energies and characteristics. The compiled data table is included in this section while the excitation functions are found in appendix A, the angular distributions are found in appendices B and C, and the Doppler shifts are included in appendices D and E. Figure 9 is a visual representation of some of the more interesting levels in the level scheme and transitions between them.

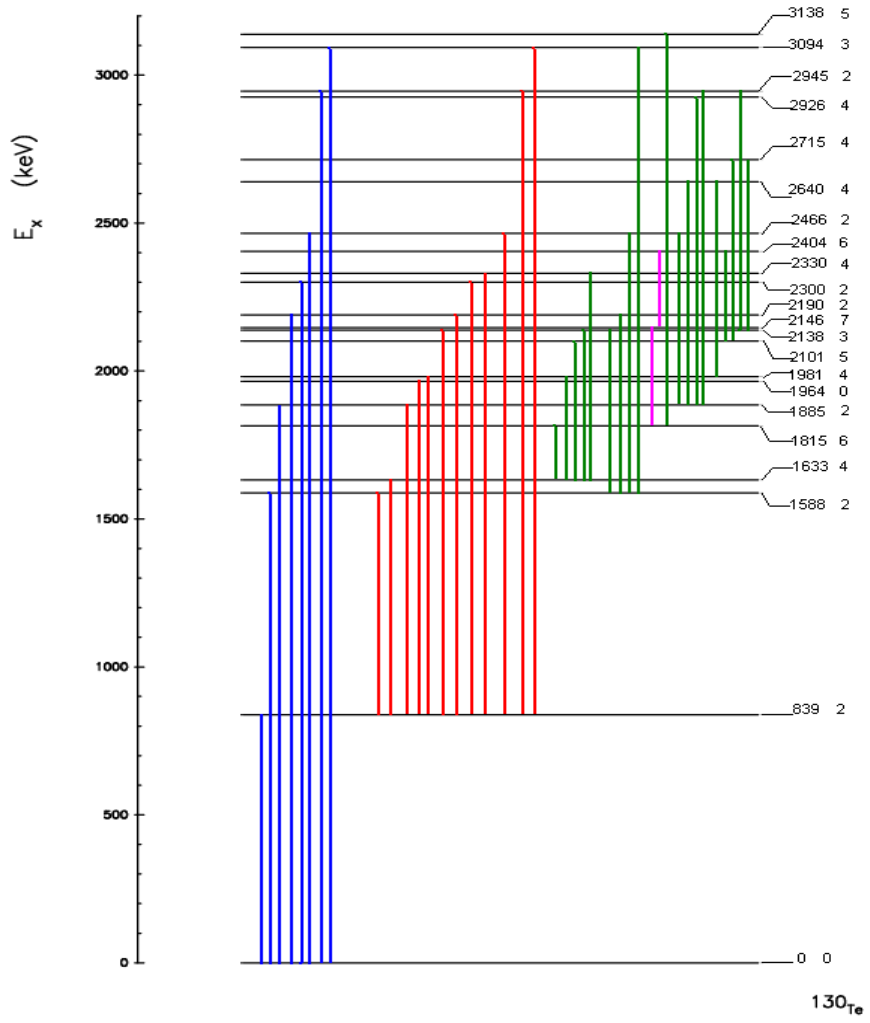

Figure 9. An abbreviated version of the ^{130}Te level scheme. Values at the right are level energies in keV and state spins. Blue lines represent transitions to the gound state, red lines represent transitions to the first excited state, and green lines represent other transitions. The violet lines represent the transitions of interest involving the 2146 keV energy level described below.

Difficulties in gamma ray placement into and building the level scheme can come from many different problems. Many times, the spectrum peaks for a particular excitation function have low yields, and there is much scatter among the data points. Sometimes the excitation energy of a state is too high to get an adequate number of data points for an extrapolation to find the threshold. Occasionally, there is background radiation at the same frequency as the gamma ray that must be taken into account. On rare occasions, there are two gamma rays from the nucleus with nearly the same energy. All of these things cause difficulty when trying to determine the threshold of the gamma rays.

One of the most perplexing problems was that of the 2146-keV level. In the excitation functions, I observed no gamma rays with a threshold of that energy. Therefore, since I saw no gamma rays coming from that energy, I thought there must not be an energy level there. The problem was that several excited states appeared to decay into a state at 2146 keV. Specific evidence included a gamma ray with energy 258 keV and a threshold at about 2400. Upon examining the excitation functions, I saw that there was a gamma ray with energy 331 keV that appeared to have the same threshold and general shape as the gamma ray with energy 258 keV, but would not fit coming from the same level. At this point, I consulted previous data on ^{130}Te and found that there was indeed a level documented at 2146 keV [BNL02]. The recorded spin of the state was 7^-, which would explain why I could not observe the state directly. The inelastic neutron scattering excitation process used for the experiment would not be able to impart seven units of angular momentum into the nucleus, and therefore any population of that state would be indirect, as via decay of higher states into that state. The gamma ray with energy 331 keV that appeared to come from a level at 2404 keV actually is from the 2146-keV state. The reason for the delayed threshold is that the 2146-keV state could not be populated until the 2404-keV state which fed it was populated. Therefore, their thresholds appear the same. And since the population of the 2146-keV state depended on the decay of the 2404-keV state (via the 258-keV gamma ray), the gamma-ray shapes could be similar.

The 285-keV gamma ray is responsible for difficulties when determining another level placement. Its position is a transition from the 2171-keV level to the 1886-keV level. It appears that the gamma-ray peak could be a "doublet," or two ^{130}Te gamma rays with the about same energy. This is observed when two different decays with two sets of initial and final states have about the same energy difference. The excitation has a severe kink near 2430 keV. This could indicate a doublet with gamma ray coming from a level at that energy, but unfortunately, there is background radiation at that gamma-ray energy. The germanium crystal can produce a 285-keV gamma ray itself, so the second apparent threshold will remain speculation.

Several transitions were identified with help from the gamma-gamma coincidence data. For example, the 334-keV gamma ray has a threshold around 2440 keV, and could be from 2435, 2500, or 2472. But the gamma ray is in coincidence with a 468-keV (2101 keV-1633 keV) gamma ray, so I picked the transition between levels at 2435 keV and 2101 keV for the 334-keV gamma ray.

Another help in distinguishing gamma rays for level placements are the shapes of their excitation functions. Two excitation functions are said to have the same shape if the yields of all the points

in one excitation function normalized to a single point in it are the same as the yields of all the respective points in another excitation function normalized to the respective single point in that plot. Excitation functions' distinguishing shape characteristics include the slope at different points, unique kinks in the line, and how smooth the line is. The shape of the excitation function of a gamma ray is characteristic of the branching ratio and the spin energy level it came from. For example, the 385-keV gamma ray could have been from any of three levels around 2700, its excitation function's shape was closest to other gamma rays from the 2789-keV level. The 491-keV gamma was placed from 2895 keV because it looks similar to the 288-keV gamma ray, which comes from a level at 2895 keV. Similarly, the 521-keV gamma ray looks like the 2117-keV gamma from the 2956-keV level, so it was placed as well from that level. The 575 keV and 614-keV gamma rays apparently both come from 2714 keV. A characteristic kink in the 2138-keV level gamma rays indicated that the 1031-keV gamma ray was one of them.

Some gamma rays have baffling characteristics and the transitions are not well understood. For example, the 468.1 keV (2101 keV – 1633 keV) is a very strong line with a strong excitation function whose yield grows continuously with a kink at 2850 keV. This type of "growing" behavior is neither normal nor expected. The level at 2101 keV is a popular choice for a final state for gamma decays, which might have something to do with the busy excitation function. Unfortunately, the only decay from this state, the 468-keV gamma ray, is too low in energy to determine the lifetime.

Sometimes gamma rays show up at inconvenient places. For example, a 753.52-keV gamma ray has a strong presence in the excitation function data, but it was not observed in the angular distribution, perhaps due to the duration of individual runs. It turns out from examining the accumulated data on the other tellurium isotopes that it is from either ^{128}Te or ^{126}Te. A few gamma rays from trace elements of other tellurium isotopes in the sample are always present. Analyzing the data and previously know literature, a gamma ray at 636 keV also appears to be from ^{126}Te, and the 743.3-keV gamma from ^{128}Te [BNL02]. Background radiation from other elements in the target room can also be found in the detector spectra. Copper, iron, and germanium gamma rays are the most common.

The techniques outlined above were used to place the approximately 170 observed transitions into a scheme of nearly 100 levels lying up to 3.4 MeV in excitation energy. Spectroscopic information about each state; the spin, lifetime, decay branching ratios, and multipole mixing ratios, have been extracted for many of these states.

Placing levels into an energy scheme using excitation functions and coincidence data was relatively easy compared to determining lifetimes and other angular-dependent spectroscopic properties. The yield of a particular gamma ray is much less sensitive to angular dependence than it is the amount of energy deposited in the sample by the neutrons. Also, with the very small changes in energy observed for Doppler shifts, it is often difficult to extract a meaningful lifetime. These difficulties make the calculation of actual transition rates extremely challenging.

Angular distributions were done at neutron energies of both 2.2 MeV and 3.3 MeV in order to get more reliable data for the lower energy levels, as decays from higher energies tend to have an

effect on the observed quantities measured for the lower energy states. Running with lower energy neutrons does have significant drawbacks, though, the major one being that often there are not enough detector counts to get good statistics. Good statistics are necessary to reduce the scatter among the data points.

Lifetimes were determined for approximately 50 of the identified excited states of ^{130}Te. Many of the states for which lifetimes were not calculated simply did not have adequate statistics in the angular data. Often what was observed appeared to be a negative slope, which is a physical impossibility. The DSAM requires identification of the transition energies to <0.1 keV for each angle. Radioactive ^{226}Ra sources were measured between each tellurium run to ensure the most accurate energy calibration for each angle.

From the plots of gamma-ray yield versus detector angle, branching and multipole mixing ratios were extracted for approximately 100 transitions. Angular momenta were assigned to most states, with new spins being assigned to almost 50 energy levels. As with the lifetime determinations, analysis was complicated by scatter in the data points. Spin and ratio assignment relies heavily upon the quality of the fit of CINDY's Legendre polynomial for that gamma ray, as well as the fits of other gamma rays from the same state. In many cases, it was impossible to determine definitely the spin of a state.

Transitions to zero-spin states that could be identified as having a bowed-up or bowed-down angular distribution identified their source states as having a spin of two or one, respectively, as a gamma ray can only carry one or two units of angular momentum. This determination did not require the use of CINDY as these transitions are purely E1 or E2 in type and multipolarity. Other transitions required the use of the CINDY code because the different possible combinations of angular momentum vectors to yield the difference in angular momentum between two states must be compared to see which is most plausible. Decays from states with zero spin have flat angular distributions. Therefore, the yields of the 1125-keV gamma ray from the second spin zero level at 1964 keV were used to normalize all data points.

F. Transition Rates

Reduced transition probabilities, "transition rates," for different multipole transitions were calculated for gamma rays from the spectroscopic information discussed above. Suitable references for this material are Firestone [Fi98] and Lilley [Li01]. A state's transition probability, P(level), is defined as the reciprocal of the mean lifetime, $1/\tau$. The partial gamma-ray transition probability is defined by:

$$P_\gamma(XL)=P(level)\ \ N_\gamma(XL) / (\Sigma\ N_d) \qquad [3]$$

Where P(level) is the transition probability for the entire state, N_γ is the intensity of the gamma ray of interest, $\Sigma\ N_d$ is the sum of the intensities of all of the transitions from the level. The argument XL denotes the radiation type, X, which is either electric, "E," or magnetic, "M," and the multipolarity, L, which is 1 or 2. This equation can more simply be expressed as the branching ratio divided by the lifetime, BR/τ. For pure transitions (E1 or E2), this equation is

sufficient for the partial gamma-ray transition probability. The equations for a single decaying state's gamma-ray transition that is mixed-mode (E2 and M1 present) are given by:

$$P_\gamma(M1)=P(level)/[1+\delta^2+\alpha_\gamma(M1)+\delta^2\alpha_\gamma(E2)] \quad [4]$$

$$P_\gamma(E2)=P(level)/[1+\delta^{-2}+\alpha_\gamma(E2)+\delta^{-2}\alpha_\gamma(M1)] \quad [5]$$

Where δ is the mixing ratio, and α_γ is the internal conversion coefficient, which for essentially all transitions represents a minimal effect. If more than one gamma-ray decays from a state that depopulates via a mixed-mode decay, equations [3] and [4] or [5] must be combined. The result is:

$$P_\gamma(M1)= BR / (\tau[1+\delta^2]) \quad [6]$$

$$P_\gamma(E2)= BR / (\tau[1+\delta^{-2}]) \quad [7]$$

The quantity of interest is the reduced transmission probability which is calculated as:

$$B(XL) = \frac{L[(2L+1)!!]^2\hbar}{8\pi(L+1)}\left(\frac{\hbar c}{E_\gamma}\right)^{2L+1} P_\gamma(XL) \quad [8]$$

where the units for energy, length, and time are MeV, fm, and second, respectively. The B(XL) are traditionally converted to "Weisskopf units" in order to easily compare the transition probabilities from different experimental techniques. The conversion factor is dependent upon nuclear mass and the type and multipolarity of the transition. The conversion factors are as follows:

$$B(E1)_w = B(E1) / 1.65 \quad [9.a]$$
$$B(E2)_w = B(E2) / 39.11 \quad [9.b]$$
$$B(M1)_w = B(M1) / 1.79 \quad [9.c]$$

As transition rates take into account every observed property of the gamma rays, they are excellent indicators of agreement or disagreement with model calculations.

All spectroscopic information extracted from the data for ^{130}Te is presented in Table I. Transition rates are presented in Weisskopf units. Uncertainties are presented in the same units as their respective values of interest.

Table I. Level scheme and spectroscopic information for the excited states of tellurium-130. Uncertainties presented have been symmetrized.

J^{π}	Initial State E_i (keV)	Transition Energy E_γ (keV)	XL	BR	Final State E_f (keV)	note	Mixing Ratio $\tan^{-1}(\delta)$	τ (ps)	τ uncert.	Reduced Transition Rates B(XL) E1 (W.u.)	E1 uncert. (W.u.)	E2 (W.u.)	E2 uncert. (W.u.)	M1 (W.u.)	M1 uncert. (W.u.)
2+	839.49	839.49	E2	1.00	0			3.32	0.07			1.51E+01	3.11E-01		
2+	1588.17	1588.09	E2	0.02	0			2.32	0.34			1.68E-02	2.16E-03		
		748.76	M1+E2	0.98	839		1					2.66E+01	3.42E+00	9.36E-03	1.21E-03
4+	1632.98	793.49	E2	1.00	839										
6+	1815.38	182.39	E2	1.00	1633			14100	7200			7.31E+00	2.47E+00		
2+	1885.60	1885.60	E2	0.02	0			.453	.016			2.92E-02	9.80E-04		
		1046.11	M1+E2	0.98	839		1.38					3.49E+01	1.17E+00	2.17E-03	7.28E-05
0+	1964.66	1125.17	E2	1.00	839			2.97	2.42			3.90E+00	1.75E+00		
4+	1981.45	1141.92	E2	0.43	839			2.97	1.22			1.56E+00	4.53E-01		
		348.52	M1+E2	0.57	1633		-0.13					1.31E+01	3.81E+00	1.42E-01	4.12E-02
5-	2101.13	468.15	E1	1.00	1633										
3+	2138.45	550.30	M1+E2	0.43	1588		0.63	4.00	3.88			1.54E+01	7.60E+00	1.34E-02	6.59E-03
		505.47	M1+E2	0.19	1633		1.04					2.27E+01	1.12E+01	3.04E-03	1.50E-03
		1299.03	M1+E2	0.38	839		0.31					4.98E-02	2.45E-02	1.25E-03	6.15E-04
7-	2146.05	330.67	E1	1.00	1815			166000	8100	6.33E-08	2.94E-09				
2	2171.51	285.60	M1+E2	0.89	1886	a	-0.66	0.85				4.27E+03		8.81E-01	
		1332.34	M1+E2	0.11	839									1.75E-03	
2+	2190.21	601.57	M1+E2	0.07	1588		0.97	0.587	0.050			2.21E+01	1.74E+00	5.72E-03	4.50E-04
		1350.98	M1+E2	0.41	839		1.41					3.15E+00	2.48E-01	2.31E-04	1.81E-05
		2190.48	E2	0.52	0							3.65E-01	2.87E-02		
2+	2282.43	2282.42	E2	0.21	0			0.111	0.002			6.26E-01	1.14E-02		
		1442.95	M1+E2	0.79	839		1.29					2.20E+01	3.89E-01	5.80E-03	1.03E-04

J^{π}	Initial State E_i (keV)	Transition Energy E_γ (keV)	XL	BR	Final State E_f (keV)	note	Mixing Ratio $\tan^{-1}(\delta)$	τ (ps)	τ uncert.	Reduced Transition Rates B(XL) E1 (W.u.)	E1 uncert. (W.u.)	E2 (W.u.)	E2 uncert. (W.u.)	M1 (W.u.)	M1 uncert. (W.u.)
2+	2300.14	1460.58	M1+E2	0.96	839	b		0.628	0.048						
		2300.20	E2	0.04	0	b									
4+	2330.64	1491.14	E2	0.20	839			0.798	0.079			7.05E-01	6.37E-02		
		697.68	M1+E2	0.80	1633		-0.06					4.56E-01	4.10E-02	9.36E-02	8.43E-03
6-	2404.34	258.17	M1+E2	0.50	2146										
		303.33	M1+E2	0.50	2101		0.03								
4-	2435.41	334.28	M1+E2	1.00	2101		-0.06								
2	2447.52	1608.03	M1+E2	1.00	839	a	1.16	0.121	0.030			1.34E+01	2.75E+00	9.99E-03	2.06E-03
4+	2449.41	816.43	M1+E2	1.00	1633		-0.25	0.376	0.041			9.34E+00	9.14E-01	1.45E-01	1.42E-02
2+	2466.80	581.09	M1+E2	0.05	1886		-0.31	0.808	0.119			1.68E+00	2.17E-01	8.44E-03	1.09E-03
		878.66	M1+E2	0.04	1588		-0.22					9.97E-02	1.28E-02	2.34E-03	3.02E-04
		1627.35	M1+E2	0.80	839		-1.54					1.81E+00	2.33E-01	6.92E-06	8.91E-07
		2466.91	E2	0.11	0							3.12E-02	4.01E-03		
2(3)	2475.95	590.30	M1+E2	0.20	1886	a	-0.03	1.51	0.27			3.48E-02	5.38E-03	2.05E-02	3.17E-03
		887.86	M1+E2	0.29	1588		-0.22					3.43E-01	5.29E-02	8.22E-03	1.27E-03
		1636.51	M1+E2	0.51	839		1.41					5.84E-01	9.03E-02	6.27E-05	9.68E-06
3-	2526.96	938.46	E1	0.03	1588		-0.06	1.11	0.16	1.38E-05	1.71E-06				
		425.63	E2	0.01	2101	c						2.00E+01	2.47E+00		
		641.25	E1	0.10	1886		0			1.24E-04	1.54E-05				
		1687.53	E1	0.78	839		-0.03			5.58E-05	6.88E-06				
		894.62	E1	0.07	1633	d				3.39E-05	4.19E-06				
3(2)	2574.89	436.22	M1+E2	0.07	2138	a,d		0.908	0.140						
		986.72	M1+E2	0.22	1588		-1.54					5.51E+00	7.36E-01	7.75E-06	1.04E-06
		942.02	M1+E2	0.63	1633		0.03					1.77E-02	2.36E-03	2.65E-02	3.54E-03
		1735.58	M1+E2	0.07	839		-0.19					3.86E-03	5.16E-04	4.79E-04	6.40E-05
2(4)+	2580.93	992.74	M1+E2	0.10	1588		1.04	0.289	0.018			5.69E+00	3.31E-01	2.94E-03	1.71E-04
		1741.53	M1+E2	0.90	839		0.6					1.29E+00	7.49E-02	1.27E-02	7.39E-04

J^{π}	Initial State E_i (keV)	Transition Energy E_γ (keV)	XL	BR	Final State E_f (keV)	note	Mixing Ratio $\tan^{-1}(\delta)$	τ (ps)	τ uncert.	Reduced Transition Rates B(XL) E1 (W.u.)	E1 uncert. (W.u.)	E2 (W.u.)	E2 uncert. (W.u.)	M1 (W.u.)	M1 uncert. (W.u.)
2(3)	2604.70	1764.99	M1+E2	0.82	839	a	-0.35	0.493	0.131			2.39E-01	5.04E-02	8.51E-03	1.79E-03
		414.45	M1+E2	0.18	2190		0.13					1.02E+01	2.15E+00	1.57E-01	3.30E-02
2(3)	2605.75	1017.65	M1+E2	1.00	1588	a	-1.19	0.775	0.240			2.13E+01	5.04E+00	5.37E-03	1.27E-03
1	2607.10	2607.06	M1+E2	0.67	0			0.101	0.004					1.18E-02	4.45E-04
		1767.65	M1+E2	0.33	839		-1.22					3.54E+00	1.33E-01	2.25E-03	8.49E-05
4	2639.54	753.92	E2	0.23	1886	a									
		658.16	M1+E2	0.77	1981		0.75								
3	2673.80	535.35	M1+E2	1.00	2138	a	0.47								
2(1)	2688.44	2688.29	M1+E2	0.84	0			0.050	0.002					2.73E-02	9.59E-04
		802.87	M1+E2	0.07	1886		-1.22					7.32E+01	2.57E+00	9.62E-03	3.38E-04
		1849.07	M1+E2	0.09	839		-1.26					1.54E+00	5.40E-02	8.27E-04	2.90E-05
	2709.40	1121.31		1.00	1588	e									
4-	2714.58	575.89	E1	0.06	2138		-0.03								
		613.69	M1+E2	0.94	2101		1.13								
3-(4)	2733.28	1144.73	E1	0.10	1588		0.81	0.175	0.011	1.39E-04	8.02E-06				
		1100.35	E1	0.66	1633		-0.72			1.07E-03	6.21E-05				
		402.78	E1	0.08	2331	f				2.70E-03	1.56E-04				
		1894.03	E1	0.16	839		0.53			5.25E-05	3.04E-06				
4+(5)	2736.17	1103.08	M1+E2	0.31	1633		-1.16								
		920.91	E2	0.69	1815		0.56								
1	2742.47	411.81		1.00	2331										

J^{π}	Initial State E_i (keV)	Transition Energy E_γ (keV)	XL	BR	Final State E_f (keV)	note	Mixing Ratio $\tan^{-1}(\delta)$	τ (ps)	τ uncert.	Reduced Transition Rates B(XL) E1 (W.u.)	E1 uncert. (W.u.)	E2 (W.u.)	E2 uncert. (W.u.)	M1 (W.u.)	M1 uncert. (W.u.)
3(2)	2744.51	2743.52		0.02	0			0.266	0.007						
		1156.27		0.08	1588		-1.38								
		1905.33		0.45	839		-0.09								
		859.27		0.35	1886		-0.06								
		1111.97		0.12	1633		0								
5(4)	2747.83	932.37	M1+E2	0.16	1815	a	-1.48	0.287	0.036			1.65E+01	1.84E+00	1.81E-04	2.01E-05
		1114.93	M1+E2	0.84	1633	e									
3(4)+	2766.26	1178.04	M1+E2	0.40	1588		0.16	0.402	0.035			2.33E-01	1.87E-02	1.89E-02	1.52E-03
		1926.74	M1+E2	0.19	839		0.75					1.71E-01	1.37E-02	1.12E-03	8.95E-05
		880.65	M1+E2	0.27	1886		-0.69					1.06E+01	8.51E-01	1.84E-02	1.48E-03
		1133.45	M1+E2	0.14	1633		0.81					2.08E+00	1.67E-01	3.68E-03	2.95E-04
3	2776.29	309.38	M1+E2	1.00	2467	a	-0.63								
3	2789.17	903.33	M1+E2	0.35	1886	a	1.16								
		1949.63	M1+E2	0.60	839		-0.03								
		385.31	?	0.05	2404	d									
	2795.11	188.05		1.00	2607	d									
	2809.45	1221.33		0.59	1588	e									
		205.00		0.41	2604	e									
	2819.33	647.48		0.78	2172	g									
		343.45		0.22	2476	g									
4,5,6+	2833.32	1200.34	M1+E2	1.00	1633	d									
4,5,6+	2834.96	1995.42	E2	0.26	839		-0.35	0.359	0.072			4.77E-01	7.99E-02		
		853.52	M1+E2	0.74	1981		0.94					6.19E+01	1.04E+01	3.66E-02	6.13E-03
3	2887.84	2048.11	M1+E2	0.60	839	a,d	-0.25	> 2				1.06E-03		1.04E-04	
		587.76	M1+E2	0.18	2300		-0.09					2.19E-02		1.42E-03	
		2887.97	?	0.21	0										

J^{π}	Initial State E_i (keV)	Transition Energy E_γ (keV)	XL	BR	Final State E_f (keV)	note	Mixing Ratio $\tan^{-1}(\delta)$	τ (ps)	τ uncert.	Reduced Transition Rates B(XL) E1 (W.u.)	E1 uncert. (W.u.)	E2 (W.u.)	E2 uncert. (W.u.)	M1 (W.u.)	M1 uncert. (W.u.)
(2-5)	2895.31	490.63		0.40	2404										
		288.76		0.60	2607										
3	2908.54	1320.45	M1+E2	1.00	1588	a	-1.26								
4	2925.65	1040.05	E2	1.00	1886	a	-1.44								
3	2939.09	1053.49	M1+E2	1.00	1886	a	0.91								
2	2945.58	1059.64	M1+E2	0.11	1886	a	0.88	0.281	0.021			3.75E+00	2.59E-01	4.38E-03	3.02E-04
		807.21	M1+E2	0.15	2138		-1.54					3.23E+01	2.23E+00	3.04E-05	2.10E-06
		2106.20	M1+E2	0.37	839		-1.54					6.70E-01	4.62E-02	4.29E-06	2.96E-07
		2945.74	E2	0.36	0							1.22E-01	8.38E-03		
3	2953.44	2113.85	M1+E2	0.89	839	a	-0.69	2.03	0.91			8.71E-02	7.04E-02	8.70E-04	7.03E-04
		1365.44	M1+E2	0.11	1588		-1.07					1.90E-01	1.53E-01	1.61E-04	1.30E-04
4(3)	2956.71	2117.06	E2	0.37	839	a	-0.03	1.04	0.25			1.74E-01	3.37E-02		
		521.46	E1	0.63	2435		-0.94								
	3047.12	1414.14			1633										
4(3)	3058.14	1172.53	E2	1.00	1886	a	0.53								
4	3073.96	935.51	M1+E2	1.00	2138	a	-1.26	0.740	1.08			3.56E+01	2.11E+01	4.90E-03	2.91E-03
							-0.22								
4	3083.04	2243.55	E2	1.00	839	a	-0.56	0.184	0.044			1.99E+00	3.83E-01		
3	3094.78	1506.56	M1+E2	0.29	1588	a	-0.13	0.178	0.011			7.45E-02	4.30E-03	1.51E-02	8.69E-04
		2255.29	M1+E2	0.43	839		-0.22					4.10E-02	2.37E-03	6.35E-03	3.66E-04
		3094.91	?	0.28	0										
1	3100.62	1135.56	M1+E2	1.00	1965	a,h									
	3110.38	3110.28		0.79	0	d		0.473	0.120						
		2270.98		0.21	839	d									

J^{π}	Initial State E_i (keV)	Transition Energy E_γ (keV)	XL	BR	Final State E_f (keV)	note	Mixing Ratio $\tan^{-1}(\delta)$	τ (ps)	τ uncert.	Reduced Transition Rates B(XL) E1 (W.u.)	E1 uncert. (W.u.)	E2 (W.u.)	E2 uncert. (W.u.)	M1 (W.u.)	M1 uncert. (W.u.)
2	3128.85	1243.03	M1+E2	0.23	1886	a	0.6	0.696	0.160			7.52E-01	1.41E-01	3.78E-03	7.07E-04
		2289.39	M1+E2	0.29	839		-1					9.90E-02	1.85E-02	3.26E-04	6.10E-05
		990.43	M1+E2	0.16	2138	d									
		3129.00	E2	0.31	0							3.14E-02	5.88E-03		
4(3)	3132.21	1246.61	E2	1.00	1886	a	0.81								
5	3137.91	1322.54	M1+E2	1.00	1815	a	0.72								
3(2)	3146.83	956.34	M1+E2	1.00	2190	a	-1.44	0.137	0.091			1.87E+02	7.48E+01	4.50E-03	1.80E-03
4	3154.49	2314.88	E2	0.48	839	a	-1.19	0.285	0.044			5.28E-01	7.08E-02		
		1521.64	M1+E2	0.52	1633		-0.35					5.47E-01	7.34E-02	1.45E-02	1.94E-03
5	3165.26	1183.85	M1+E2	1.00	1981	a	-1.16								
							-0.35								
(4,5,6)	3167.12	1065.99	E1	1.00	2101	a	-1.13	0.799	0.799	3.96E-04	1.99E-04				
4	3169.03	1002.36		0.49	2166	a	-0.75	> 3							
		1030.85	M1+E2	0.51	2138		-0.79					1.54E+00		2.45E-03	
3	3176.82	1291.16	M1+E2	0.84	1886	a	-1.22								
		2337.39	M1+E2	0.16	839	e									
2	3196.19	3196.19	E2	1.00	0	a		0.121	0.020			4.88E-01	6.59E-02		
4	3224.89	1086.44	M1+E2	1.00	2138	a	-1.04	0.909	0.570			1.13E+01	4.38E+00	6.98E-03	2.71E-03
							-0.44								
3	3242.31	3242.03	?	0.67	0	a		0.189	0.020						
		2403.09	M1+E2	0.33	839		0.6					1.46E-01	1.39E-02	2.75E-03	2.60E-04
5	3249.55	1616.57	M1+E2	1.00	1633	a	-0.79	1.35	0.18			7.07E-01	1.13E-01	2.76E-03	4.43E-04
		846.82	?		2404	d									
7,8+	3287.14	882.97	E1		2404										

J^{π}	Initial State E_i (keV)	Transition Energy E_γ (keV)	XL	BR	Final State E_f (keV)	note	Mixing Ratio $\tan^{-1}(\delta)$	τ (ps)	τ uncert.	Reduced Transition Rates B(XL) E1 (W.u.)	E1 uncert. (W.u.)	E2 (W.u.)	E2 uncert. (W.u.)	M1 (W.u.)	M1 uncert. (W.u.)
	3308.36	563.49			2745										
3(4)	3319.27	2479.78	M1+E2	1.00	839	a	1.16	0.297	0.37			6.28E-01	3.49E-01	1.12E-03	6.20E-04
5	3340.00	1358.00	M1+E2	0.09	1981	a	-0.85								
		1454.19	?	0.65	1886	e									
		384.26	M1+E2	0.26	2957	d									
5	3355.95	1540.58	M1+E2	1.00	1815	a	-0.97								
3-	3362.59	1547.21	?	1.00	1815	e									
5	3381.32	1565.94	M1+E2	1.00	1815	a	0.06	0.099	0.125			8.03E-02	4.49E-02	8.31E-02	4.65E-02
5	3385.88	1752.90	M1+E2	1.00	1633	a	-0.75	0.088	0.046			6.60E+00	2.26E+00	3.56E-02	1.22E-02
	3388.41	1057.56			2331	i									
		553.70		1.00	2835	d		0.021	0.027						
	3389.96	1504.36		1.00	1886	d									
	3394.20	627.97			2766										
4	3396.90	1206.41	E2	1.00	2190	a	0.44	0.449	0.944			1.82E+01	1.23E+01		
4	3399.77	1208.93	E2	1.00	2190	a	-0.53	0.139	0.201			5.77E+01	3.41E+01		
		271.12			3129										
4	3403.10	274.00	E2	0.75	3129	a	0.75	0.635	1.196			1.60E+04	1.04E+04		
		998.75		0.25	2404	e									
	3405.50	276.50		1.00	3129	d		0.001	0.004						
	3406.40	1075.74		1.00	2331			0.642	0.630						
	3407.60	312.82			3095										

J^{π}	Initial State E_i (keV)	Transition Energy E_γ (keV)	XL	BR	Final State E_f (keV)	note	Mixing Ratio $\tan^{-1}(\delta)$	τ (ps)	τ uncert.	Reduced Transition Rates B(XL) E1 (W.u.)	E1 uncert. (W.u.)	E2 (W.u.)	E2 uncert. (W.u.)	M1 (W.u.)	M1 uncert. (W.u.)
5	3410.58	1079.93	M1+E2	1.00	2331	a	0.75								

a New level.
b Flat angular distribution.
c Angular distribution inconsistent with spin-3.
d Poor quality angular distribution data.
e Significant portion of the yield is beam induced background.
f Unlikely to be spin-3.
g Questionable level existance.
h Dipole-shaped angular distribution.
i Previously placed with this level, not observed in these data.

IV. MODEL DISCUSSION

The next step of the project is to try to uncover the structural features of the ^{130}Te nucleus. Independent particle models are good for describing systems of a few nucleons, and collective models are used to describe large nuclei when it would be impossible to track all of the individual nucleons. The ultimate goal would be to understand the features of the nuclear force that determine the balance between collective- and particle- like behavior. To look at the collective features, experimental results are compared to the calculations of a collective behavior model. Likewise, to look at particle features, results are compared to particle behavior model calculations. Hybrid models are used to predict relative particle aspects of larger nuclei by combining aspects of both collective and particle models.

Theorists are continually developing complex codes to simulate the actions of excited nuclei. A number of these treat the nucleus in the "liquid drop" fashion, proposing that all excited states can be reproduced as a combination of vibrations, deformations, and rotations of a fluid nucleus. An older, more complete traditional fluid model, the General Collective Model (GCM) has re-emerged [Gn69, Gn71, Tr91, Va97, Za97]. The GCM solves the problem of the liquid drop sloshing around in a deformed potential well. In the GCM, the potential energy is described as a function of two deformation variables.

The independent-particle models are not fit to describe situations where large numbers (greater than three or four) of nucleons are involved and the collective models are not capable of describing situations where only a few nucleons are responsible for the excitations. Hybrid models seek to combine features of both. The Particle-Core Coupling Model (PCM) [He67] treats the tellurium nuclei as two valence nucleons orbiting a spherical core. The two valence nucleons are then allowed to interact with each other and with the core, and the core is allowed to undergo simple vibrations. It is hoped that by adjusting the strength of the interaction between the valence particles and the core (similar to tidal forces), one can "dial up" the particular tellurium isotope of interest. Weaker tidal strengths may be appropriate for the vibrational-like ^{120}Te, while a stronger tidal strengths may be appropriate for ^{130}Te, where particle characteristics are more pronounced.

A. Initial Observations

The lighter tellurium nuclei, ^{120}Te and ^{122}Te, have groups of equally spaced levels suggestive of a harmonic oscillator. The heavier nuclei, $^{126\text{-}130}$Te, have several levels suggestive of individual particle orbits. Looking at the experimentally developed level scheme, it appears that the first 6^+ state is too depressed to be part of a harmonic vibrator scheme. Also, the second 0^+ state is elevated above the third 2^+, which is unusual. Figure 10 depicts the evolution of a few excited states across the isotopic chain.

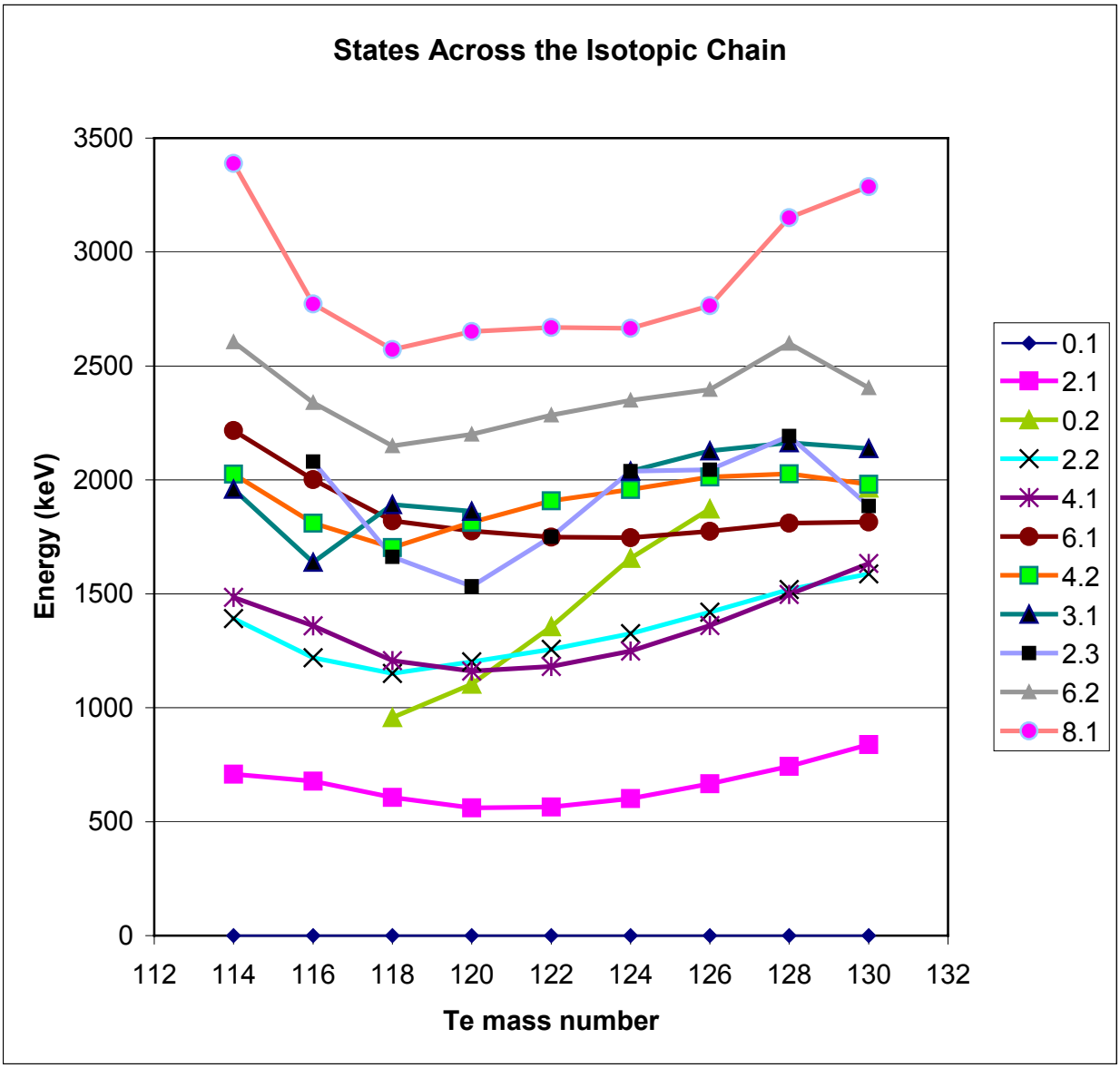

Figure 10. Selected important energy levels in nine tellurium isotopes. The notation of the legend regards the first state of spin 2 as "2.1".

Often level schemes are more important for just deciding if a model has sufficient built-in complexity (since the Hamiltonian parameters are adjusted to fit the observed states) rather than providing a sensitive test of the wave functions. We examine the electric quadrupole transition rate, B(E2), between levels to evaluate the degree of agreement. Formulae for determining the transition rate from the experimental lifetime, multipole mixing ratio, and γ-ray transition energy may be found above, as well as in other references [Kr88, Li01]. Comparisons of electric quadrupole transition rates, B(E2), for several transitions of interest are also in the PCM discussion section.

B. General Collective Model

The General Collective Model treats the nucleus as a vibrating, rotating fluid blob. Rotations and vibrations are quantum mechanical in nature and correspond to quantized quadrupole and octupole phonon excitations. The radius of the nucleus is expanded by the following function [He94]:

$$R(\theta,\phi,t)=R_0[1+\Sigma\, \alpha_{\lambda\mu}(t)Y_{\lambda\mu}(\theta,\phi)] \qquad [10]$$

where $\alpha_{\lambda\mu}$ are expansion coefficients or more specifically the time-dependent multipole deformation parameters corresponding to the different phonon excitations, and $Y_{\lambda\mu}$ are the spherical harmonics. Typically $\lambda = 2$ only. Using $R(\theta,\phi,t)$, kinetic energy terms, elasticity terms, and a nuclear potential such as Woods-Saxon, the Hamiltonian can be constructed with independent parameters for "inertia" and surface stiffness.

The GCM uses what is known as the Gneuss-Greiner form for the potential energy term in the Hamiltonian. The following terms of the potential were used [Tr91]:

$$V(\beta,\gamma) = C_2\sqrt{\frac{1}{5}}\beta^2 - C_3\sqrt{\frac{2}{35}}\beta^3\cos(3\gamma) + C_4\frac{1}{5}\beta^4 \qquad [11]$$

The deformation variables β and γ determine the deformed shape of the nucleus for a given state. Changing the β and γ coordinates will result in what is analogous to squashing or stretching a balloon in the z direction and on the sides, respectively. The GCM code takes level energies and spins given by the user and searches for the best parameters to fit those inputs. Then the user runs the code in a different mode to reproduce a level scheme with these "best" parameters. The quality of model agreement with experimental results lets the user determine which states exhibit collectivity and which states do not. To assure that the minimization routine found the absolute minimum, searches were made starting from different potential parameters selected from other tellurium nuclei.

When the GCM code analyzed a full set of experimental levels to determine potential parameters, the values it determined for C_2, C_3, and C_4 were 1905.41, 20224.14, and 4780.82 MeV, respectively. There are other, higher-order terms, but only the first three are considered to be physically justifiable. The GCM was also asked to find parameters by analyzing a reduced set of experimental values; the "problem" levels were taken out. The potential parameters found with less search levels are 2042.498, 19721.71, and 4786.108 MeV for C_2, C_3, and C_4, respectively. Figure 11 is a comparison of the experimental level scheme and the two GCM code calculations.

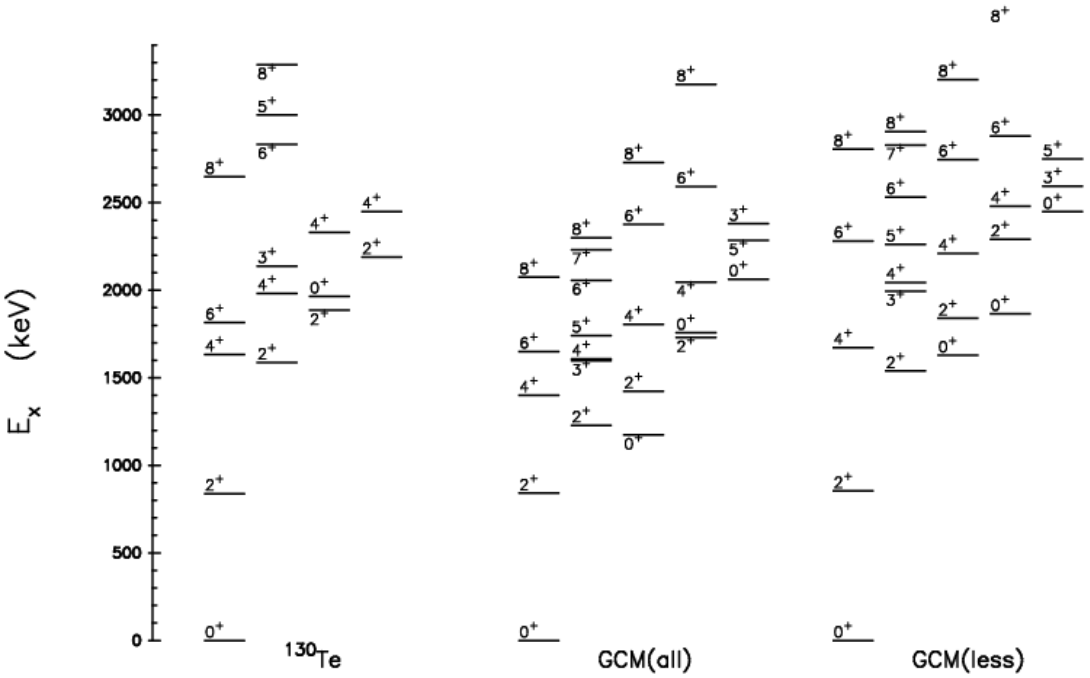

Figure 11. Comparison of the experimental ^{130}Te level scheme with GCM calculations. Levels are arranged in columns for clarity.

The experimental level scheme has little vibration-like character. The position of the first state with a value for spin of 2 and a positive parity, annotated "2_1^+", was correctly placed, but agreement in subsequent levels varied. The 4_1^+, 2_2^+, and 0_2^+ states (1st, 2nd, and 3rd columns, respectively) that could belong to a two-quadrupole phonon multiplet and should look slightly degenerate are present and are shifted in an acceptable manner, but the fragmentation of the 6^+, 4^+, 3^+, and 2^+ states of the three-phonon multiplet (second column) is not consistent with the patterns of anharmonic vibrators [Ca02]. The three-phonon states are intermingled with the two-phonon states. The 0_2^+ is shifted above the 2_3^+ in the third column. The 6_1^+ state in the first column is severely depressed from that of an equally-spaced vibrator scheme. If it followed a vibrator scheme, the first states of each spin would be evenly spaced (first column), as additional identical quadrupole phonons carry the same energy. The sequence of states that would be considered a part of the emerging γ- or β- bands (2nd and 3rd columns) of a non-spherical vibrator is scrambled.

C. Particle-Core Coupling Model

We compare our experimental results with calculations from the PCM, which treats the nucleus as two valence protons orbiting an inert core undergoing harmonic vibration [He67]. The PCM Hamiltonian is given by a collective term, a particle term, a particle-particle residual interaction term, and a proton-vibration interaction term. The 'major parameters' for the PCM model are the orbital energies for the valence protons, the strength of the pairing interaction between the valence protons, the energy of the characteristic core vibration, and the strength of the interaction between the valence protons and the core. Several related calculations were performed some years ago on various tellurium nuclei by Lopac [Lo70] and Warr [Wa98]. The calculations differ principally in their choice of the orbital energies.

Use of the PCM should allow us a better understanding of the particle versus collective nature of excited state structure as the user can vary the interaction and strength of each aspect. Five single particle orbital energies can be defined to be a basis for the particle-like effects in the nucleus. Multipole phonon energies and possible combinations may be varied as well. The variable parameters ζ_2 and ζ_3 are the "coupling constants" of the quadrupole and octupole phonons, respectively. These parameters represent the particle-phonon interaction strength. The variable parameter G is the amount of interaction between the particles, the "proton-proton pairing strength." Although the older PCM-generated schemes of Lopac and Warr were ultimately chosen to represent the PCM in comparisons with experiment, a new set of parameters were also independently developed in an attempt to reproduce the level scheme using the PCM.

While ^{130}Te has two valence protons, ^{129}Sb only has one. Since it has an extra proton beyond the closed shell at Z=50, and it is generally more difficult to break a closed shell than it is to excite a single valence particle, the energy levels of ^{129}Sb probably roughly resemble the single-particle orbital energies. In other words, the low-lying energy levels for ^{129}Sb are significantly particle-like in nature. Therefore, the tabulated energies of the excited states of ^{129}Sb were chosen as the five single particle orbital energies as follows:

$1g_{7/2}$: 0 MeV $2d_{5/2}$: 1.3 MeV $1h_{11/2}$: 1.13 MeV $2d_{3/2}$: 1.8 MeV $3s_{1/2}$: 4.5 MeV

The "core" nucleus for ^{130}Te, ^{128}Sn, has a closed proton shell, and its first excited state, the quadrupole excitation, should exhibit a high degree of collectivity. On such a basis, ^{128}Sn's first excited state energy, 1.2 MeV, was chosen as the ^{130}Te quadrupole phonon energy. Since it is thought that the valence protons in ^{130}Te are involved in particle behaviors, only the neutrons were allowed to take part in the quadruple phonon excitations, and no octupole phonon excitations were used at all. Three quadrupole phonons in all were allowed.

The five single-particle energies and the quadrupole phonon energy were entered as fixed parameters in the PCM input files. Often the parameters ζ and G are fixed by global equations or are within a defined range dependent upon the nuclear number and mass. For this experiment, the energy parameters were fixed, and these coupling strength parameters were varied in order to find the values that yielded the best agreement with experiment throughout the set of excited

states. Seventy-two sets of calculations were done using these energies, varying the pairing strength parameter, G, from 0.04 to 1.00, and the quadrupole phonon coupling constant, ζ_2, from 0.1 to 3.6. Ratios of PCM-predicted energies to the experimentally determined energies were plotted as the dependent variable in a two-parameter space. Figure 12 illustrates.

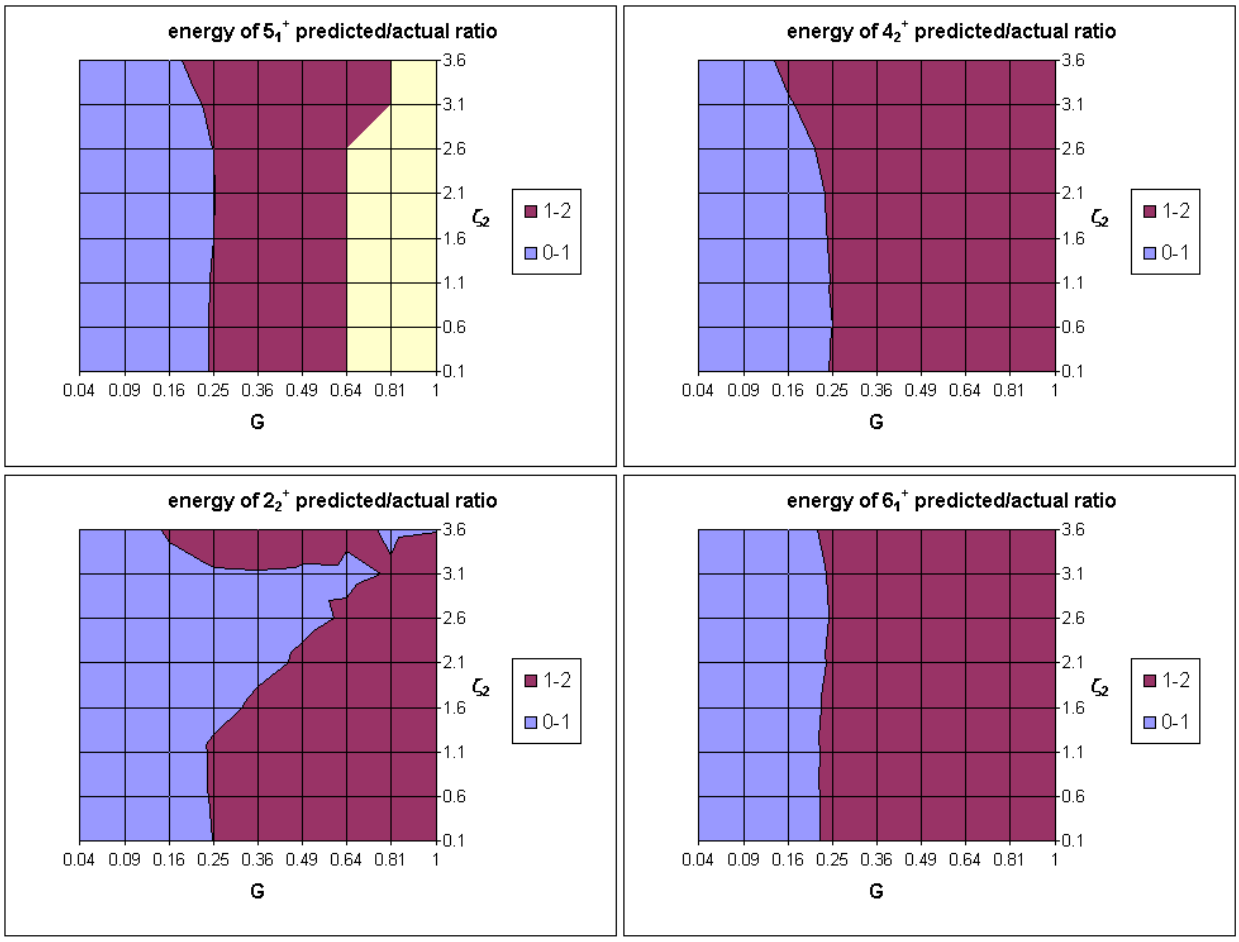

Figure 12. The ratio of the PCM-predicted value over the experimental value is plotted as a function of both the pairing strength and the quadrupole phonon coupling constant. The boundary between the red and blue regions is where the predicted value equals the experimental value.

Most of the parameter space plots look similar, and it is easy to point out which states are not easily recreated with this energy set. The best choice appears to be G=0.25 and ζ_2=1.1. These coordinates were closest to the ratio=1 line for most of the plots.

From the plots, one observes that increasing G will push up the PCM-predicted state energies. Looking at the plot of the 6_1^+ state, one can see that the optimal value for G is less than what was chosen, and based on the results that the state was calculated to be too high, conclude that the proton-proton interaction is less than predicted for this particular state. Based on the results from the GCM, it appears that the 6_1^+ state is indeed particle-like. Although that particular instance is an extreme case, it appears that many of the levels are mostly unaffected by a change in the proton-phonon interaction strength. Notable exceptions to this are the 0_2^+, 2_1^+, and 4_1^+ levels,

which exhibit extreme dependence on the proton-phonon coupling, suggestive of mixed-character states. While increasing ζ_2 for those states reduces their energy, the opposite appears to occur in many of the other states, including the later 2^+ and 4^+ states. Figure 13 illustrates the comparison between the experimentally determined level energies and the results of this model.

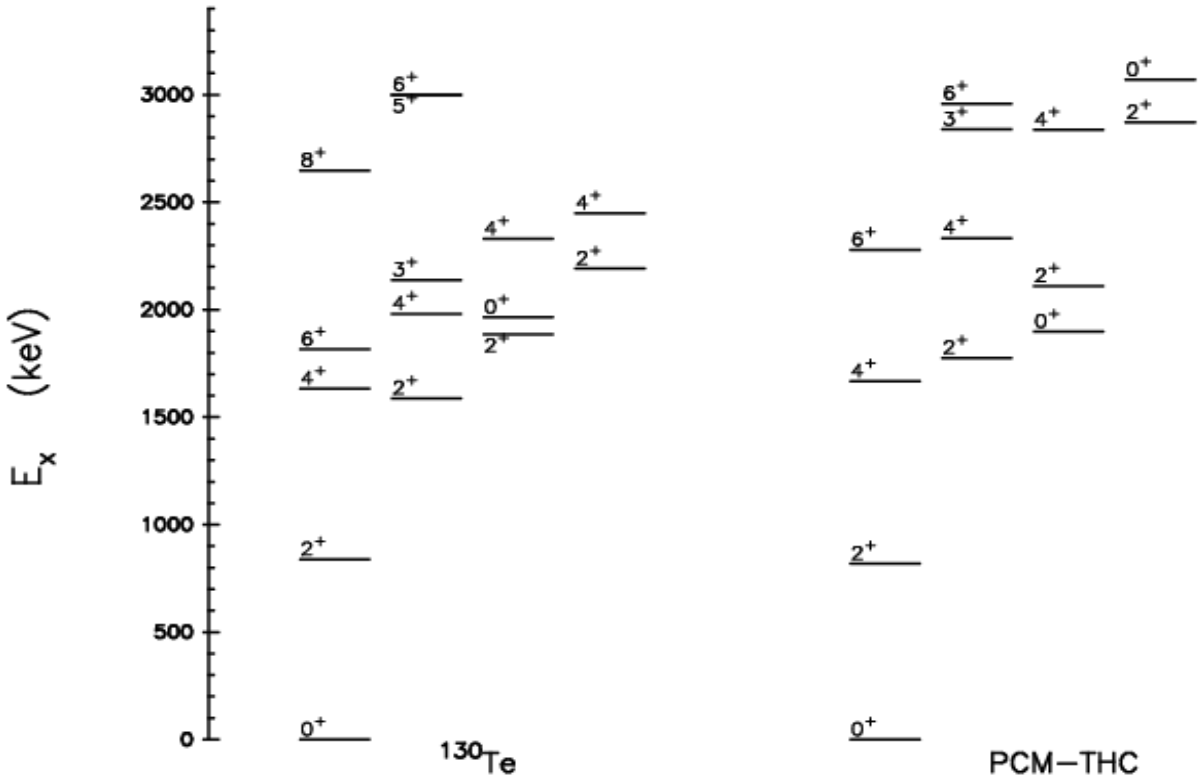

Figure 13. Comparison of the experimental ^{130}Te level scheme with our PCM calculations. Levels are arranged in columns for clarity.

Although many useful conclusions were drawn from analyzing the level energy dependences on G and ζ_2, the resulting level scheme for the chosen values does not reproduce any of the irregularities of the observed tellurium nucleus. For this reason, the PCM calculations previously done by Lopac and Warr were chosen for further evaluation of the PCM. Figure 14 illustrates the comparison between the experimentally determined level energies and the results of the model.

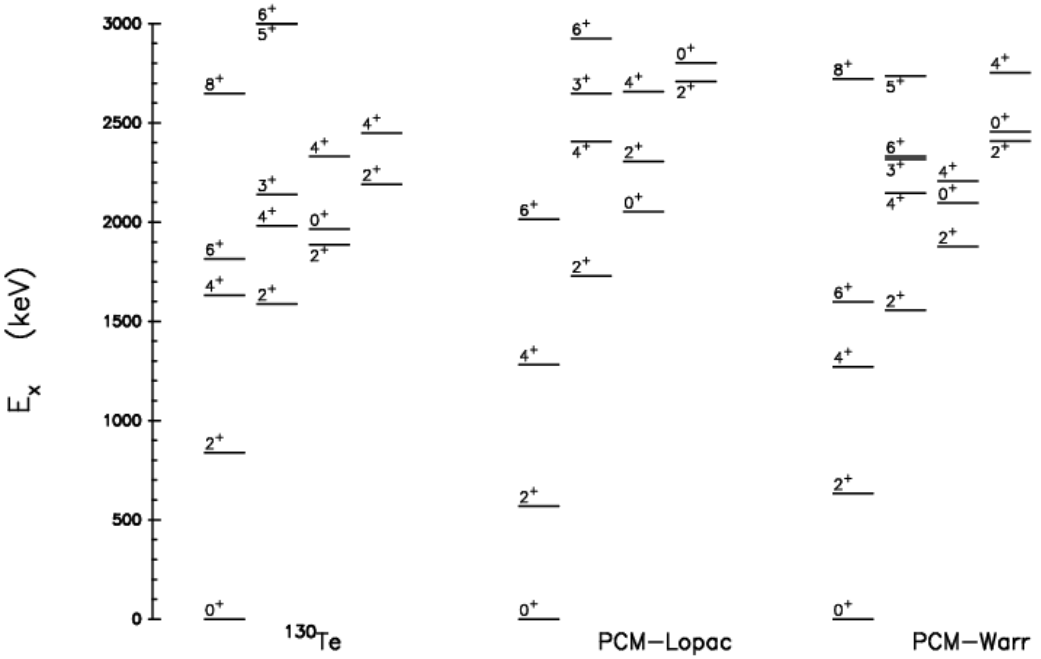

Figure 14. Comparison of the experimental ^{130}Te level scheme with the Lopac and Warr PCM calculations. Levels are arranged in columns for clarity.

The proton orbital energies in the Lopac calculation were selected to best reproduce what was known about the tellurium nuclei in the year ~1970. This calculation now has difficulty reproducing the current level sequences. The depressed 6^+ state is not reproduced. The Lopac calculation is more representative of an oscillator with a γ-deformation dependent potential (related to the C_3 term in the GCM potenial of equation [11]) [Ca02].

The proton orbital energies in the Warr calculation were based upon a regional shell model study by Kisslinger [Ki63] and the Ph.D. thesis of Wenes [We83]. The $d_{5/2}$ and $d_{3/2}$ orbital energies are significantly higher than those in the Lopac calculation. The resulting level sequence produced does a reasonable job of reproducing the ordering of states, the only major discrepancy is the elevated position of the second 2^+ state with respect to the 4_1^+. Because the PCM calculation done by Warr yielded reasonably sound results for the level scheme, it is known the PCM is sufficiently complex to model the ^{130}Te, and further evaluation regarding the accuracy of parameters is warranted. The electric quadrupole transition rates (B(E2)) are therefore compared (see Table II).

Table II. Selected transition rates in ^{130}Te. B(E2) values are given in W.u. Results are grouped according to a pure vibrational model interpretation. Entries denoted '-' are not measured. Blank entries do not apply.

Initial State	Final State	Experiment	Lopac [Lo70] Calculation	Warr [Wa98] Calculation
Single-phonon excitation				
2_1^+	0_1^+	15.1(3) a	31	28
Two-phonon excitations				
4_1^+	2_1^+	-	44	34
2_2^+	2_1^+	26.6(34)	24	35
2_2^+	0_1^+	0.016(2)	1.7	0.0015
0_2^+	2_1^+	3.9(18)	20	20
Three-phonon excitations				
6_1^+	4_1^+	7.3(25) a	35	21
4_2^+	4_1^+	13.0(38)	6.9	14
4_2^+	2_2^+	not observed	13	24
4_2^+	2_1^+	1.6(5)	4.9	7.5
3_1^+	2_1^+	0.050(2)	3.1	0.36
3_1^+	2_2^+	15.4(76)	32	17
3_1^+	4_1^+	22.7(112)	4.7	6.8
2_3^+	2_1^+	34.9(12) or 2.22(7)	0.71	3.5
2_3^+	2_2^+	-	0.78	0.0001
2_3^+	4_1^+	-	-	-
0_3^+	2_1^+	-	0.0071	0.12
0_3^+	2_1^+	-	9.7	25
Ground state decays of spin-2 states				
2_1^+	0_1^+	15.1(3)	31	28
2_2^+	0_1^+	0.016(2)	1.7	-
2_3^+	0_1^+	0.029(1)	0.20	-
2_4^+	0_1^+	0.37(3)	0.0016	-

a) Value from other experiment literature, Ref [Va01].

There does not appear to be any clear correspondence between the measured rates and predicted rates, either in absolute size or in a simple relative large-versus-small viewpoint. The actual 2_1^+, 0_2^+, and 6_1^+ states are not as collective as predicted by these two PCM parameter sets. It is difficult to make structure conclusions for the remaining levels. As an inspection of the experimental level schemes of the tellurium nuclei was expected to be dominated by a mixture of two-valence proton and anharmonic vibrational structures, more exploration with parameter sets in the PCM is warranted. One possible approach is to take orbital energies from experimental information in the underlying Sb nuclei again, this time using a different parameter set and phonon energy[Co68, Is67]. To determine particle effects to a higher degree of accuracy, it would be wise to undertake an independent-particle model calculation. Such a calculation was not started for this research, nor has it been attempted by more experienced shell-model theorists.

V. SUMMARY

Nuclear structure research is not a trivial process. It requires much time and effort devoted to planning, experimentation, and analysis. The excited states of tellurium-130 have been identified from gamma-ray spectra which were measured following inelastic neutron scattering. Data were collected in the summer of 2002 at the University of Kentucky using the particle accelerator and data acquisition system there. Excitation function data were collected in June and angular distribution data were collected in August. The data have been analyzed, and the level scheme has been generated. Over half (approximately 52%) of the levels were previously undiscovered. Level and transition properties, such as lifetimes, spins, mixing ratios, branching ratios were determined. Transition rates were also calculated. Model calculations were performed using the Particle-Core Coupling Model and the General Collective Model. Comparisons were made between the experimental results and new and previously existing model calculations. The GCM was unable to reproduce the nuclear structure behavior exhibited in tellurium-130. A previously existing PCM calculation was found to reproduce the level scheme, but the agreement with transition rate data is lacking. As the experimental level scheme suggests that the structure is dominated by a mixture of two-valence proton and anharmonic vibrational structures, a more thorough exploration with new parameter sets in the PCM is warranted. It also appears that more particle-like structure is active in several levels of tellurium-130 than was previously thought. An independent particle shell model calculation would be the best method to develop a better understanding of the nuclear structure.

REFERENCES

[Be94] T. Belgya, B. Fazekas, G. Molnar, R. A. Gatenby, E. L. Johnson, E. M. Baum, D. Wang, D. P. DiPriete, and S. W. Yates, in *Proceedings of the 8th International Symposium on Capture Gamma-Ray Spectroscopy and Related Topics*, Fribourg, Switzerland, 1993, edited by J. Kern (World Scientific, Singapore, 1994), p. 878.

[BNL02] Tellurium databases maintained at the National Nuclear Data Center, www.nndc.bnl.gov, January 2002.

[BNL03] Internal conversion coefficient calculations available at the National Nuclear Data Center, www.nndc.bnl.gov, January 2003.

[Ca02] M.A.Caprio, R.F.Casten, and J.Jolie, Phys. Rev. C **65**, 034304 (2002).

[Ch97a] B. Champine, et al., "Nuclear Structure of the Tellurium-128 and –130 Nuclei.", Capstone paper USNA Dept Physics 1997 [unpublished].

[Ch97b] B.Champine, P.Burkett, C.Davoren, S.Etzkorn, W.Faulkner, B.Meehan, and M.Skubis, "Nuclear Structure of the Stable Tellurium Isotopes." Proceedings: Eleventh National Conference on Undergraduate Research **11**, 1531 (1997).

[Co] C.Collard, G. Alexander, and S. F. Hicks. private communication.

[Co68] M. Conjeaud, S.Harar, and Y. Cassagnou, Nucl. Phys. **A 117**, 449 (1968).

[Et97] S.J. Etzkorn, S. J. "Decay Properties and Lifetimes of States in ^{124}Te from (n,n'γ)." Thesis, U. of Dallas, 1997.

[Fi98] R.B. Firestone Table of Isotopes 8th Ed. New York: J. Wiley and Sons, 1998.

[Gn69] G. Gneuss, U. Mosel, W. Greiner, Phys. Lett. **30B** 397 (1969).

[Gn71] G. Gneuss, W. Greiner, Nucl Phys. **171** 449 (1971).

[He67] K. Heyde and P. J. Brussard, Nucl. Phys. **A 104**, 81 (1967).

[He94] K. Heyde, Basic Ideas and Concepts in Nuclear Physics, Philadelphia: Institute of Physics, 1994.

[Is67] T. Ishimatsu, K.Yagi, H.Ohmura, T.Nakajima, and H.Orihara, Nucl. Phys. **A 104**, 481 (1967).

[Ki63] L.S. Kisslinger and R.A.Sorensen, Rev. Mod. Phys. **35**, 835 (1963).

[Ki02] K.Kitao, Y.Tendow, and A.Hashizume, Nuclear Data Sheets **96**, 241 (2002).

[Kr88] K.S. Krane, Introduction to Nuclear Physics, New York: J.Wiley & Sons, 1988.

[Li01] J. Lilley, Nuclear Physics: Principles and Applications, New York: J.Wiley & Sons, 2001.

[Lo70] V. Lopac, Nucl. Phys. **A 155**, 513 (1970).

[Ph76] G.W. Phillips and K. W. Marlow, "Program HYPERMET for automatic analysis of gamma-ray spectra from germanium detectors", Nucl. Instrum. Methods **137**, 525 (1976).

[Sh66] E. Sheldon, and D. M. van Patter, Rev. Mod. Phys. **38**, 143 (1966).

[Ta99] J.A.Tanyi, J.R.Vanhoy, S.F. Hicks, M.C.Burns, N.Warr, S.W.Yates, "Level Scheme of ^{126}Te Using Inelastic Scattering from (n, n' γ) Reaction Studies", Capstone paper USNA Dept Physics 1999 [unpublished].

[Ta01] J.A.Tanyi, T.Churchill, K.A.Crandell, J.R.Vanhoy, M.C.Burns, P.A.Roddy, S.F.Hicks, Z.Ammar, T.B.Brown, M.Merrick, N.Warr, S.W.Yates, In *Proceedings: Eleventh National Conference on Undergraduate Research 2001*, Edited by R.D. Yearout, Asheville: Univ North Carolina at Asheville Press, (in press, Fall 2001).

[Tr91] Troltenier, D., J. A. Maruhn, and P. O. Hess, "Numerical Applications of the Generalized Collective Model." *Computational Nuclear Physics 1: Nuclear Structure*. Ed. K. Langanke, J. A. Maruhn, and S. E. Koonin, Berlin: Springer-Verlag, p.105 (1991).

[UF96] FITPIC spectra fitting program version 5.1-8, University of Fribourg Nuclear Structure Group, Fribourg, Switzerland, 1996.

[Va97] J.R. Vanhoy, "Nuclear Structure Trends in N=84 and Z=52", In "Workshop on Nuclear Physics with GEANIE at LANSCE" ,Ed. J.Becker and D.Strottman, LANL Rpt LA-UR-97-3743, p.65 (1997).

[Va01] J.R.Vanhoy, S.F.Hicks, N.Warr, G.K.Alexander, C.A.Aubin, P.G.Burkett, M.C.Burns, B.R.Champine, R.T.Coleman, C.J.Collard, F.Corminboeuf, K.A.Crandell, S.J.Etzkorn, P.E.Garrett, L.Genilloud, J.Jolie, J.Kern, J.L.Shenker, B.K.Sklaney, J.A.Tanyi , M.M.Walbrun, M.Yeh, Heavy Ion Physics **12**, 287 (2001).

[Va02] J.R.Vanhoy, R.T. Coleman, K.A.Crandell, S.F.Hicks, B.K.Sklaney, M.M.Walbrun, N.Warr, P.E.Garrett, S.W.Yates, J.Jolie, F.Corminboeuf, L.Genilloud, J.Kern, J.L.Schenker, submitted to Phys. Rev. C (Apr '03).

[Wa88] PKS Neutron Time of Flight Peak Fitting Program, IBM370 version, modified by: D. Wang, UK; J.R.Vanhoy, USNA, 1988.

[Wa98] N.Warr, S.Drissi, P.E.Garrett, J.Jolie, J. Kern, H.Lehmann, S.J. Mannanal, and J.-P.Vorlet, Nucl. Phys. **A 636**, 379 (1998).

[We83] G. Wenes, Ph.D. Thesis, Laboratorium voor Kernfysica, Rijksuniveriteit Gent (1983).

[Wi75] K.B. Winterbon, Nucl. Phys. **A 246** 293 (1975).

[Za97] V.Zamfir, "The Geometric Collective Model Revisited", In "Workshop on Nuclear Physics with GEANIE at LANSCE" ,Ed. J.Becker and D.Strottman, LANL Rpt LA-UR-97-3743, p.70 (1997).

APPENDICES

Appendix A: Excitation Functions

The excitation functions are plotted as well as the plot of gamma ray energy versus incident neutron energy. The vertical bars on each point represent the error for the individual point, while the horizonal bars in the energy plot represent the error for the whole set.

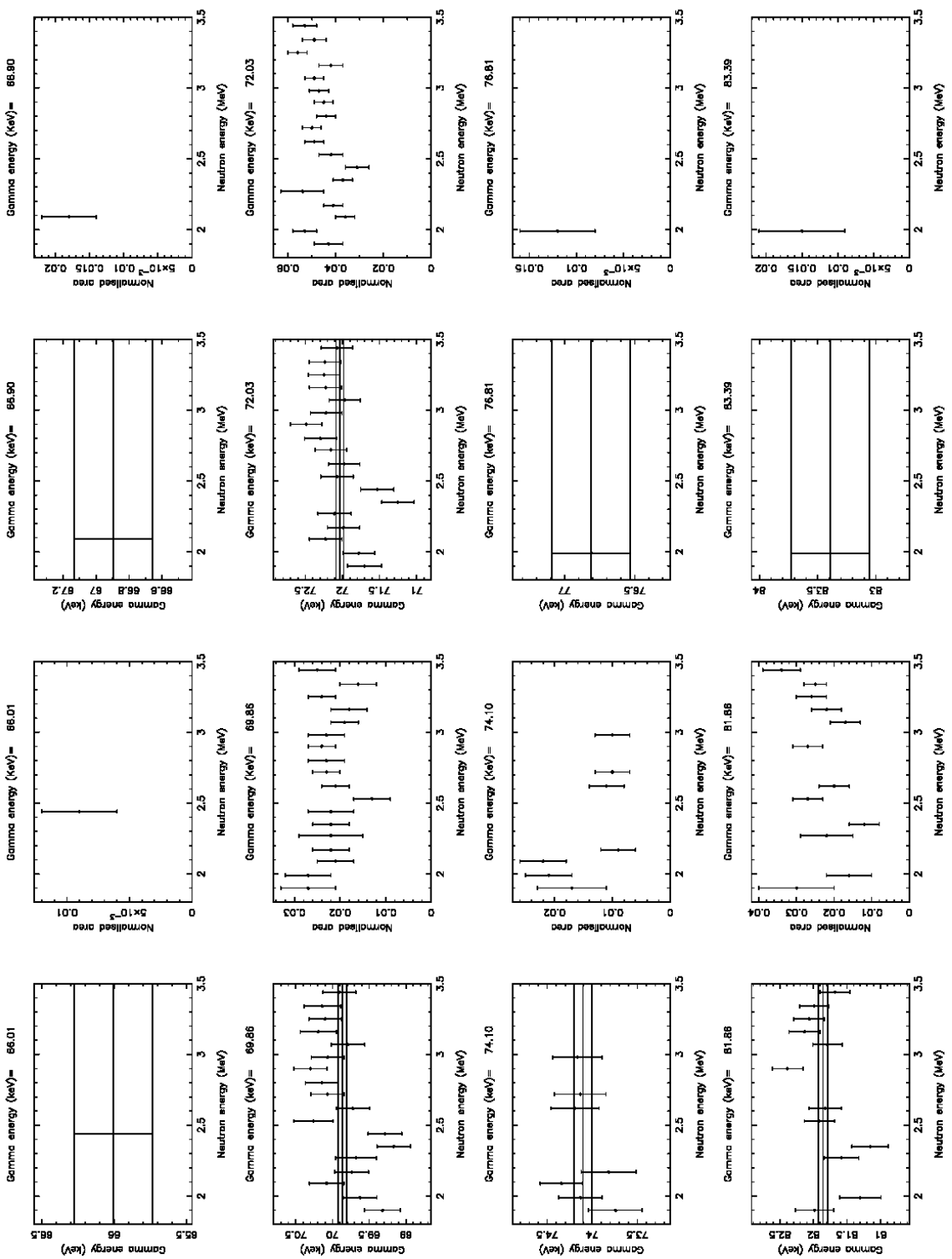
Gamma energy (keV)= 66.01
Gamma energy (keV)= 69.86
Gamma energy (keV)= 74.10
Gamma energy (keV)= 81.88
Gamma energy (keV)= 66.90
Gamma energy (keV)= 72.03
Gamma energy (keV)= 76.81
Gamma energy (keV)= 83.39
Gamma energy (keV)= 66.90
Gamma energy (keV)= 72.03
Gamma energy (keV)= 76.81
Gamma energy (keV)= 83.39
Neutron energy (MeV)
Normalised area
Gamma energy (keV)

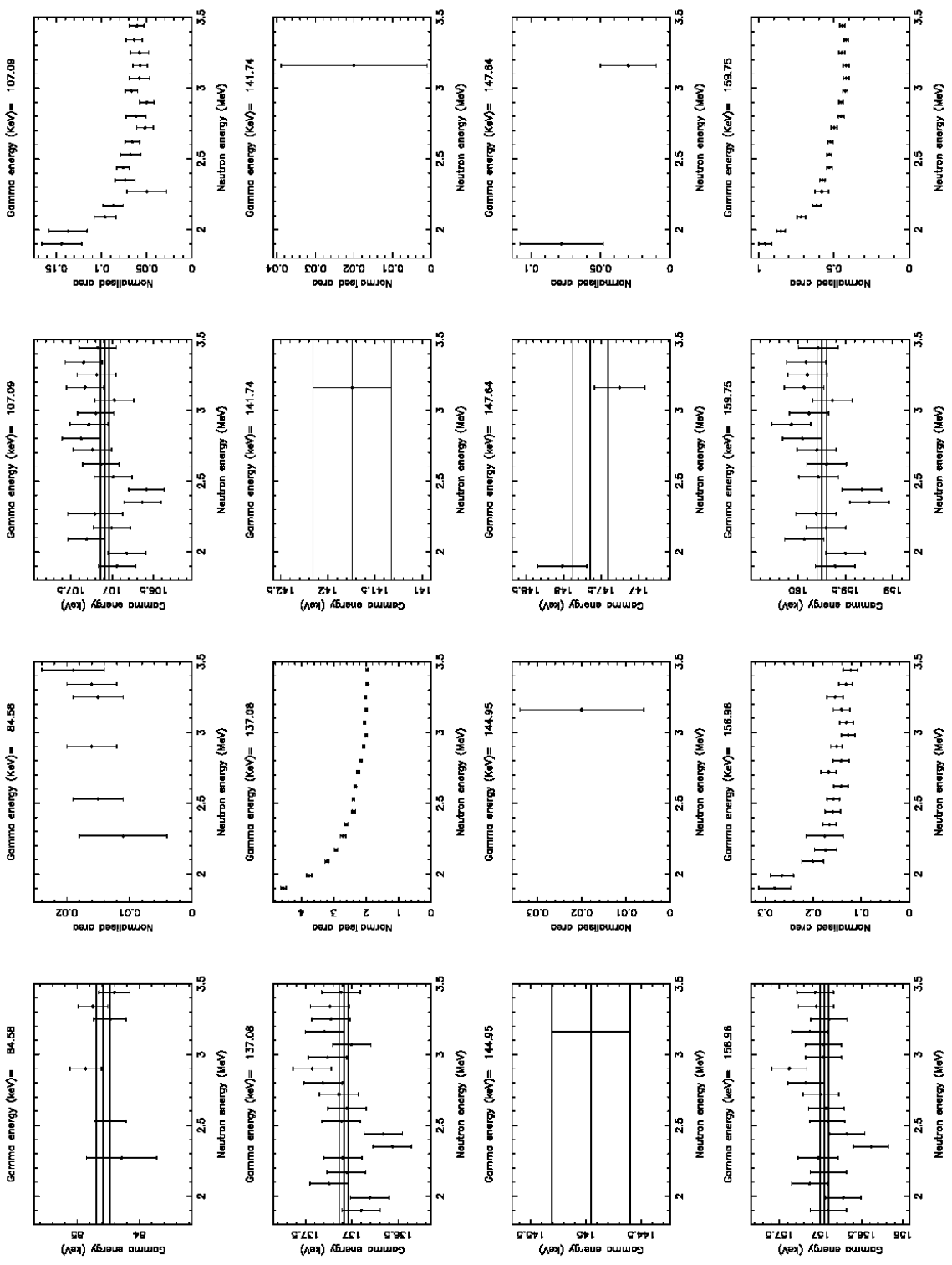
Gamma energy (keV)= 84.58
Gamma energy (keV)= 137.08
Gamma energy (keV)= 144.95
Gamma energy (keV)= 156.96
Gamma energy (keV)= 107.09
Gamma energy (keV)= 141.74
Gamma energy (keV)= 147.64
Gamma energy (keV)= 159.75
Gamma energy (keV)= 107.09
Gamma energy (keV)= 141.74
Gamma energy (keV)= 147.64
Gamma energy (keV)= 159.75
Gamma energy (keV)= 84.58
Gamma energy (keV)= 137.08
Gamma energy (keV)= 144.95
Gamma energy (keV)= 156.96
Neutron energy (MeV)
Normalised area
Gamma energy (keV)

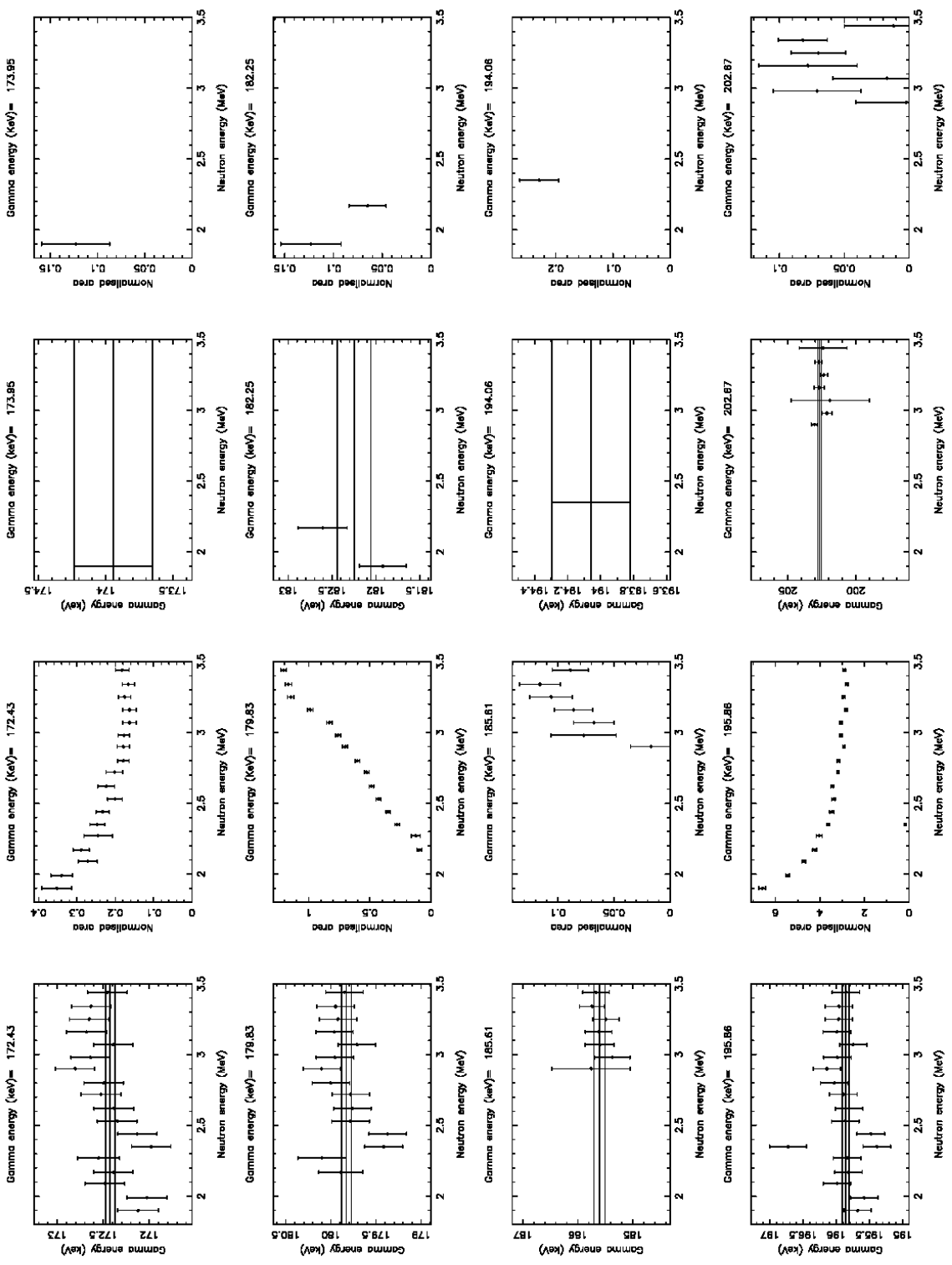
Gamma energy (keV)= 172.43
Gamma energy (keV)= 179.83
Gamma energy (keV)= 185.61
Gamma energy (keV)= 195.86
Gamma energy (keV)= 173.85
Gamma energy (keV)= 182.25
Gamma energy (keV)= 194.06
Gamma energy (keV)= 202.87
Gamma energy (keV)= 173.95
Gamma energy (keV)= 182.25
Gamma energy (keV)= 194.06
Gamma energy (keV)= 202.87
Neutron energy (MeV)
Normalized area
Gamma energy (keV)

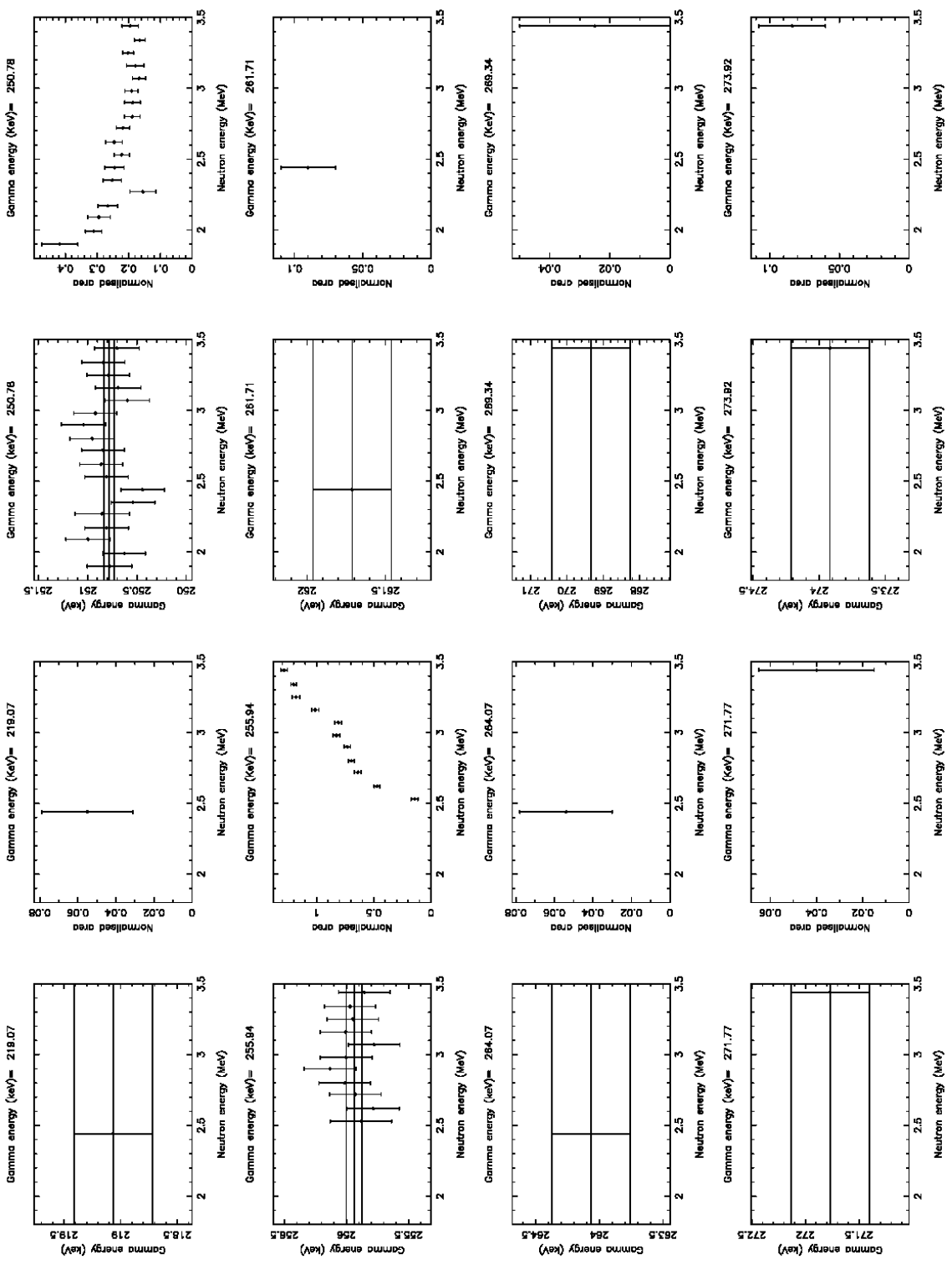
Gamma energy (keV)= 218.07
Gamma energy (keV)= 219.07
Gamma energy (keV)= 250.78
Gamma energy (keV)= 255.94
Gamma energy (keV)= 261.71
Gamma energy (keV)= 264.07
Gamma energy (keV)= 269.34
Gamma energy (keV)= 271.77
Gamma energy (keV)= 273.92
Neutron energy (MeV)
Normalised area
Gamma energy (keV)

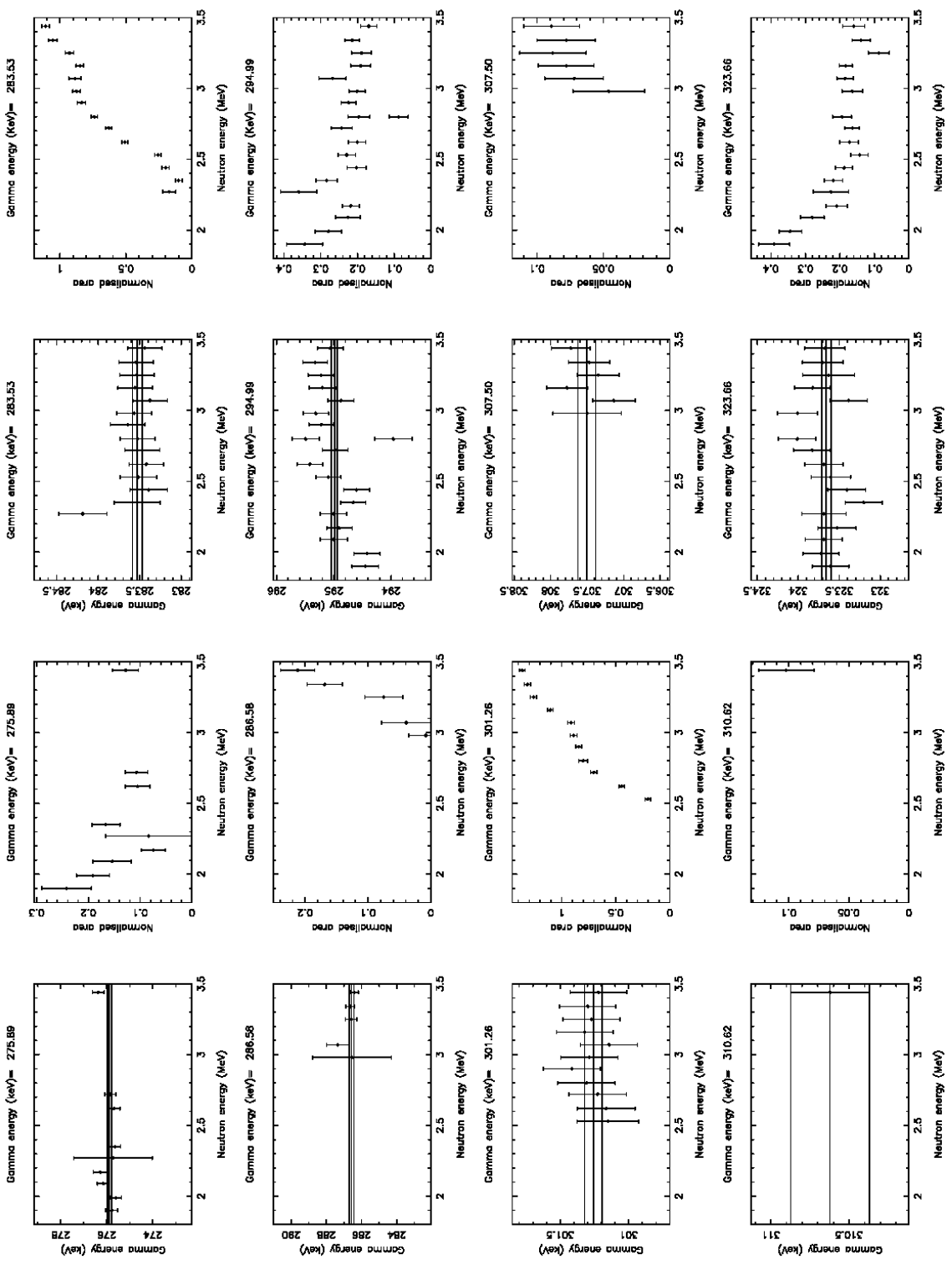
Gamma energy (kev)= 275.89
Gamma energy (kev)= 286.58
Gamma energy (kev)= 301.26
Gamma energy (kev)= 310.62
Gamma energy (kev)= 283.53
Gamma energy (kev)= 294.99
Gamma energy (kev)= 307.50
Gamma energy (kev)= 323.66
Gamma energy (KeV)= 283.53
Gamma energy (KeV)= 294.99
Gamma energy (KeV)= 307.50
Gamma energy (KeV)= 323.66
Gamma energy (kev)
Normalised area
Neutron energy (MeV)

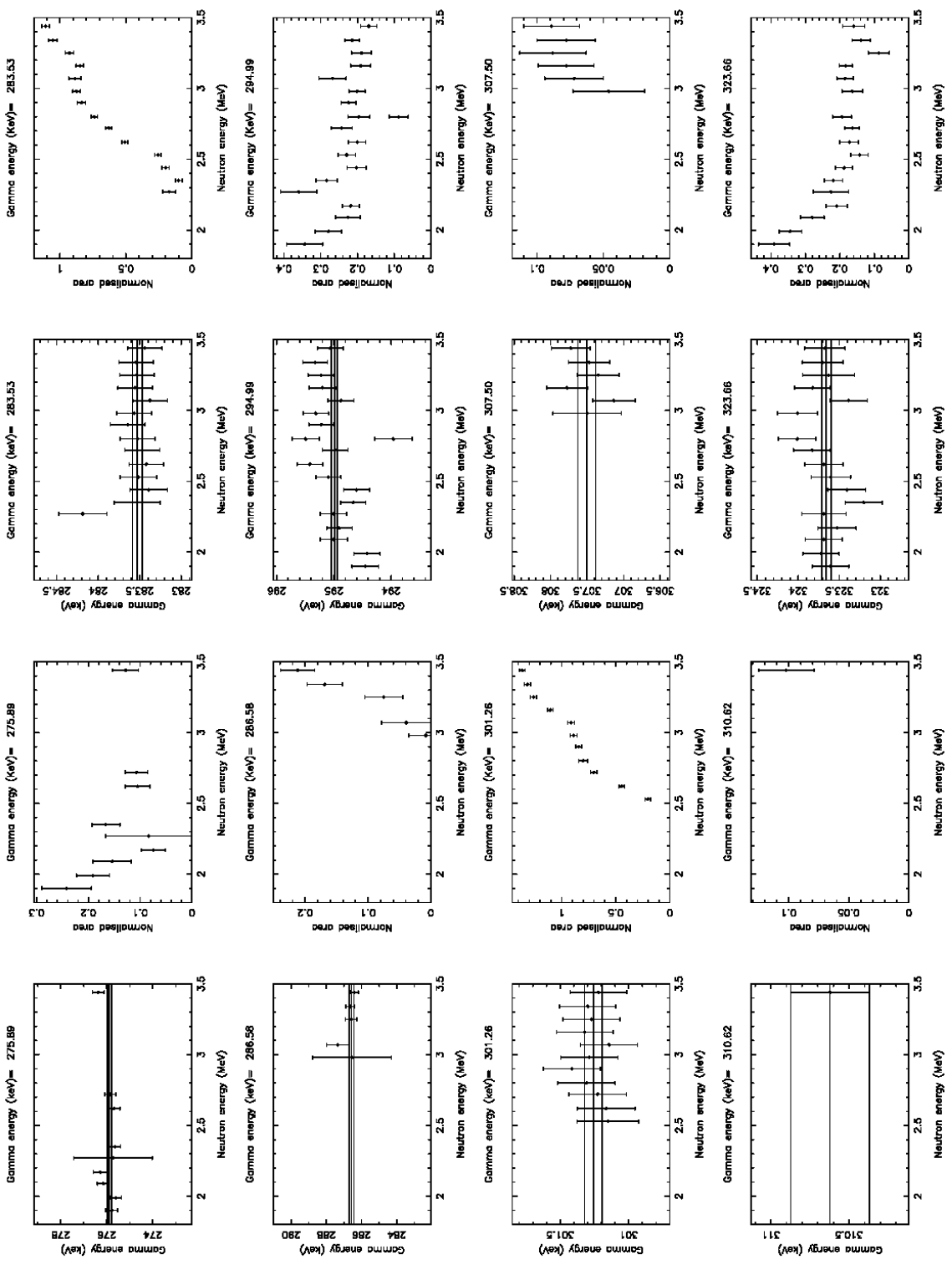
Gamma energy (KeV)= 283.53
Normalised area
Neutron energy (MeV)
Gamma energy (KeV)= 294.99
Normalised area
Neutron energy (MeV)
Gamma energy (KeV)= 307.50
Normalised area
Neutron energy (MeV)
Gamma energy (KeV)= 323.66
Normalised area
Neutron energy (MeV)
Gamma energy (kev)= 283.53
Gamma energy (kev)
Neutron energy (MeV)
Gamma energy (kev)= 294.99
Gamma energy (kev)
Neutron energy (MeV)
Gamma energy (kev)= 307.50
Gamma energy (kev)
Neutron energy (MeV)
Gamma energy (kev)= 323.66
Gamma energy (kev)
Neutron energy (MeV)
Gamma energy (KeV)= 275.89
Normalised area
Neutron energy (MeV)
Gamma energy (KeV)= 286.58
Normalised area
Neutron energy (MeV)
Gamma energy (KeV)= 301.26
Normalised area
Neutron energy (MeV)
Gamma energy (KeV)= 310.62
Normalised area
Neutron energy (MeV)
Gamma energy (kev)= 275.89
Gamma energy (kev)
Neutron energy (MeV)
Gamma energy (kev)= 286.58
Gamma energy (kev)
Neutron energy (MeV)
Gamma energy (kev)= 301.26
Gamma energy (kev)
Neutron energy (MeV)
Gamma energy (kev)= 310.62
Gamma energy (kev)
Neutron energy (MeV)

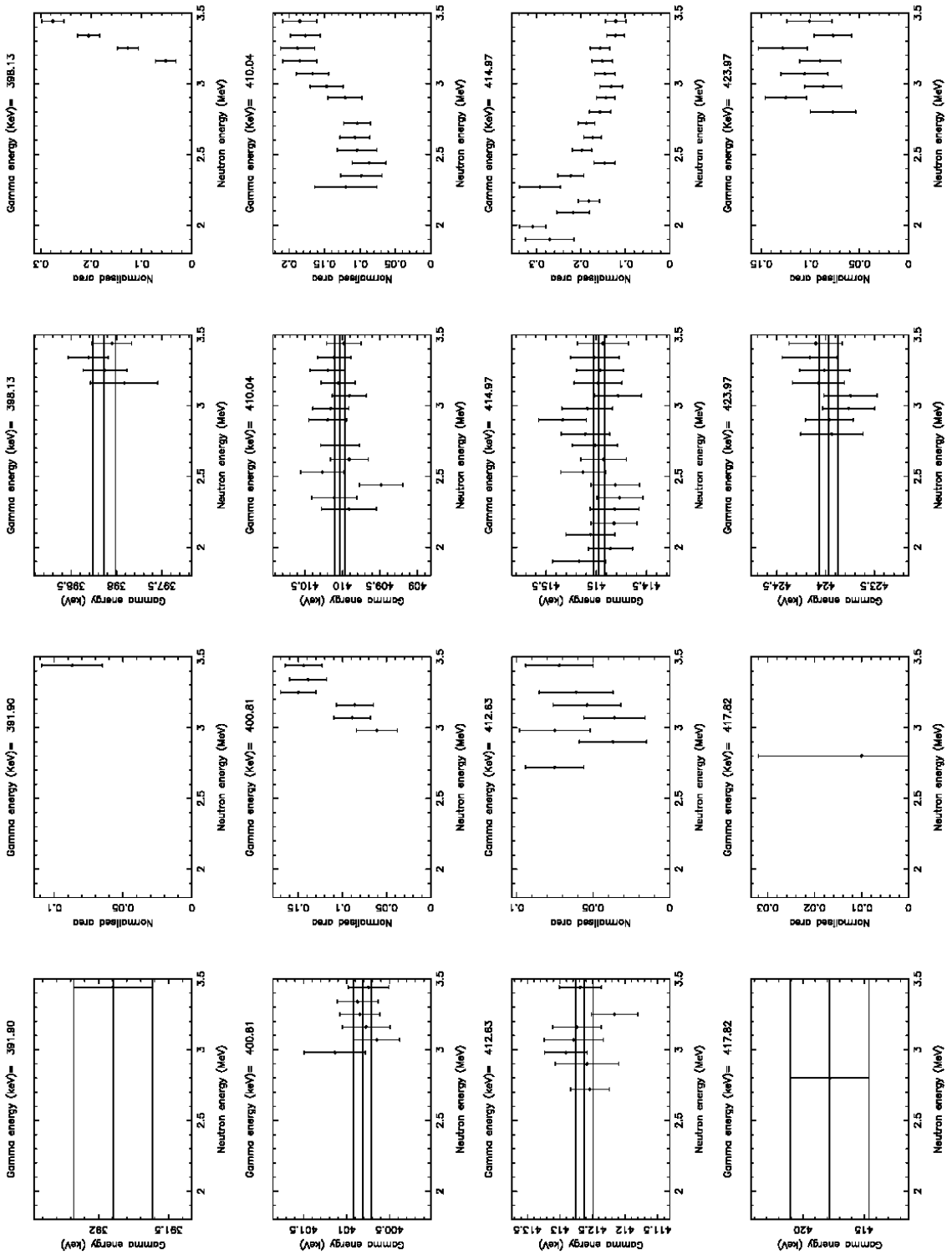
Gamma energy (keV)= 391.90
Gamma energy (keV)= 400.81
Gamma energy (keV)= 412.63
Gamma energy (keV)= 417.82
Gamma energy (keV)= 388.13
Gamma energy (keV)= 410.04
Gamma energy (keV)= 414.97
Gamma energy (keV)= 423.97
Gamma energy (keV)= 398.13
Gamma energy (keV)= 414.87
Neutron energy (MeV)
Normalized area
Gamma energy (keV)

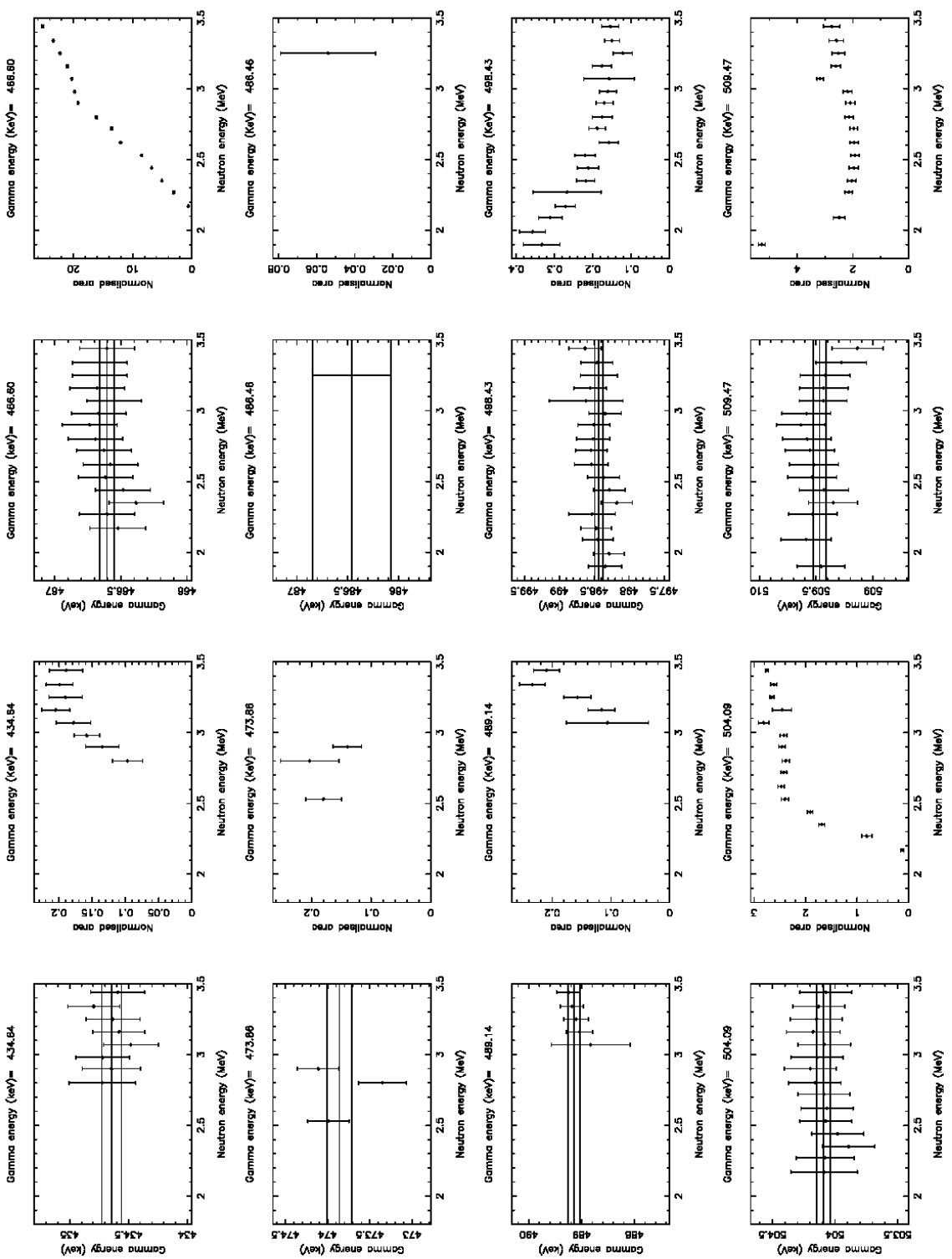
Gamma energy (keV)= 434.64
Gamma energy (keV)= 473.86
Gamma energy (keV)= 489.14
Gamma energy (keV)= 504.09
Gamma energy (keV)= 466.60
Gamma energy (keV)= 486.46
Gamma energy (keV)= 498.43
Gamma energy (keV)= 509.47
Gamma energy (keV)= 466.60
Gamma energy (keV)= 486.46
Gamma energy (keV)= 498.43
Gamma energy (keV)= 509.47
Neutron energy (MeV)
Normalised area
Gamma energy (keV)

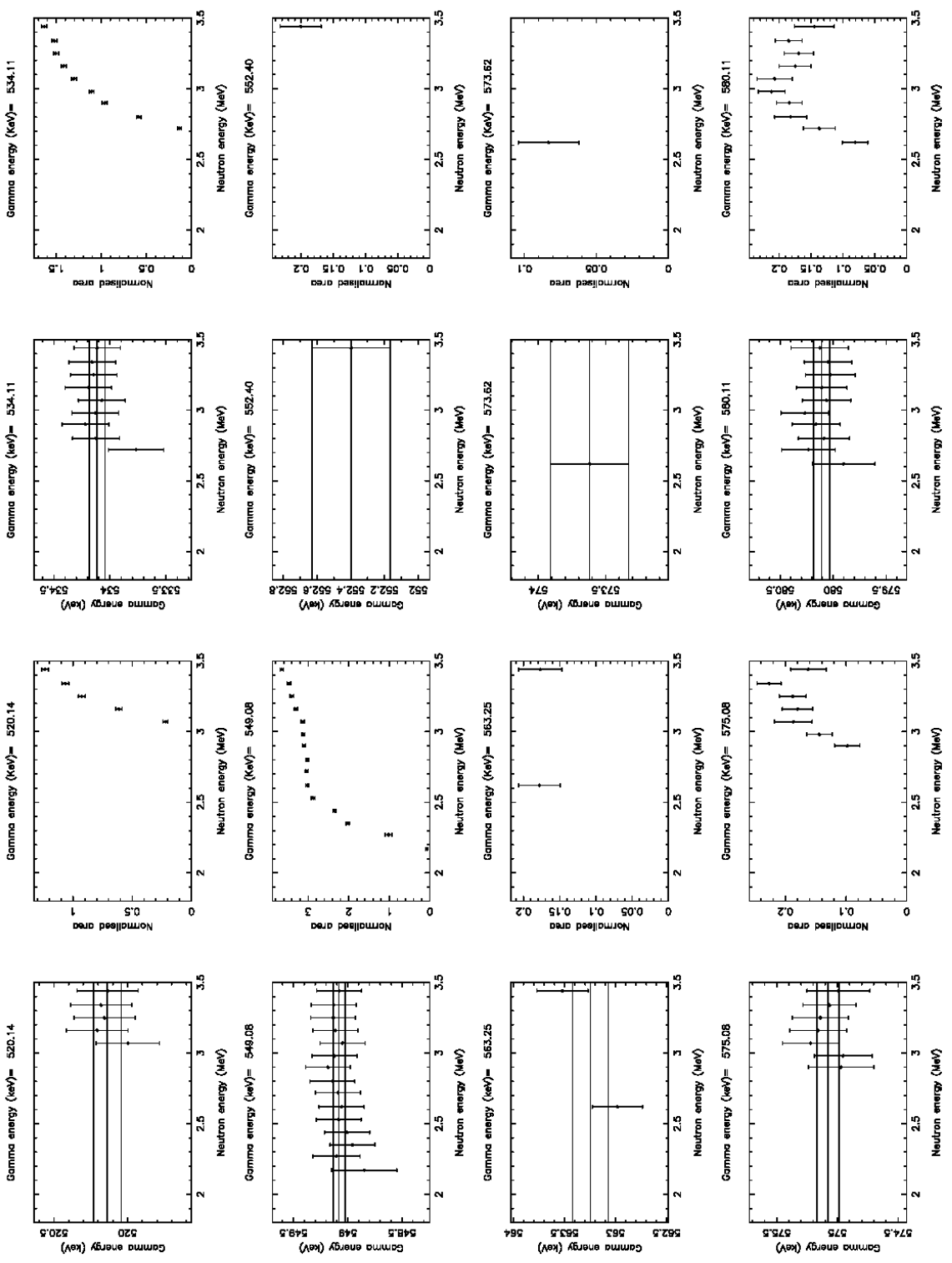
Gamma energy (kev)= 520.14
Gamma energy (KeV)= 520.14
Gamma energy (kev)= 549.08
Gamma energy (KeV)= 549.08
Gamma energy (kev)= 563.25
Gamma energy (KeV)= 563.25
Gamma energy (kev)= 575.08
Gamma energy (KeV)= 575.08
Gamma energy (kev)= 534.11
Gamma energy (KeV)= 534.11
Gamma energy (kev)= 552.40
Gamma energy (KeV)= 552.40
Gamma energy (kev)= 573.62
Gamma energy (KeV)= 573.62
Gamma energy (kev)= 580.11
Gamma energy (KeV)= 580.11
Neutron energy (MeV)
Normalised area
Gamma energy (keV)

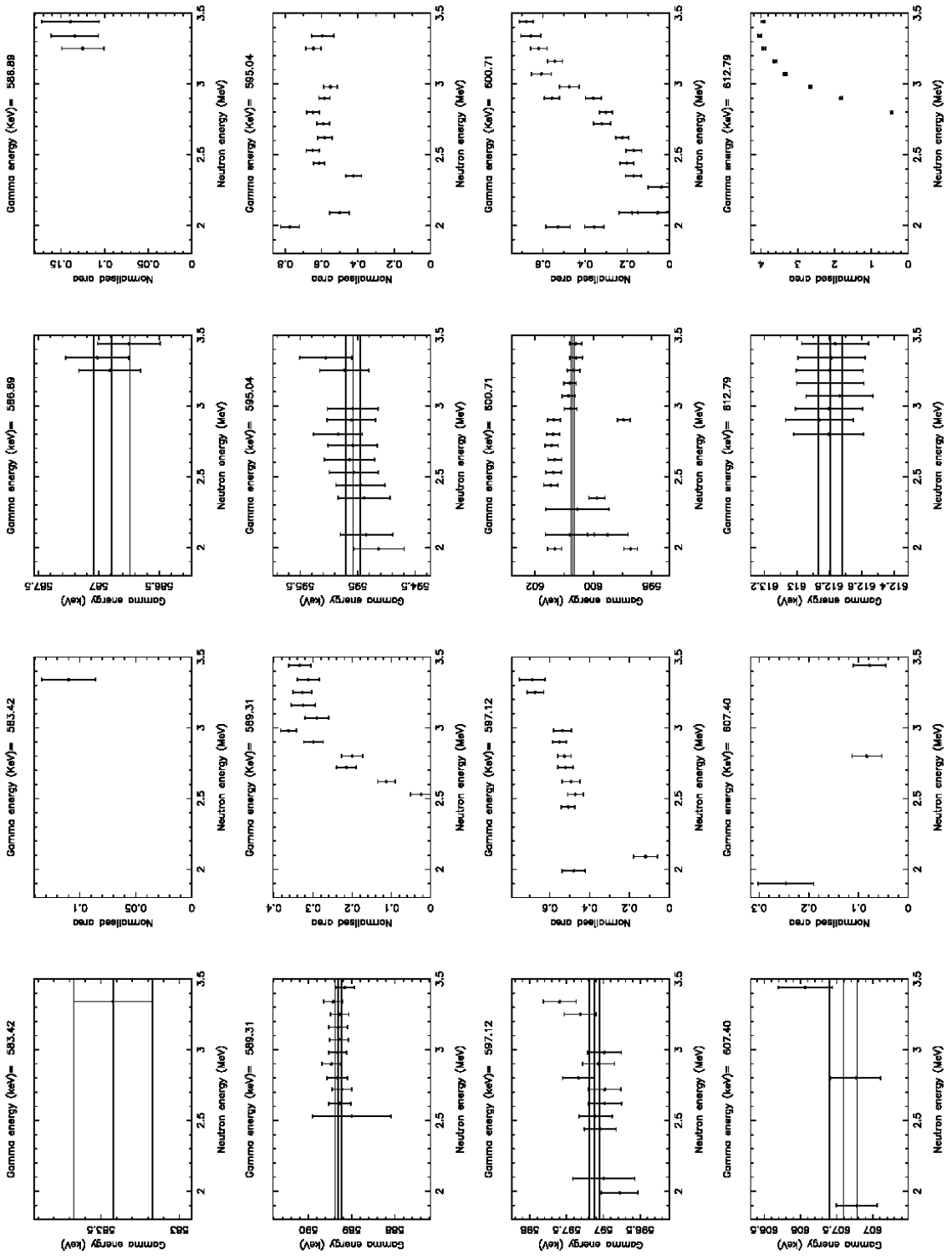
Gamma energy (keV)= 583.42
Gamma energy (keV)= 589.31
Gamma energy (keV)= 597.12
Gamma energy (keV)= 607.40
Gamma energy (keV)= 586.89
Gamma energy (keV)= 595.04
Gamma energy (keV)= 600.71
Gamma energy (keV)= 612.79
Gamma energy (keV)= 586.89
Gamma energy (keV)= 595.04
Gamma energy (keV)= 600.71
Gamma energy (keV)= 612.79
Neutron energy (MeV)
Normalised area
Gamma energy (keV)

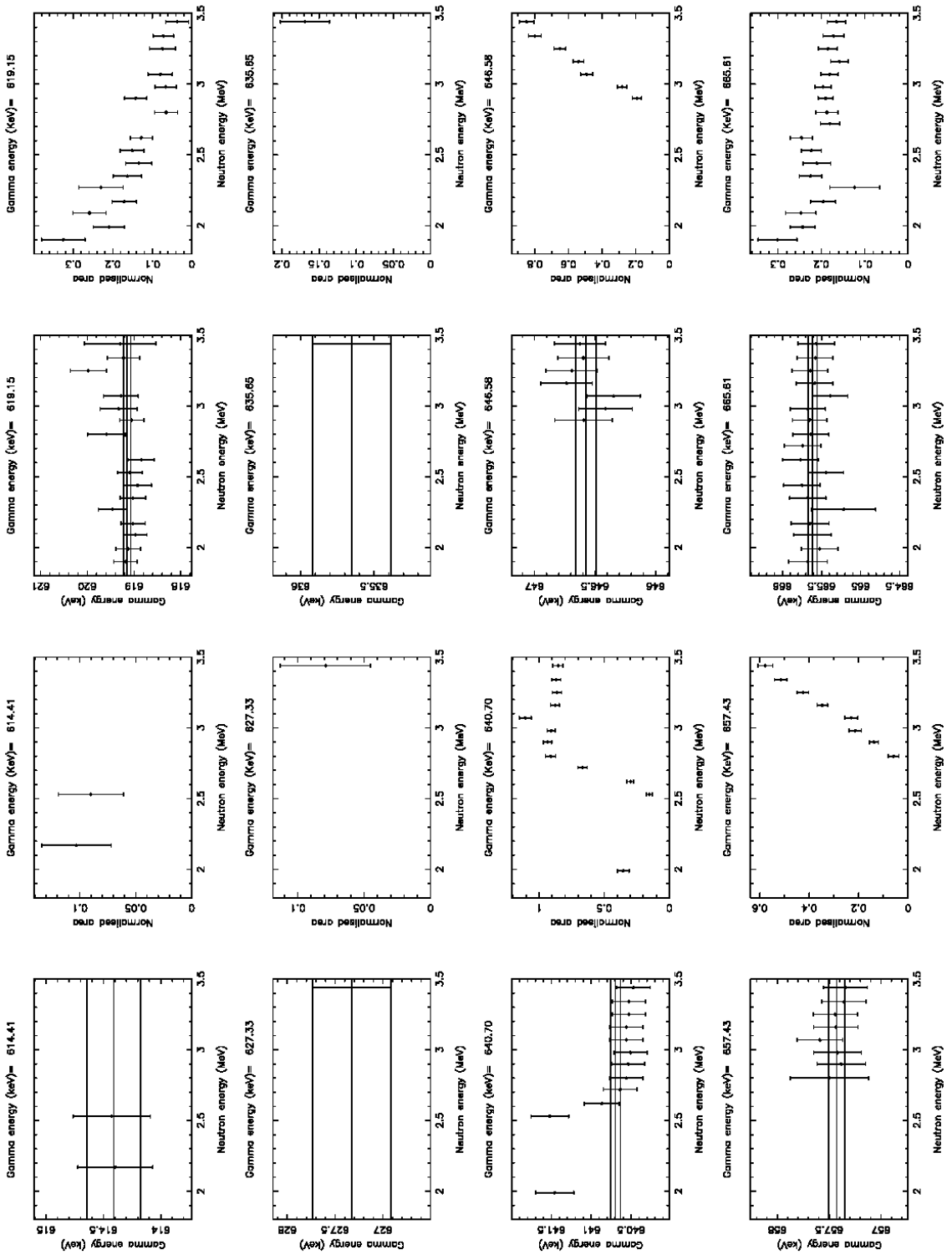
Gamma energy (keV)= 614.41
Gamma energy (keV)= 618.15
Gamma energy (keV)= 619.15
Gamma energy (keV)= 627.33
Gamma energy (keV)= 635.65
Gamma energy (keV)= 835.85
Gamma energy (keV)= 640.70
Gamma energy (keV)= 646.58
Gamma energy (keV)= 646.58
Gamma energy (keV)= 657.43
Gamma energy (keV)= 665.61
Gamma energy (keV)= 665.61
Normalised area
Neutron energy (MeV)
Gamma energy (keV)

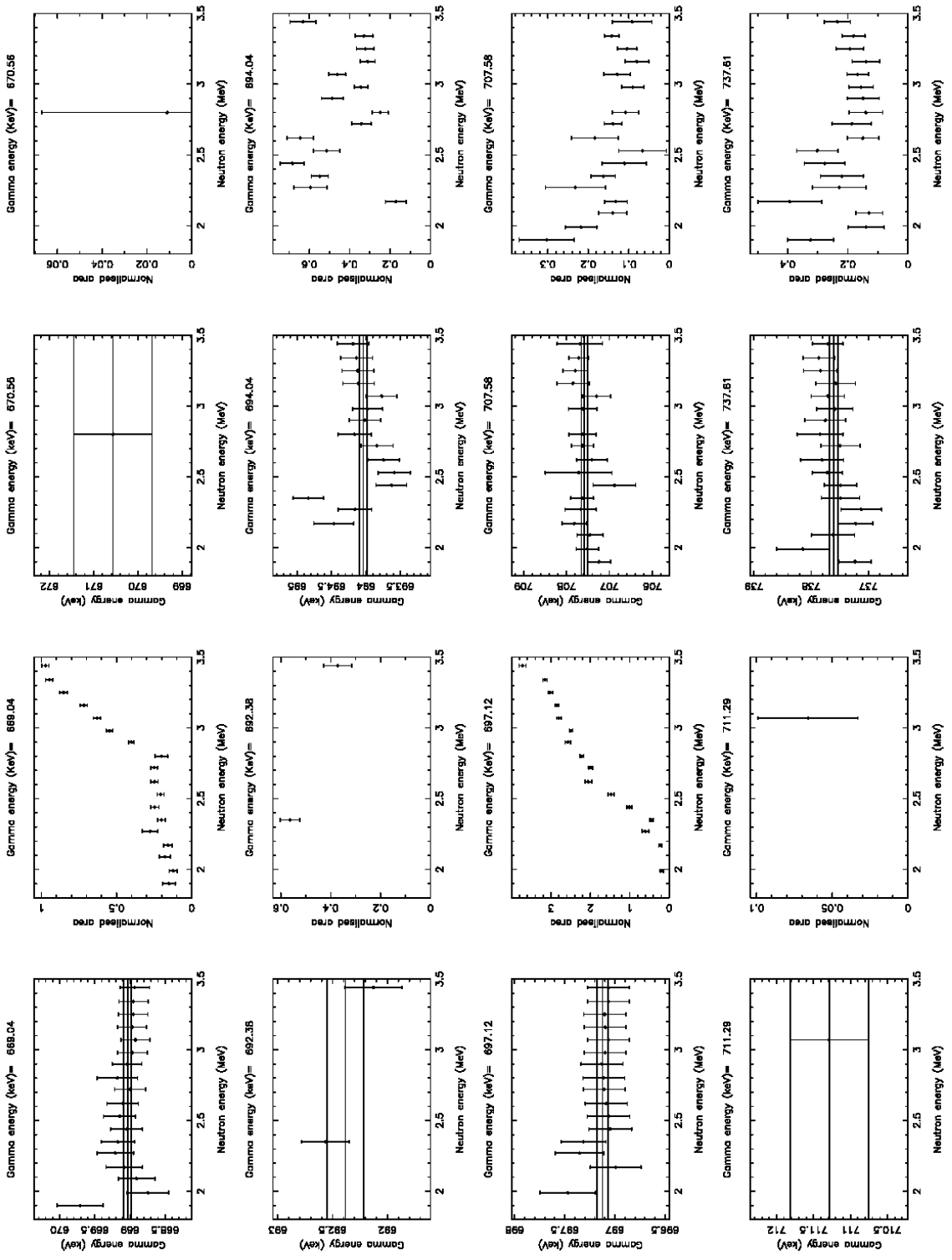
Gamma energy (keV)= 668.04
Gamma energy (keV)= 692.38
Gamma energy (keV)= 697.12
Gamma energy (keV)= 711.29
Gamma energy (keV)= 670.55
Gamma energy (keV)= 694.04
Gamma energy (keV)= 707.58
Gamma energy (keV)= 737.61
Gamma energy (keV)= 670.56
Gamma energy (keV)= 694.04
Gamma energy (keV)= 707.58
Gamma energy (keV)= 737.61
Neutron energy (MeV)
Normalised area
Gamma energy (keV)

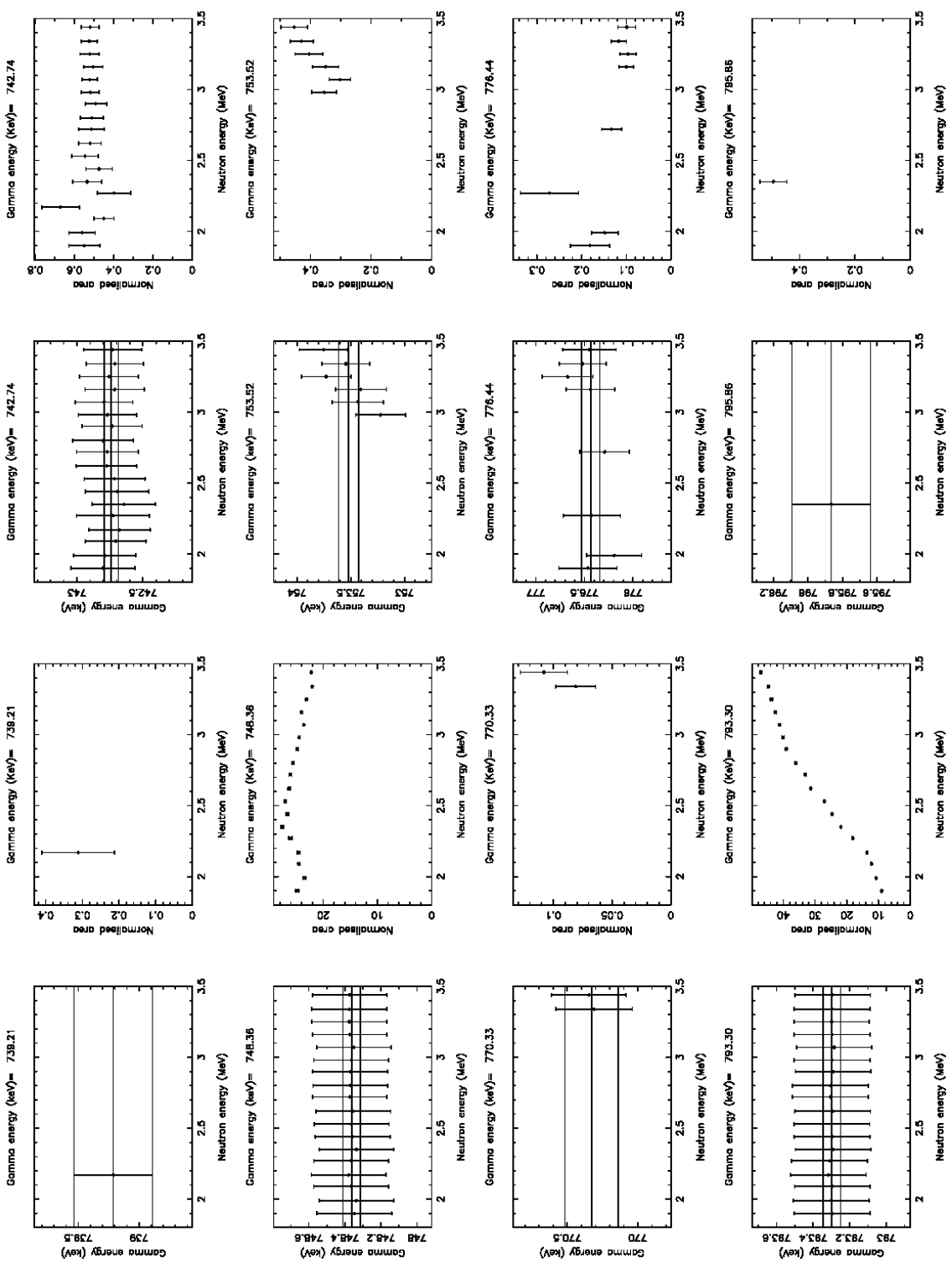
Gamma energy (keV)= 738.21
Gamma energy (keV)= 748.36
Gamma energy (keV)= 770.33
Gamma energy (keV)= 783.30
Gamma energy (keV)= 742.74
Gamma energy (keV)= 753.52
Gamma energy (keV)= 776.44
Gamma energy (keV)= 795.86
Neutron energy (MeV)
Normalized area
Gamma energy (keV)

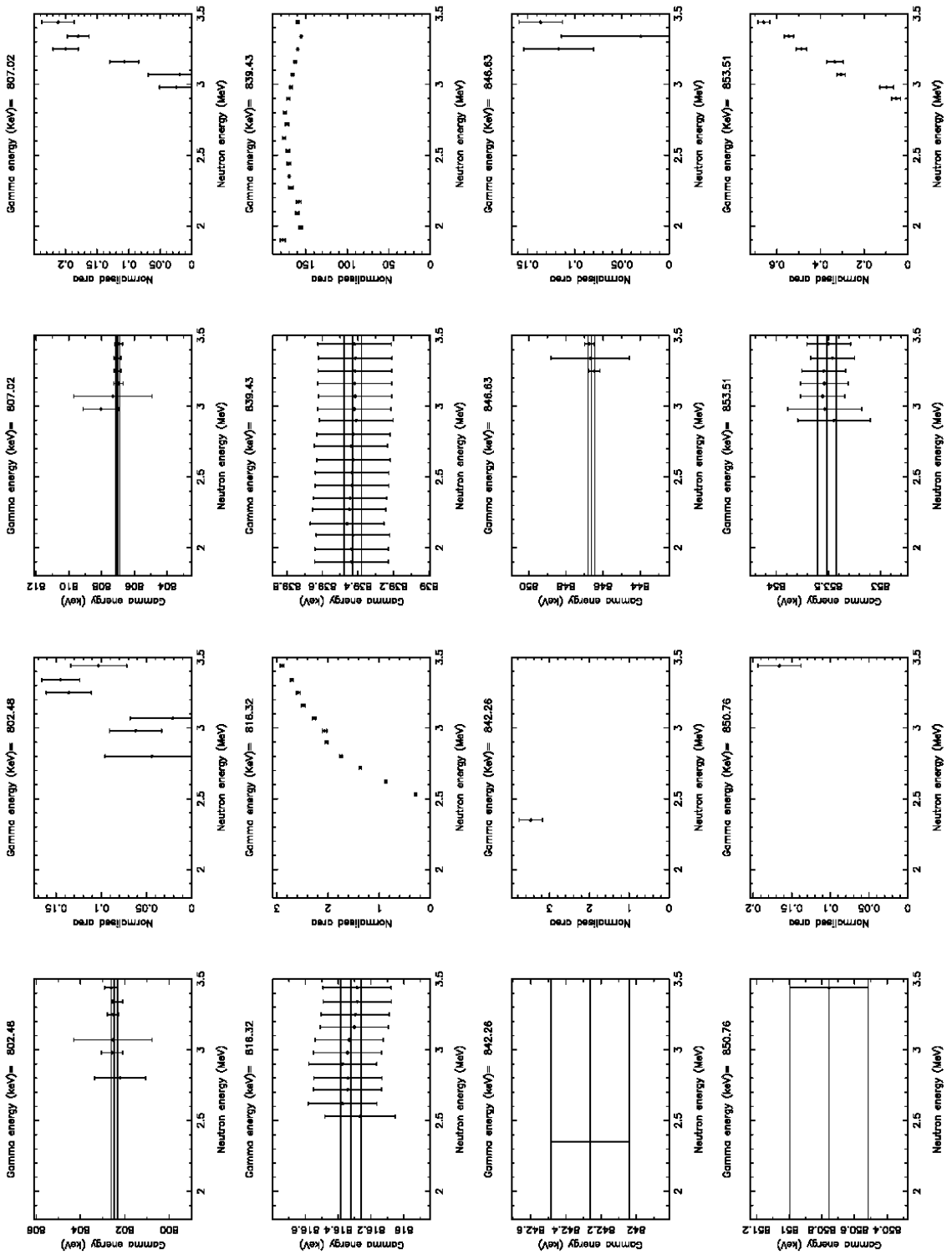
Gamma energy (keV)= 802.48
Gamma energy (keV)= 816.32
Gamma energy (keV)= 842.26
Gamma energy (keV)= 850.76
Gamma energy (keV)= 802.48
Gamma energy (keV)= 816.32
Gamma energy (keV)= 842.26
Gamma energy (keV)= 850.76
Gamma energy (keV)= 807.02
Gamma energy (keV)= 839.43
Gamma energy (keV)= 846.63
Gamma energy (keV)= 853.51
Gamma energy (keV)= 807.02
Gamma energy (keV)= 839.43
Gamma energy (keV)= 846.63
Gamma energy (keV)= 853.51
Neutron energy (MeV)
Normalised area
Gamma energy (keV)

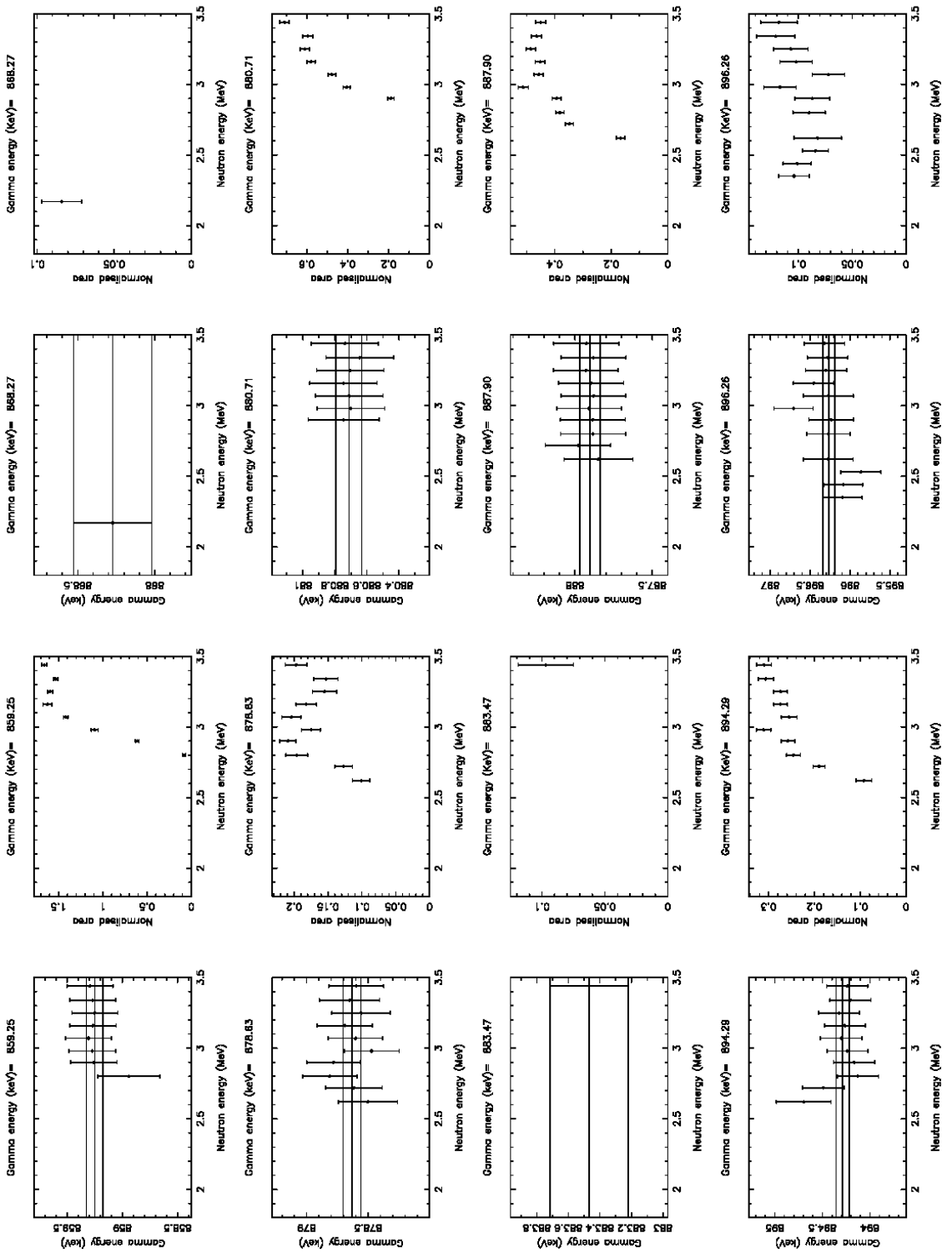
Gamma energy (keV)= 858.25
Gamma energy (keV)
Normalised area
Neutron energy (MeV)
Gamma energy (KeV)= 878.83
Gamma energy (KeV)= 883.47
Gamma energy (KeV)= 894.29
Gamma energy (keV)= 896.26
Gamma energy (keV)= 887.90
Gamma energy (keV)= 880.71
Gamma energy (KeV)= 868.27

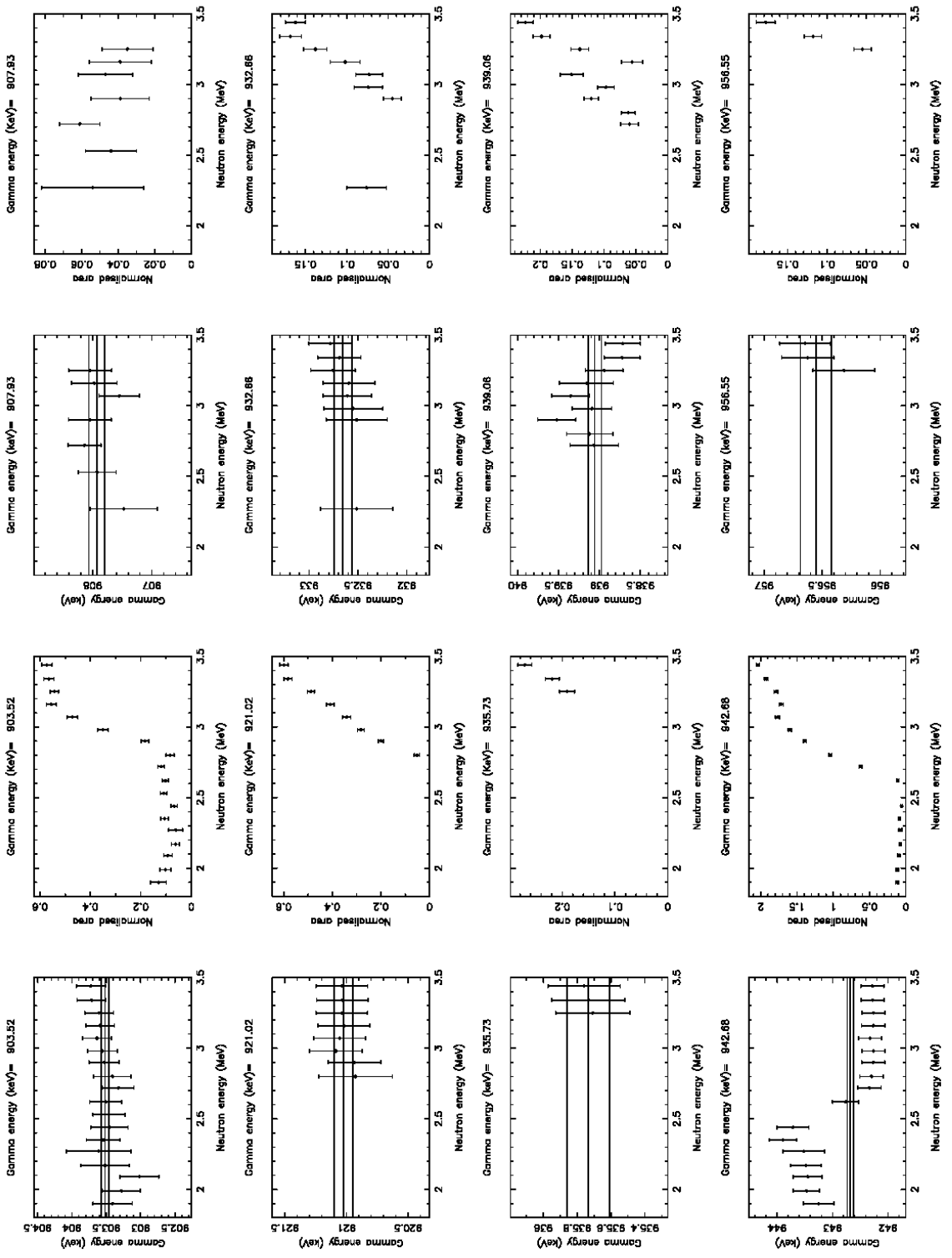
Gamma energy (keV)= 803.52
Gamma energy (keV)= 921.02
Gamma energy (keV)= 935.73
Gamma energy (keV)= 942.68
Gamma energy (keV)= 807.83
Gamma energy (keV)= 932.86
Gamma energy (keV)= 939.06
Gamma energy (keV)= 956.55
Neutron energy (MeV)
Normalised area
Gamma energy (keV)

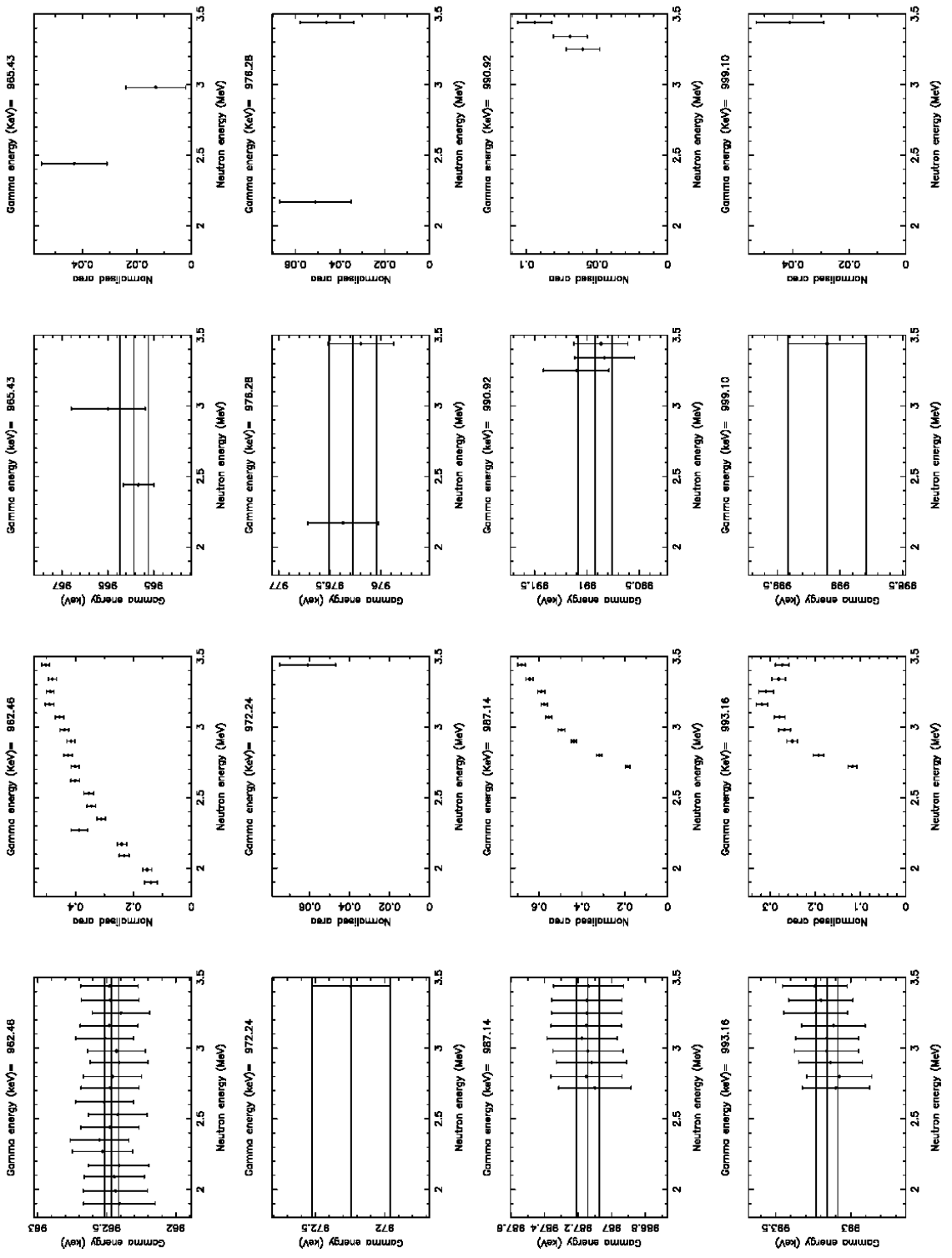
Gamma energy (keV)= 862.46
Gamma energy (keV)= 872.24
Gamma energy (keV)= 887.14
Gamma energy (keV)= 893.16
Gamma energy (keV)= 865.43
Gamma energy (keV)= 878.28
Gamma energy (keV)= 890.92
Gamma energy (keV)= 899.10
Neutron energy (MeV)
Normalised area
Gamma energy (keV)

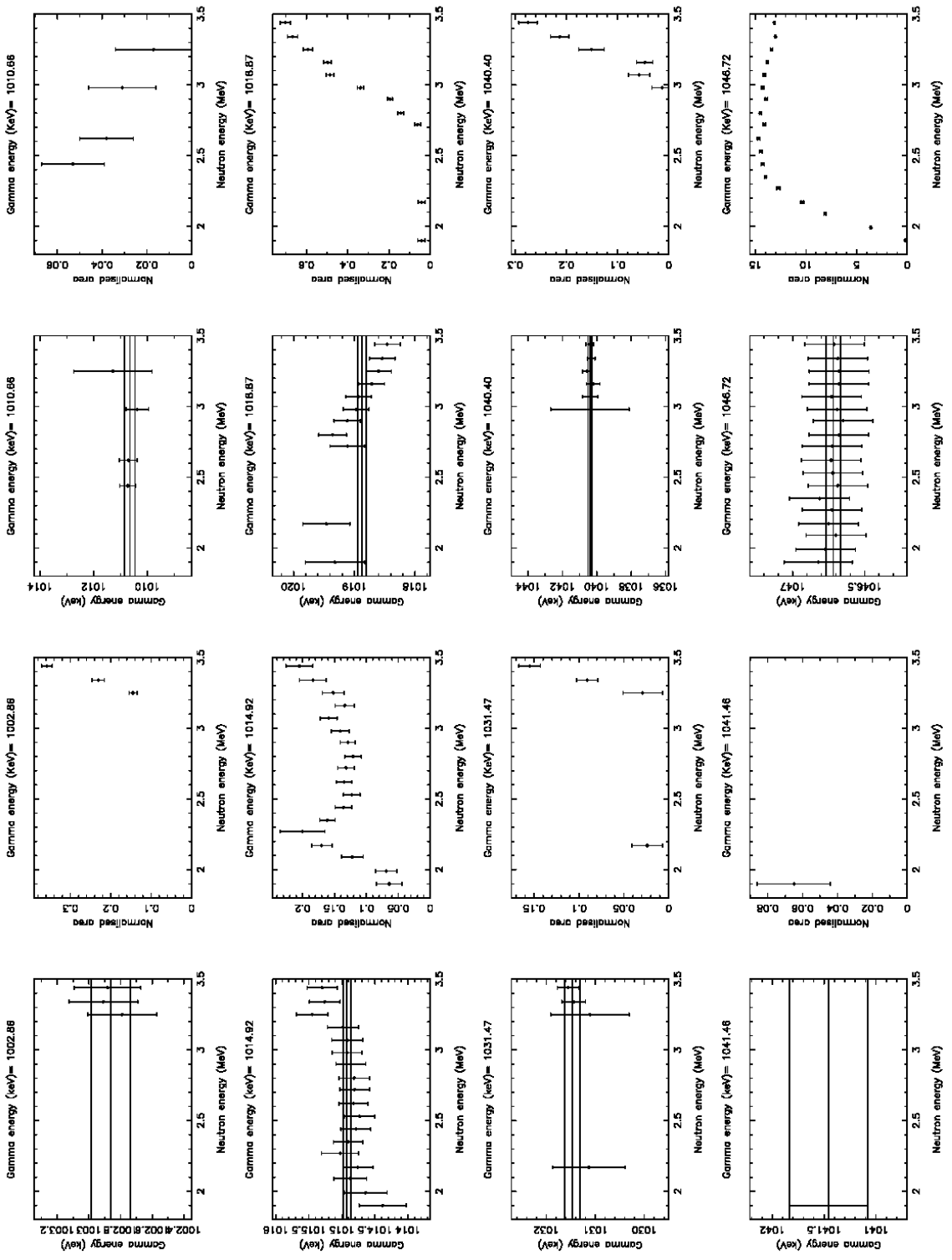
Gamma energy (keV)= 1002.86
Gamma energy (keV)= 1014.92
Gamma energy (keV)= 1031.47
Gamma energy (keV)= 1041.46
Gamma energy (keV)= 1010.66
Gamma energy (keV)= 1018.87
Gamma energy (keV)= 1040.40
Gamma energy (keV)= 1046.72
Neutron energy (MeV)
Normalised area
Gamma energy (keV)

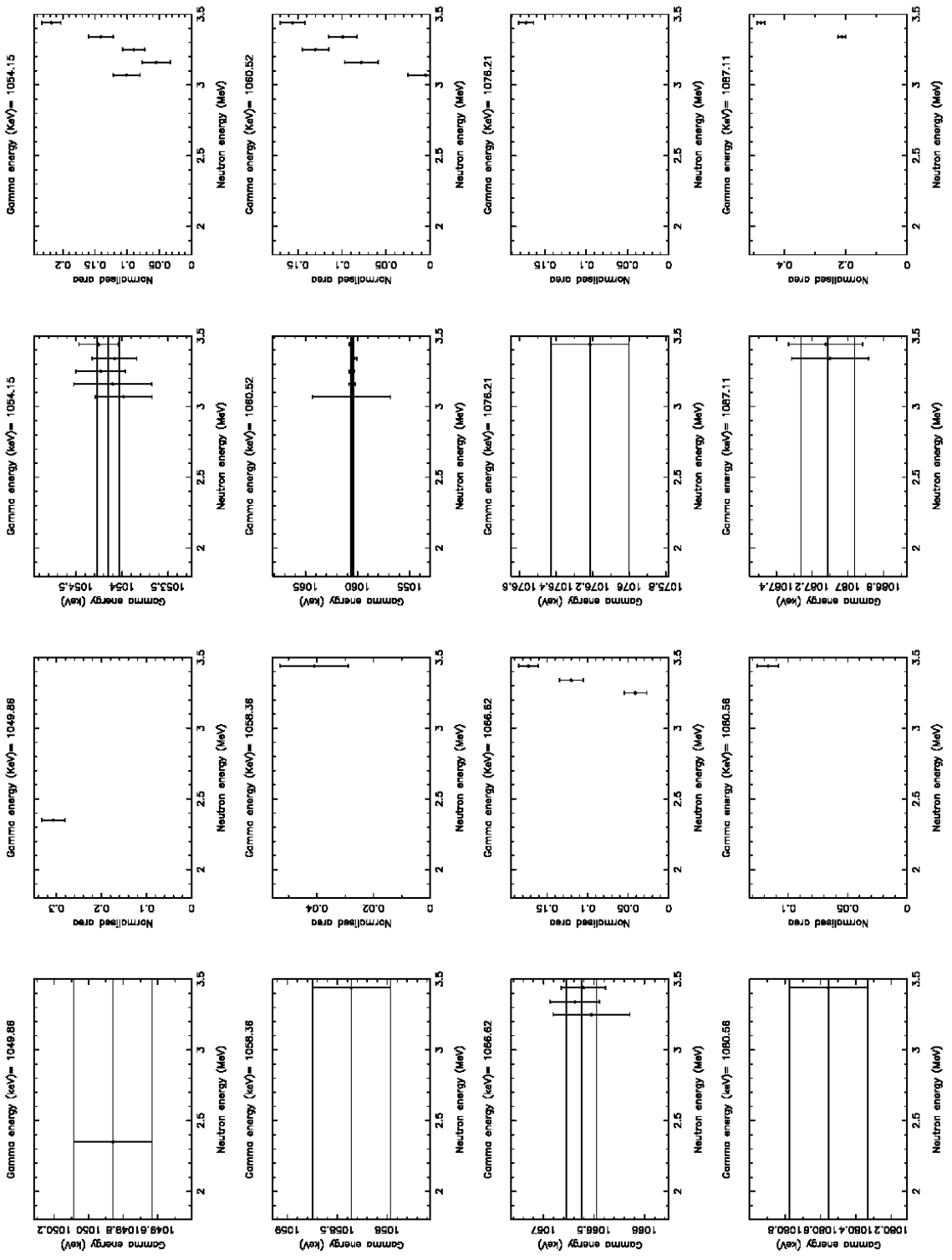
Gamma energy (keV)= 1049.86
Gamma energy (keV)= 1058.36
Gamma energy (keV)= 1066.62
Gamma energy (keV)= 1080.58
Gamma energy (keV)= 1054.15
Gamma energy (keV)= 1060.52
Gamma energy (keV)= 1076.21
Gamma energy (keV)= 1087.11
Neutron energy (MeV)
Normalised area
Gamma energy (keV)

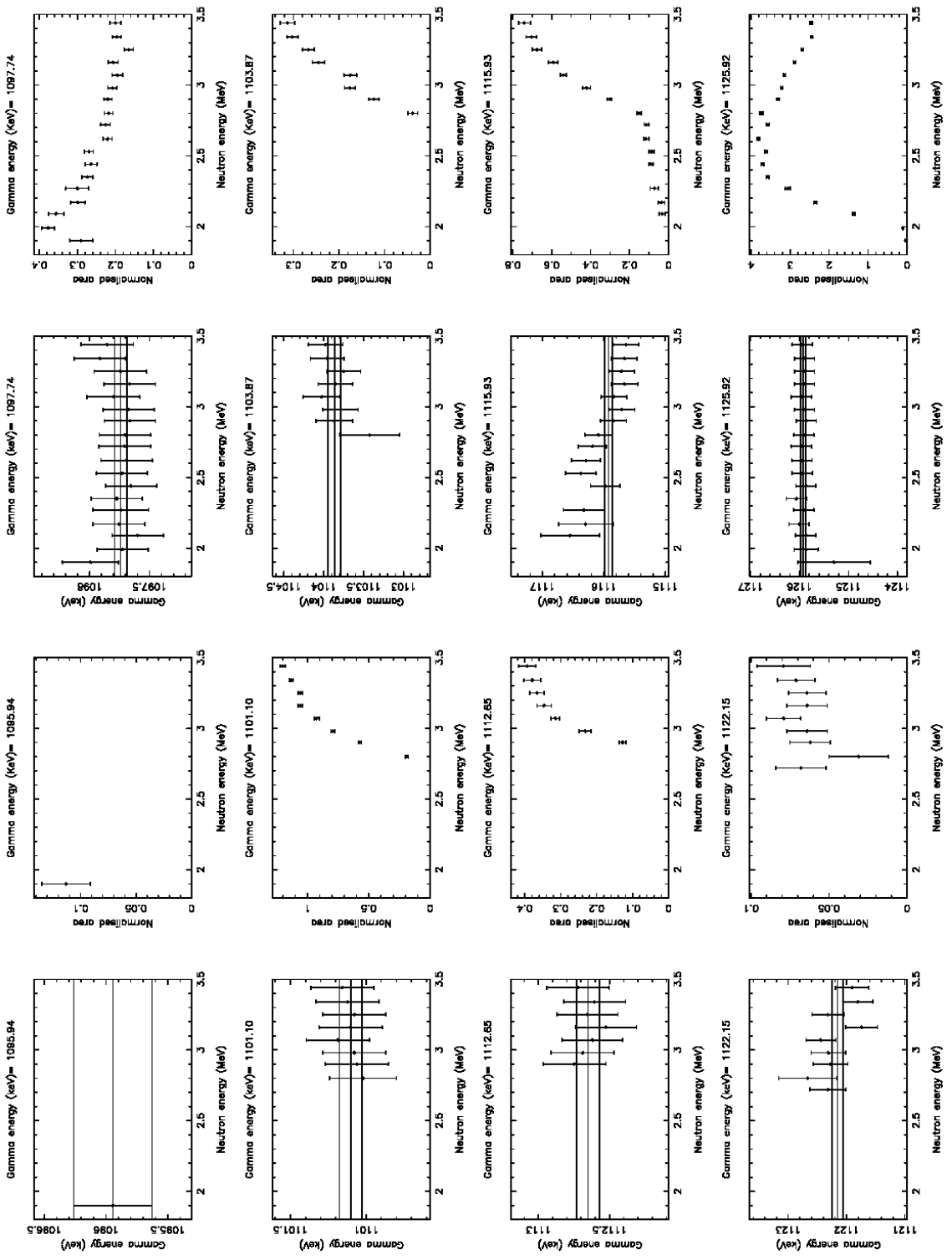
Gamma energy (keV)= 1085.94
Gamma energy (keV)= 1101.10
Gamma energy (keV)= 1112.65
Gamma energy (keV)= 1122.15
Gamma energy (keV)= 1097.74
Gamma energy (keV)= 1103.87
Gamma energy (keV)= 1115.93
Gamma energy (keV)= 1125.92
Gamma energy (keV)
Normalised area
Neutron energy (MeV)

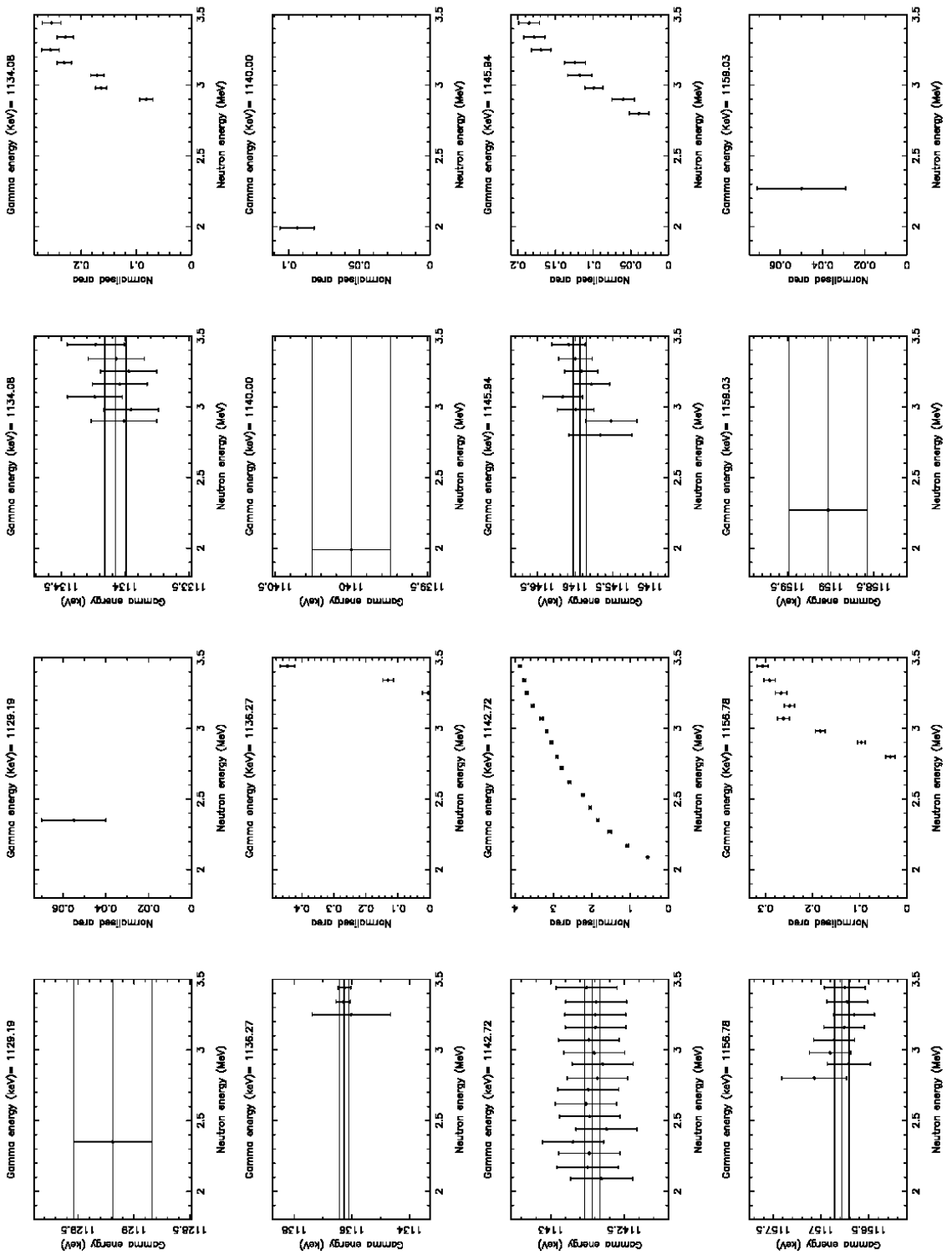
Gamma energy (keV)= 1129.19
Gamma energy (keV)
Neutron energy (MeV)
Normalised area
Gamma energy (keV)= 1136.27
Gamma energy (keV)= 1142.72
Gamma energy (keV)= 1156.78
Gamma energy (keV)= 1134.08
Gamma energy (keV)= 1140.00
Gamma energy (keV)= 1145.84
Gamma energy (keV)= 1158.03

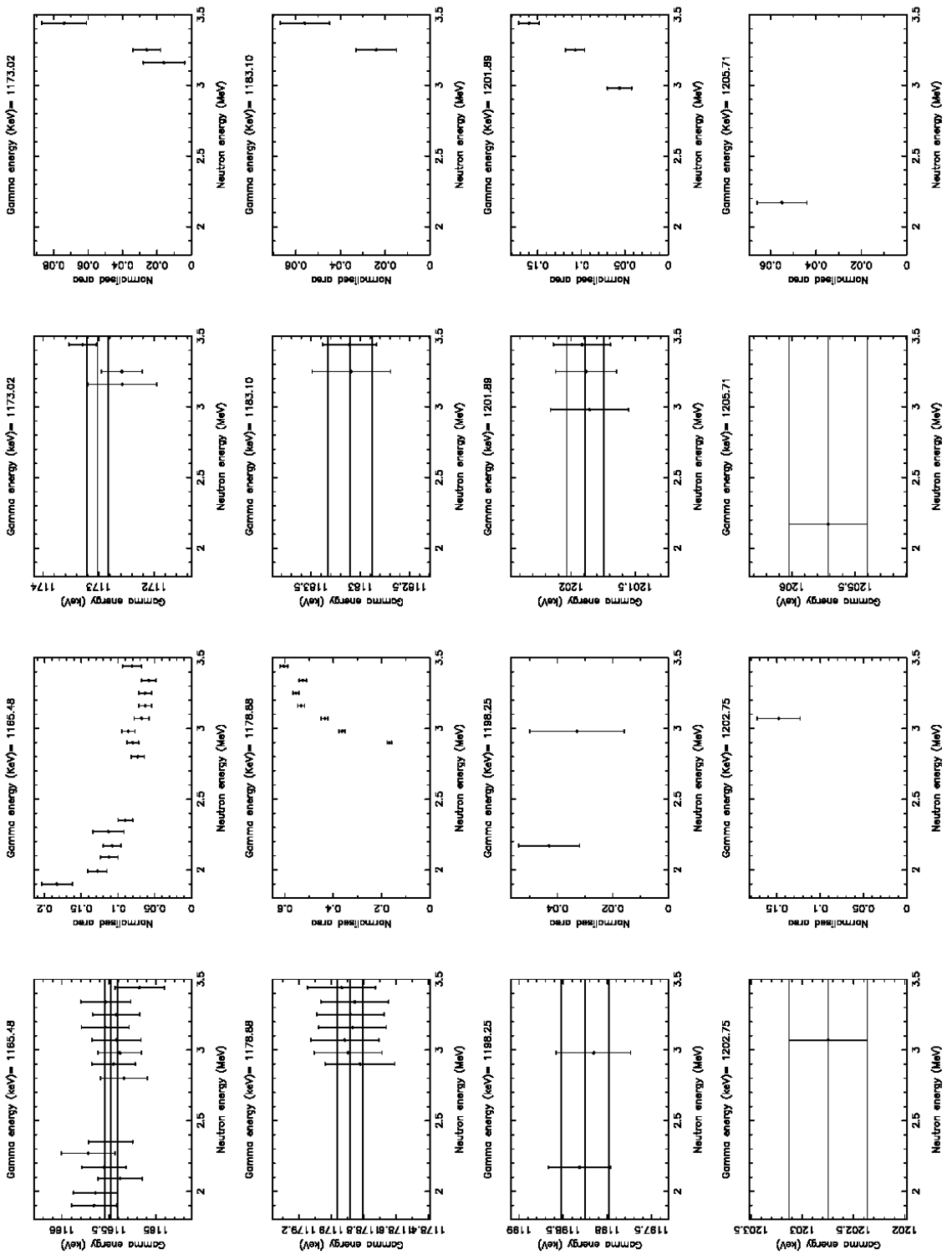
Gamma energy (keV)= 1165.48
Gamma energy (keV)= 1178.88
Gamma energy (keV)= 1188.25
Gamma energy (keV)= 1202.75
Gamma energy (keV)= 1173.02
Gamma energy (keV)= 1183.10
Gamma energy (keV)= 1201.88
Gamma energy (keV)= 1205.71
Neutron energy (MeV)
Normalised area
Gamma energy (keV)

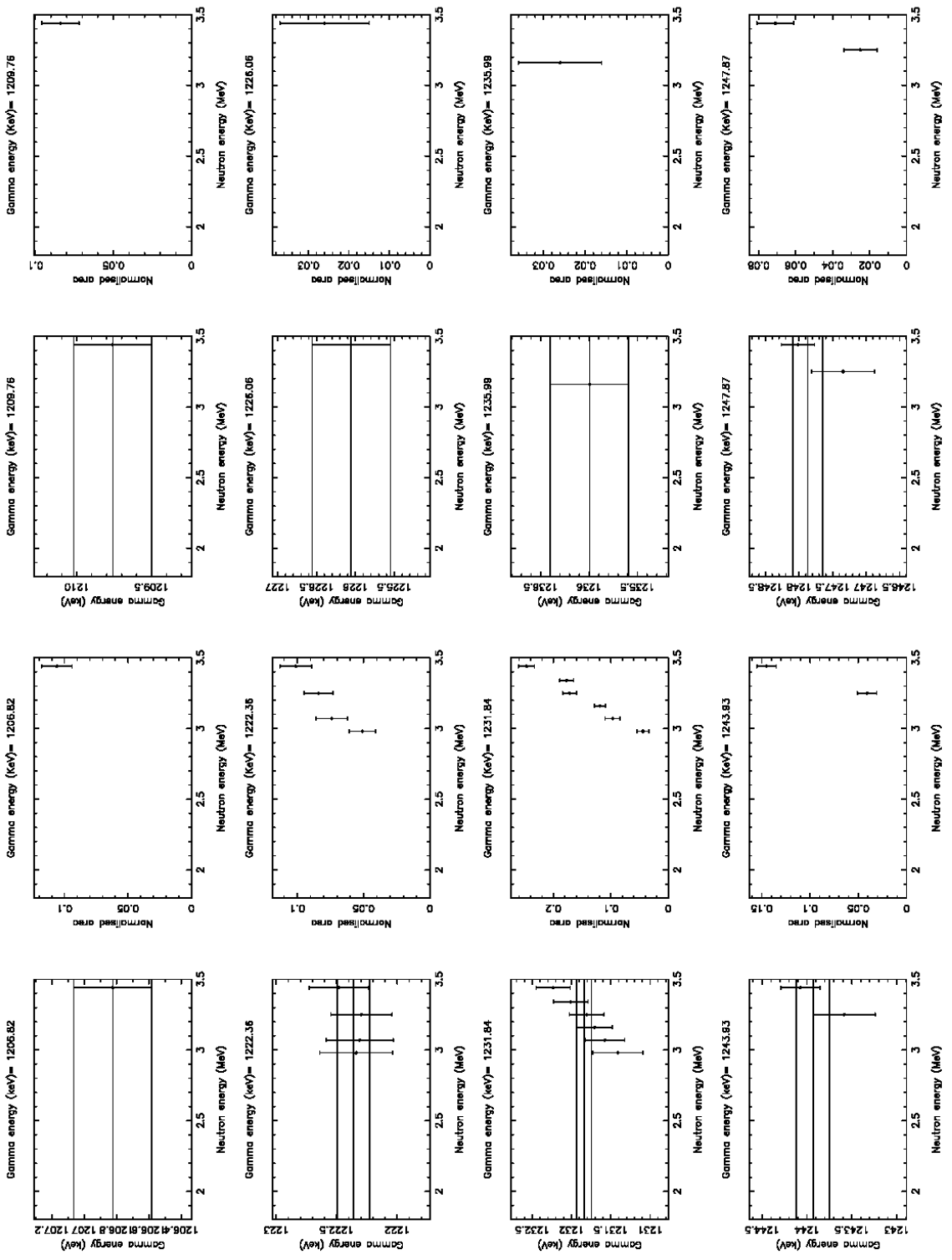
Gamma energy (keV)= 1205.82
Gamma energy (keV)= 1222.36
Gamma energy (keV)= 1231.84
Gamma energy (keV)= 1243.83
Gamma energy (keV)= 1209.76
Gamma energy (keV)= 1226.06
Gamma energy (keV)= 1235.98
Gamma energy (keV)= 1247.87
Gamma energy (keV)= 1206.82
Gamma energy (keV)= 1222.36
Gamma energy (keV)= 1231.84
Gamma energy (keV)= 1243.83
Gamma energy (keV)= 1209.76
Gamma energy (keV)= 1226.06
Gamma energy (keV)= 1235.98
Gamma energy (keV)= 1247.87
Gamma energy (keV)= 1209.76
Gamma energy (keV)= 1226.06
Gamma energy (keV)= 1235.98
Gamma energy (keV)= 1247.87
Neutron energy (MeV)
Normalised area

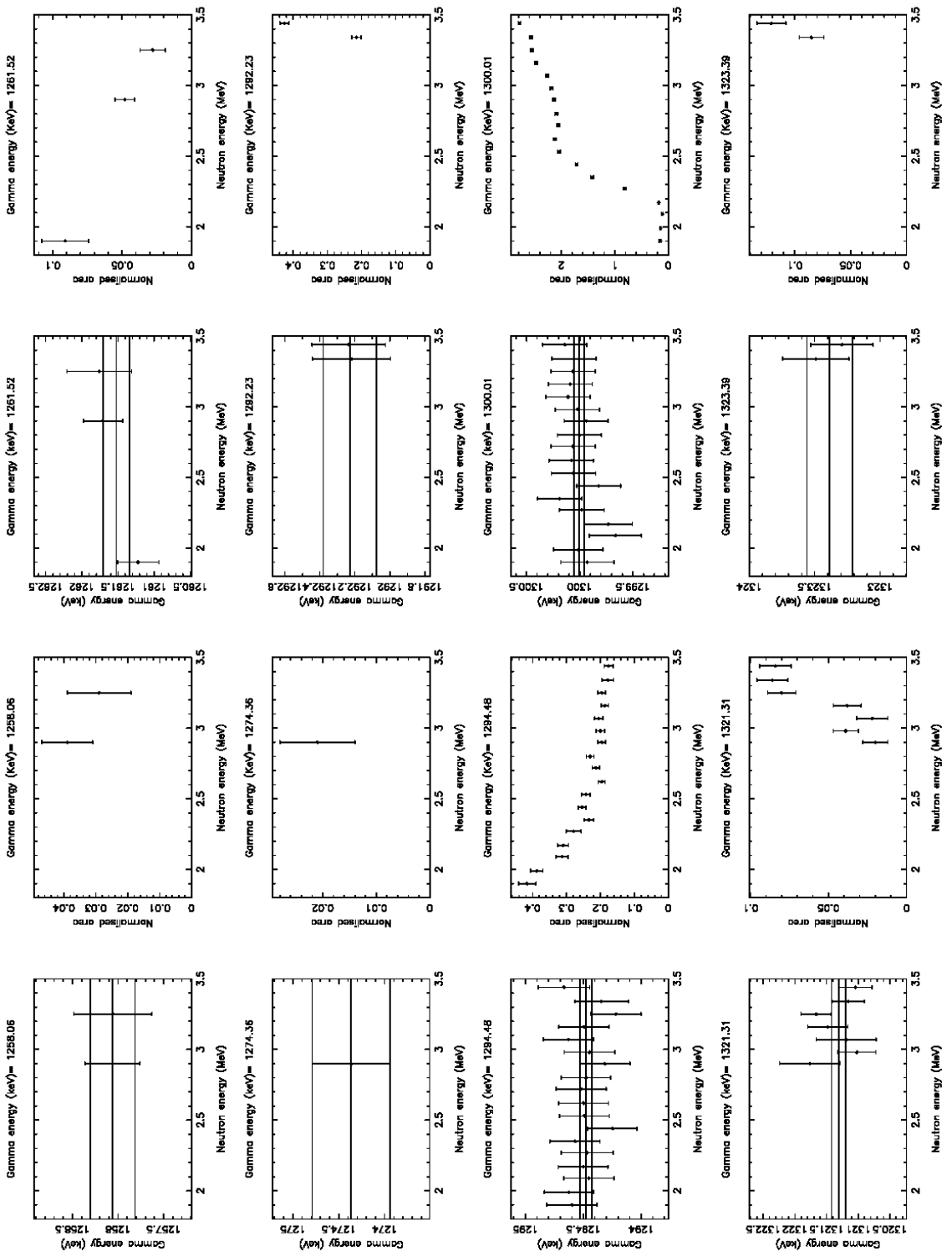
Gamma energy (keV)= 1258.06
Gamma energy (keV)= 1274.36
Gamma energy (keV)= 1284.48
Gamma energy (keV)= 1321.31
Gamma energy (keV)= 1251.52
Gamma energy (keV)= 1282.23
Gamma energy (keV)= 1300.01
Gamma energy (keV)= 1323.39
Gamma energy (keV)= 1261.52
Gamma energy (keV)= 1282.23
Gamma energy (keV)= 1300.01
Gamma energy (keV)= 1323.39
Neutron energy (MeV)
Normalised area
Gamma energy (keV)

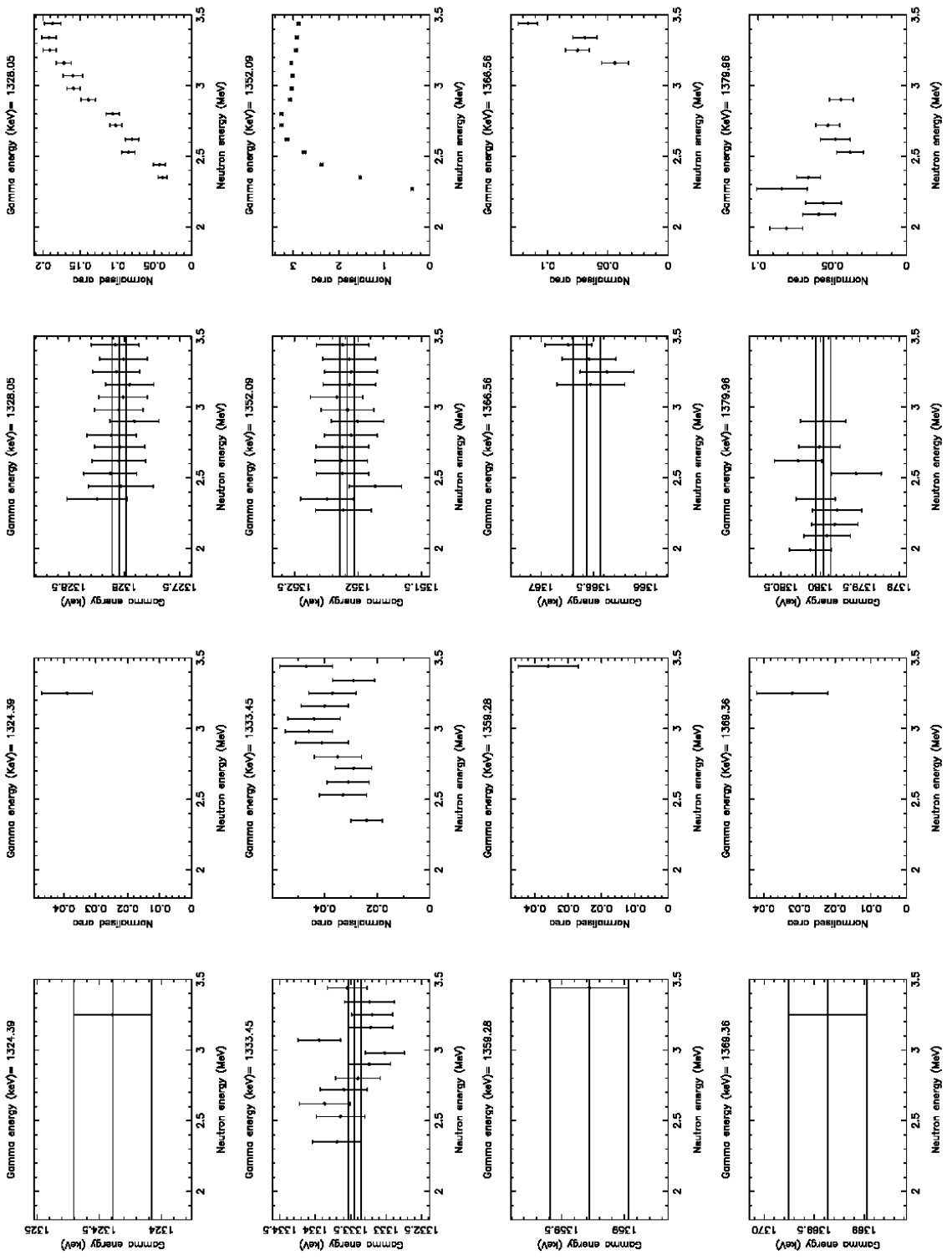
Gamma energy (keV)= 1324.39
Gamma energy (keV)= 1333.45
Gamma energy (keV)= 1358.28
Gamma energy (keV)= 1368.36
Gamma energy (keV)= 1328.05
Gamma energy (keV)= 1352.09
Gamma energy (keV)= 1366.56
Gamma energy (keV)= 1379.96
Gamma energy (keV)
Normalised area
Neutron energy (MeV)

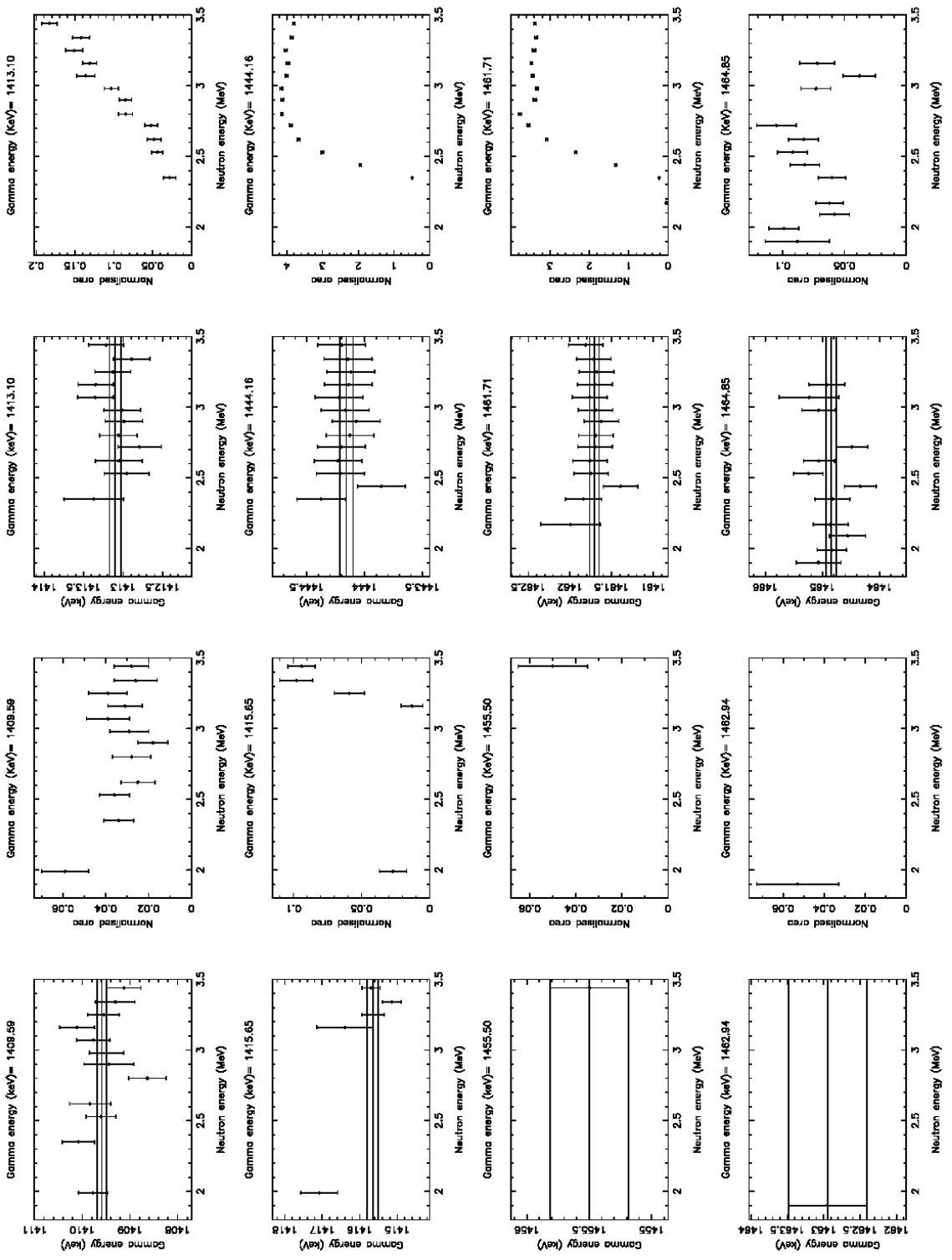
Gamma energy (keV)= 1408.59
Gamma energy (keV)= 1415.65
Gamma energy (keV)= 1455.50
Gamma energy (keV)= 1462.94
Gamma energy (keV)= 1413.10
Gamma energy (keV)= 1444.16
Gamma energy (keV)= 1461.71
Gamma energy (keV)= 1464.85
Gamma energy (keV)
Normalised area
Neutron energy (MeV)

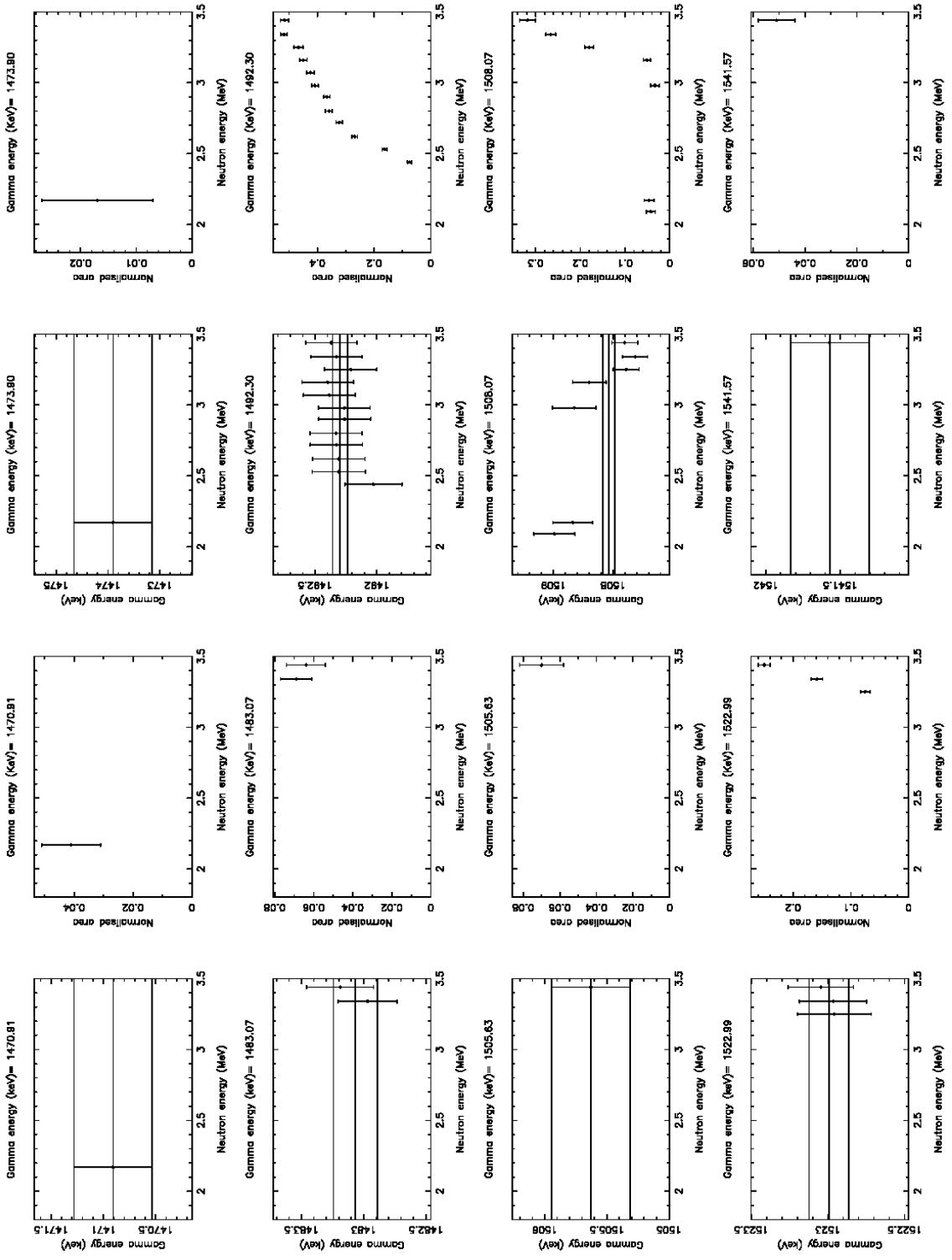
Gamma energy (keV)= 1470.81
Gamma energy (keV)= 1483.07
Gamma energy (keV)= 1505.63
Gamma energy (keV)= 1522.99
Gamma energy (keV)= 1473.80
Gamma energy (keV)= 1492.30
Gamma energy (keV)= 1508.07
Gamma energy (keV)= 1541.57
Gamma energy (keV)= 1473.80
Gamma energy (keV)= 1492.30
Gamma energy (keV)= 1508.07
Gamma energy (keV)= 1541.57
Neutron energy (MeV)
Normalised area

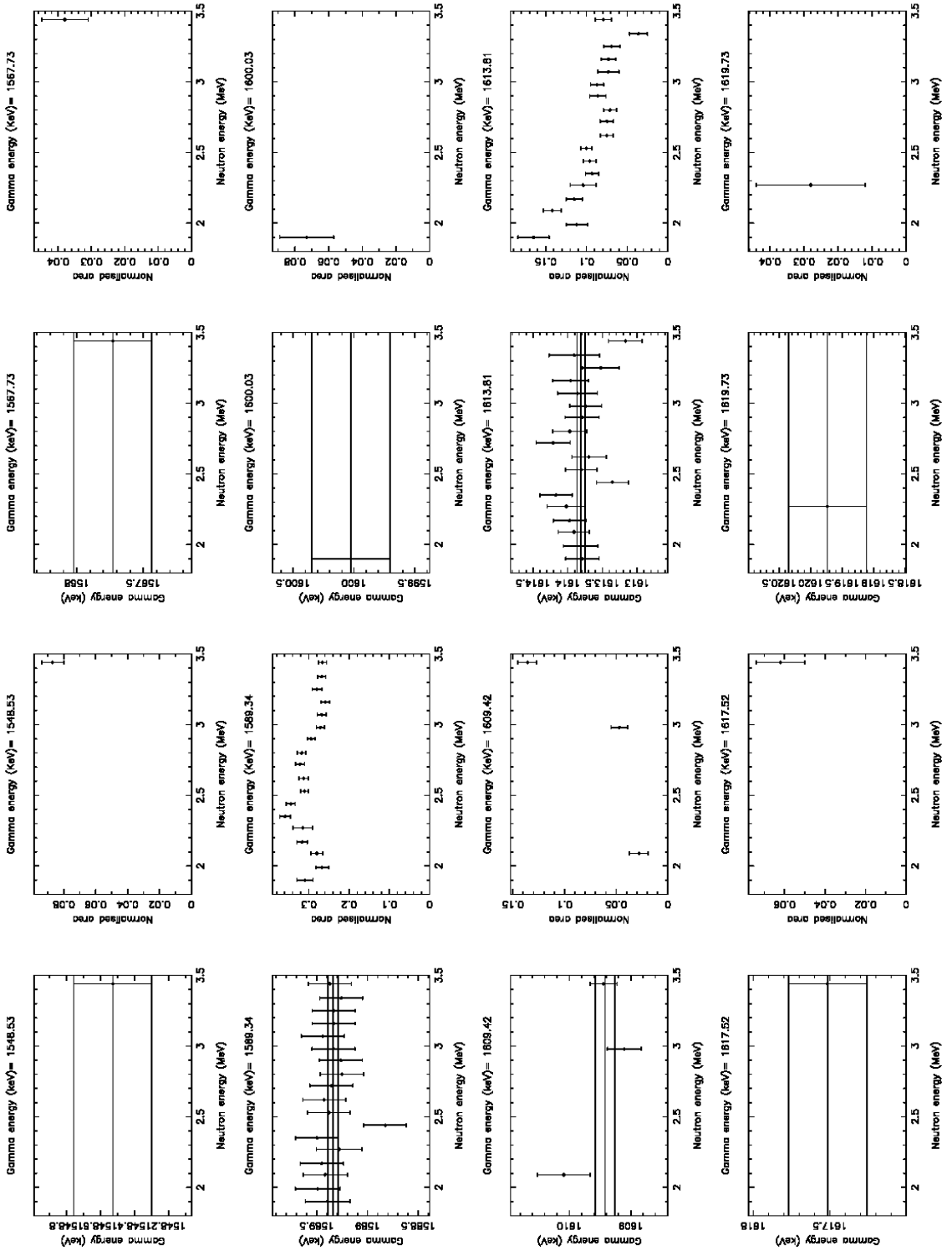
Gamma energy (keV)= 1548.53
Gamma energy (keV)= 1589.34
Gamma energy (keV)= 1609.42
Gamma energy (keV)= 1617.52
Gamma energy (keV)= 1567.73
Gamma energy (keV)= 1600.03
Gamma energy (keV)= 1613.81
Gamma energy (keV)= 1619.73
Neutron energy (MeV)
Normalised area
Gamma energy (keV)

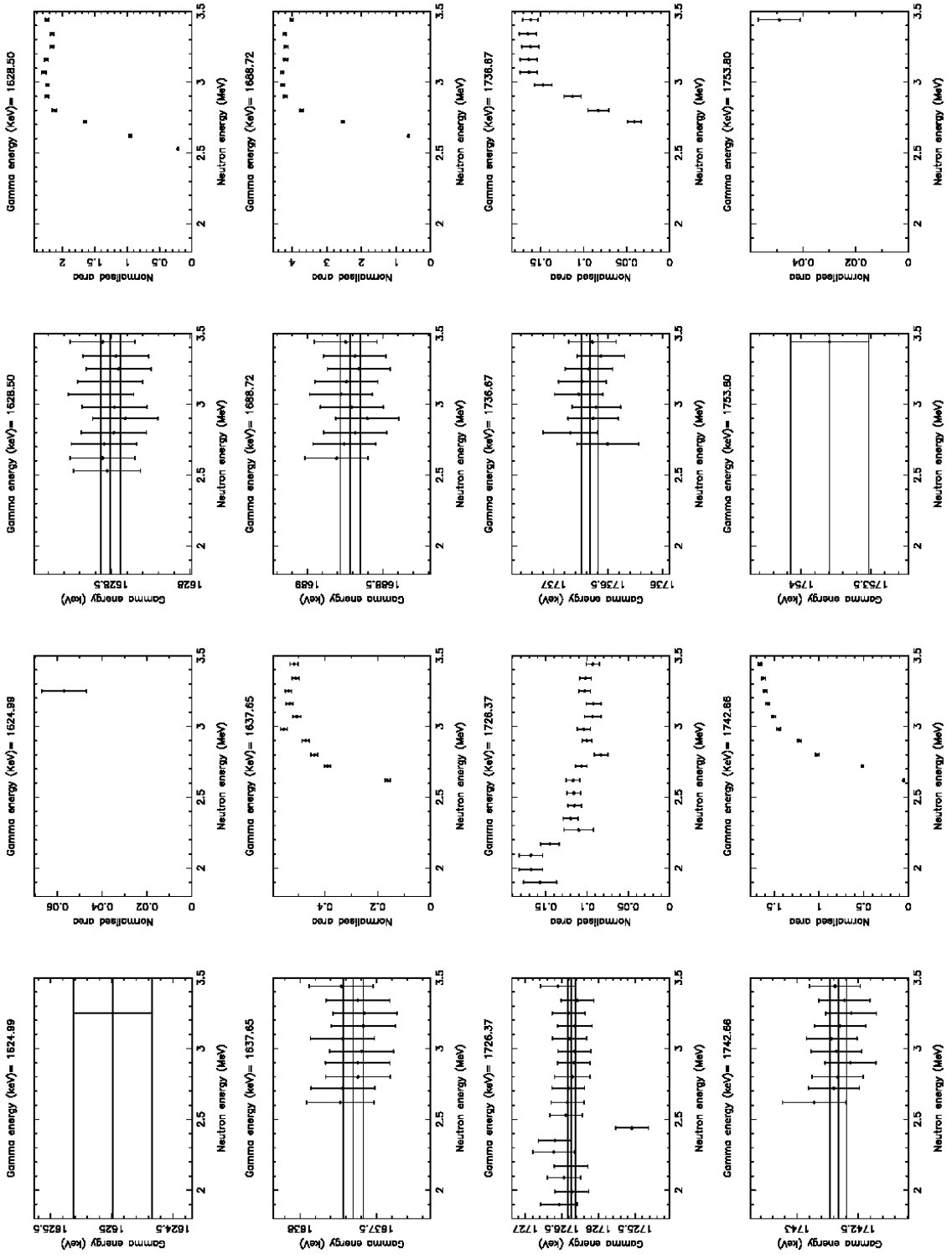
Gamma energy (keV)= 1624.89
Gamma energy (keV)= 1624.89
Gamma energy (keV)= 1637.65
Gamma energy (keV)= 1637.65
Gamma energy (keV)= 1726.37
Gamma energy (keV)= 1726.37
Gamma energy (keV)= 1742.66
Gamma energy (keV)= 1742.86
Gamma energy (keV)= 1753.80
Gamma energy (keV)= 1753.80
Gamma energy (keV)= 1736.67
Gamma energy (keV)= 1736.67
Gamma energy (keV)= 1688.72
Gamma energy (keV)= 1688.72
Gamma energy (keV)= 1628.50
Gamma energy (keV)= 1628.50
Neutron energy (MeV)
Normalised area
Gamma energy (keV)

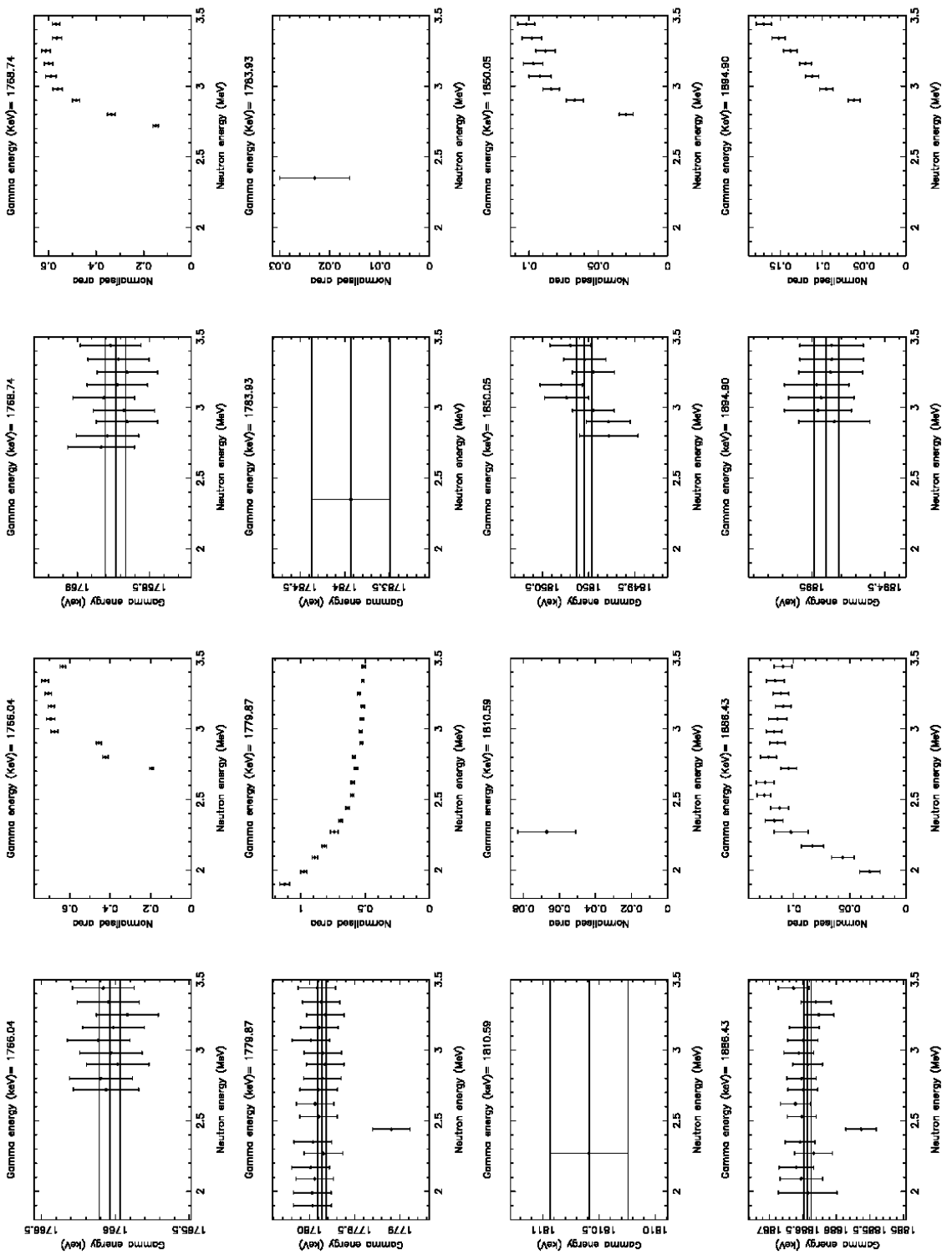
Gamma energy (keV)= 1766.04
Gamma energy (keV)= 1778.87
Gamma energy (keV)= 1810.59
Gamma energy (keV)= 1886.43
Gamma energy (keV)= 1766.04
Gamma energy (keV)= 1779.87
Gamma energy (keV)= 1810.59
Gamma energy (keV)= 1886.43
Gamma energy (keV)= 1768.74
Gamma energy (keV)= 1783.93
Gamma energy (keV)= 1850.05
Gamma energy (keV)= 1894.90
Gamma energy (keV)= 1768.74
Gamma energy (keV)= 1783.93
Gamma energy (keV)= 1850.05
Gamma energy (keV)= 1894.90
Neutron energy (MeV)
Normalised area
Gamma energy (keV)

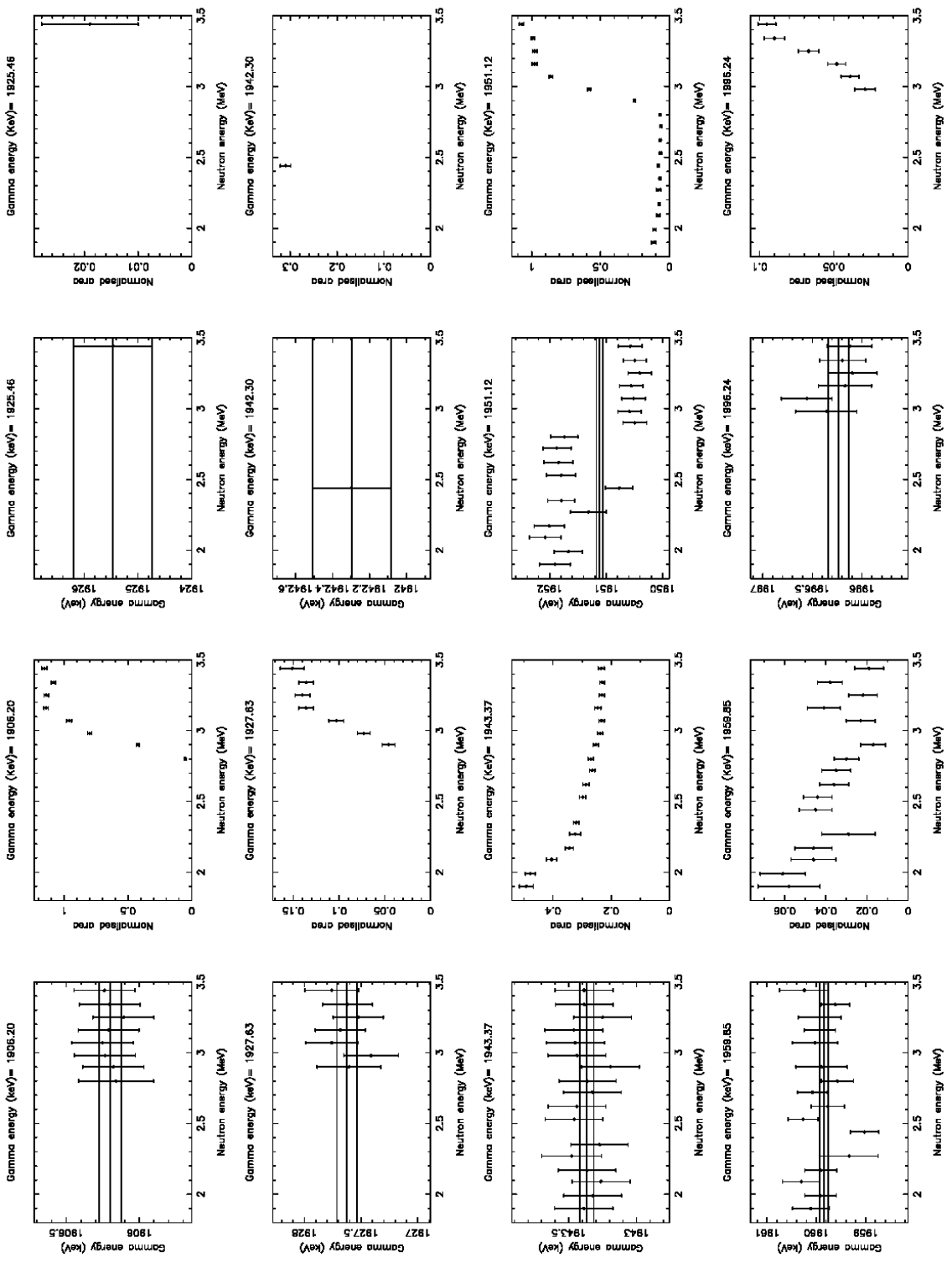
Gamma energy (keV)= 1906.20
Gamma energy (keV)= 1927.63
Gamma energy (keV)= 1943.37
Gamma energy (keV)= 1958.85
Gamma energy (keV)= 1925.46
Gamma energy (keV)= 1942.30
Gamma energy (keV)= 1951.12
Gamma energy (keV)= 1995.24
Neutron energy (MeV)
Normalised area
Gamma energy (keV)

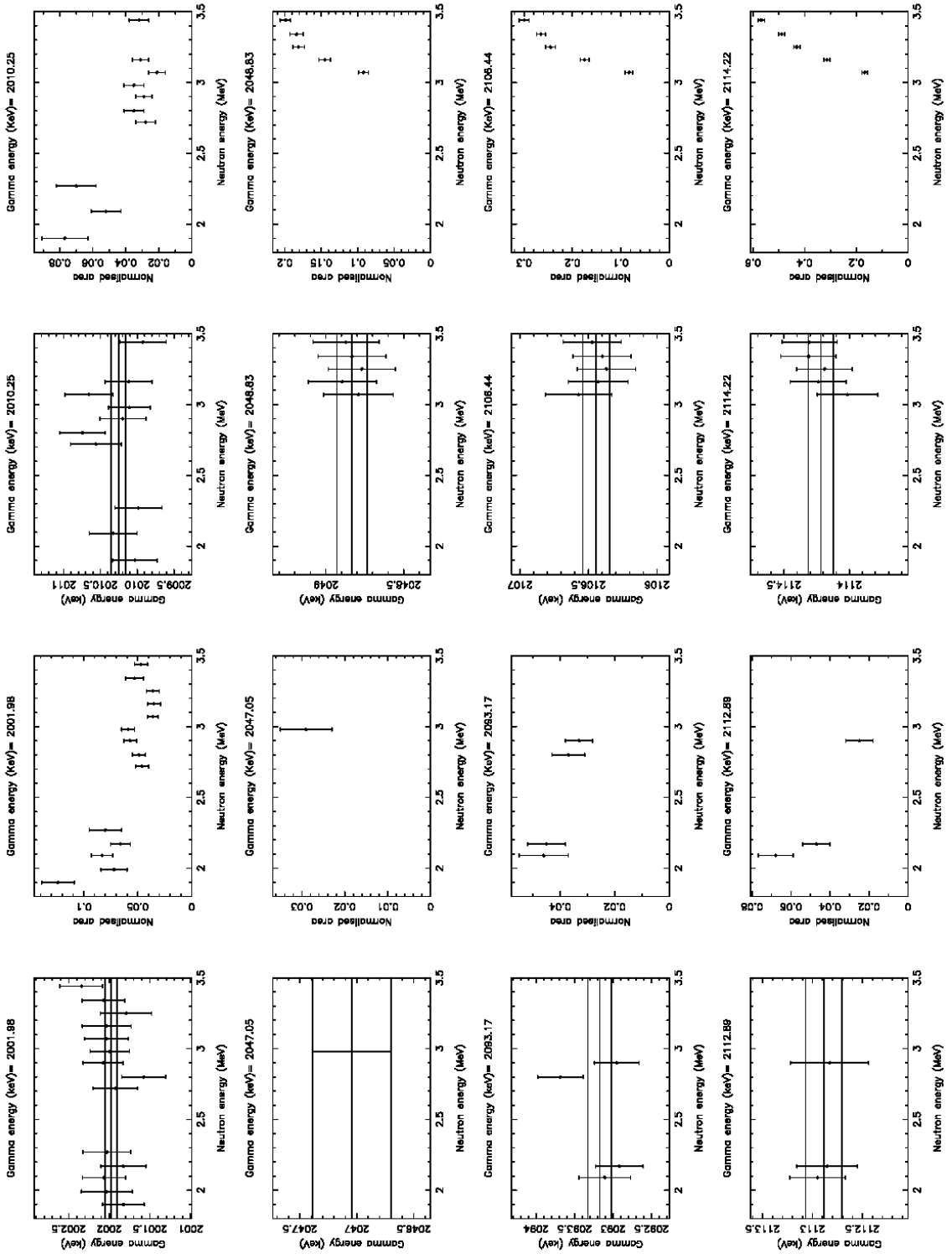
Gamma energy (keV)= 2001.98
Gamma energy (keV)= 2047.05
Gamma energy (keV)= 2083.17
Gamma energy (keV)= 2112.89
Gamma energy (keV)= 2010.25
Gamma energy (keV)= 2048.83
Gamma energy (keV)= 2106.44
Gamma energy (keV)= 2114.22
Gamma energy (keV)= 2010.25
Gamma energy (keV)= 2048.83
Gamma energy (keV)= 2106.44
Gamma energy (keV)= 2114.22
Gamma energy (keV)= 2001.98
Gamma energy (keV)= 2047.05
Gamma energy (keV)= 2083.17
Gamma energy (keV)= 2112.89
Neutron energy (MeV)
Normalised area
Gamma energy (keV)

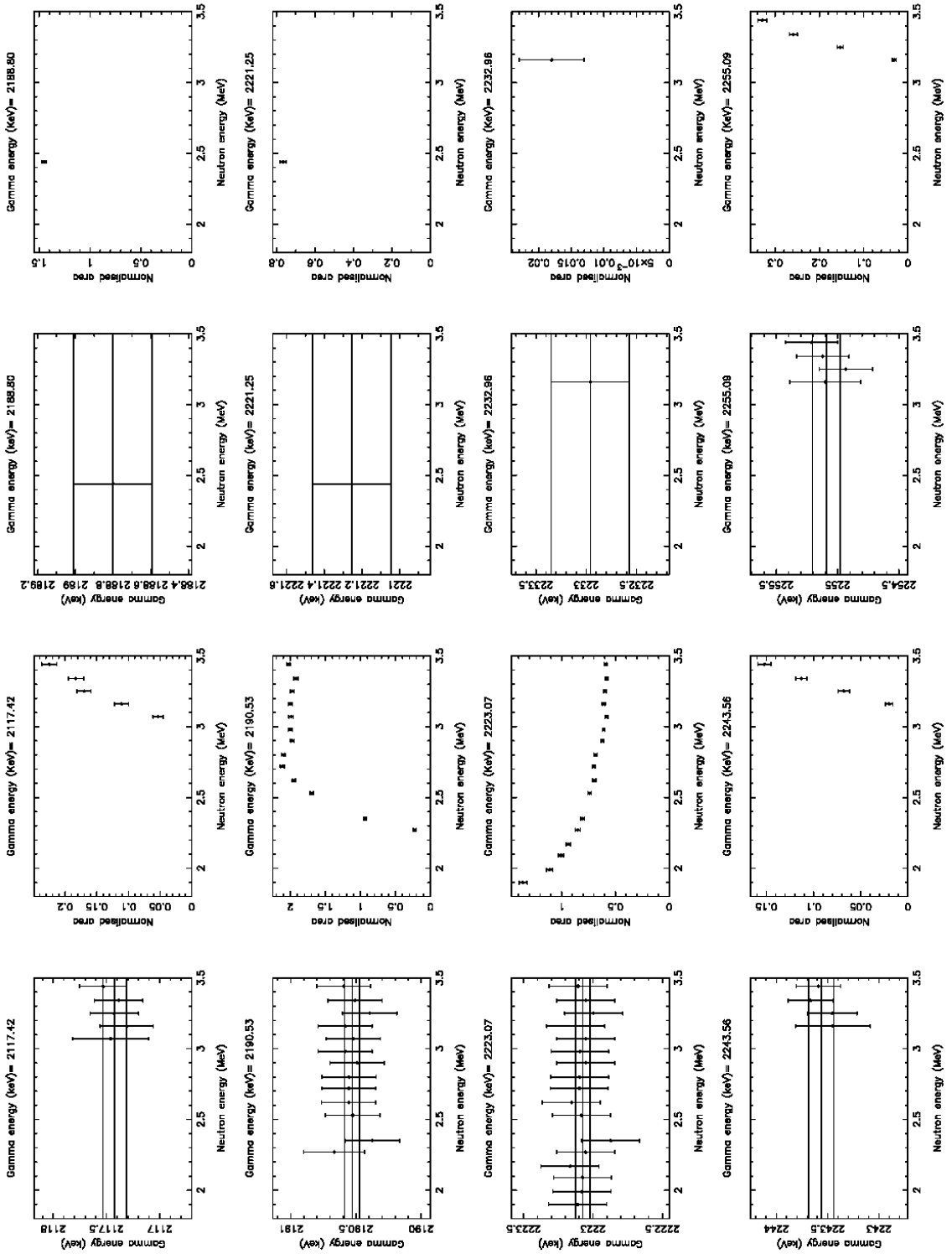
Gamma energy (keV)= 2117.42
Gamma energy (keV)= 2190.53
Gamma energy (keV)= 2223.07
Gamma energy (keV)= 2243.56
Gamma energy (keV)= 2188.80
Gamma energy (keV)= 2221.25
Gamma energy (keV)= 2232.96
Gamma energy (keV)= 2255.09
Neutron energy (MeV)
Normalised area
Gamma energy (keV)

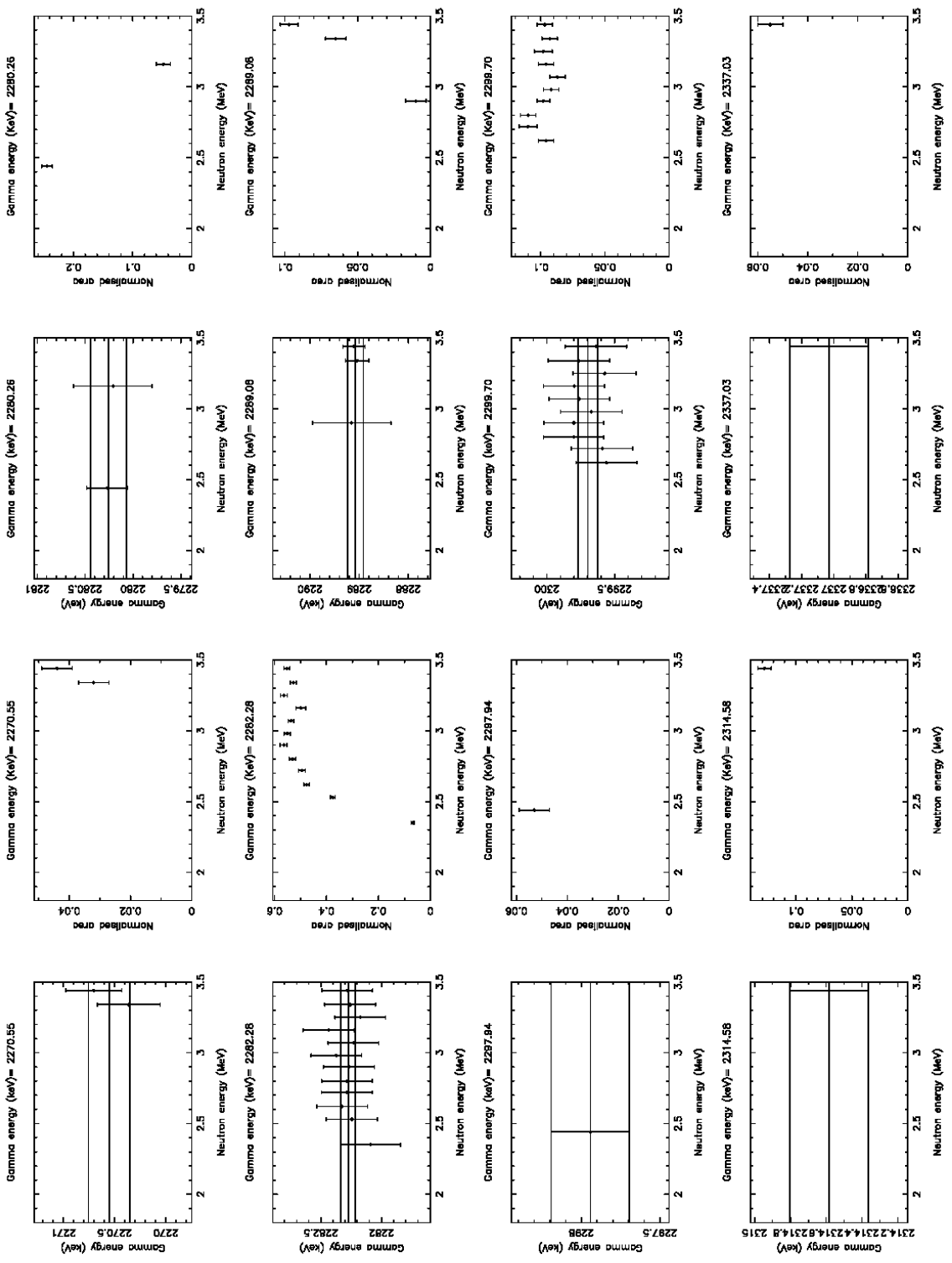
Gamma energy (keV)= 2270.55
Gamma energy (keV)= 2282.28
Gamma energy (keV)= 2287.94
Gamma energy (keV)= 2314.58
Gamma energy (keV)= 2280.26
Gamma energy (keV)= 2289.08
Gamma energy (keV)= 2299.70
Gamma energy (keV)= 2337.03
Gamma energy (keV)= 2280.26
Gamma energy (keV)= 2289.08
Gamma energy (keV)= 2299.70
Gamma energy (keV)= 2337.03
Neutron energy (MeV)
Normalised area
Gamma energy (keV)

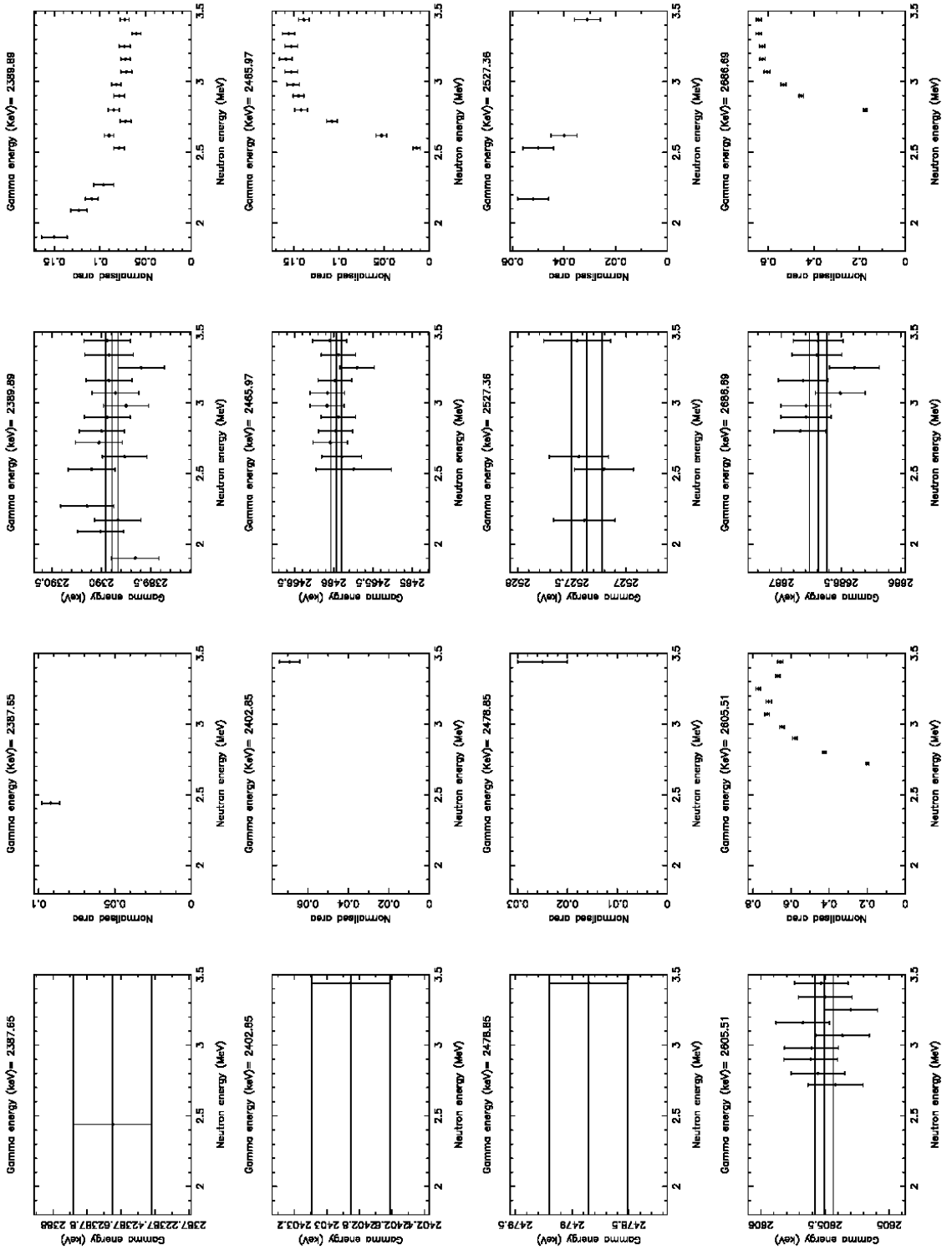
Gamma energy (keV)= 2387.65
Gamma energy (keV)= 2402.85
Gamma energy (keV)= 2478.85
Gamma energy (keV)= 2605.51
Gamma energy (keV)= 2389.89
Gamma energy (keV)= 2465.97
Gamma energy (keV)= 2527.36
Gamma energy (keV)= 2686.69
Gamma energy (keV)= 2389.88
Gamma energy (keV)= 2485.97
Gamma energy (keV)= 2527.36
Gamma energy (keV)= 2686.69
Neutron energy (MeV)
Normalised area
Gamma energy (keV)

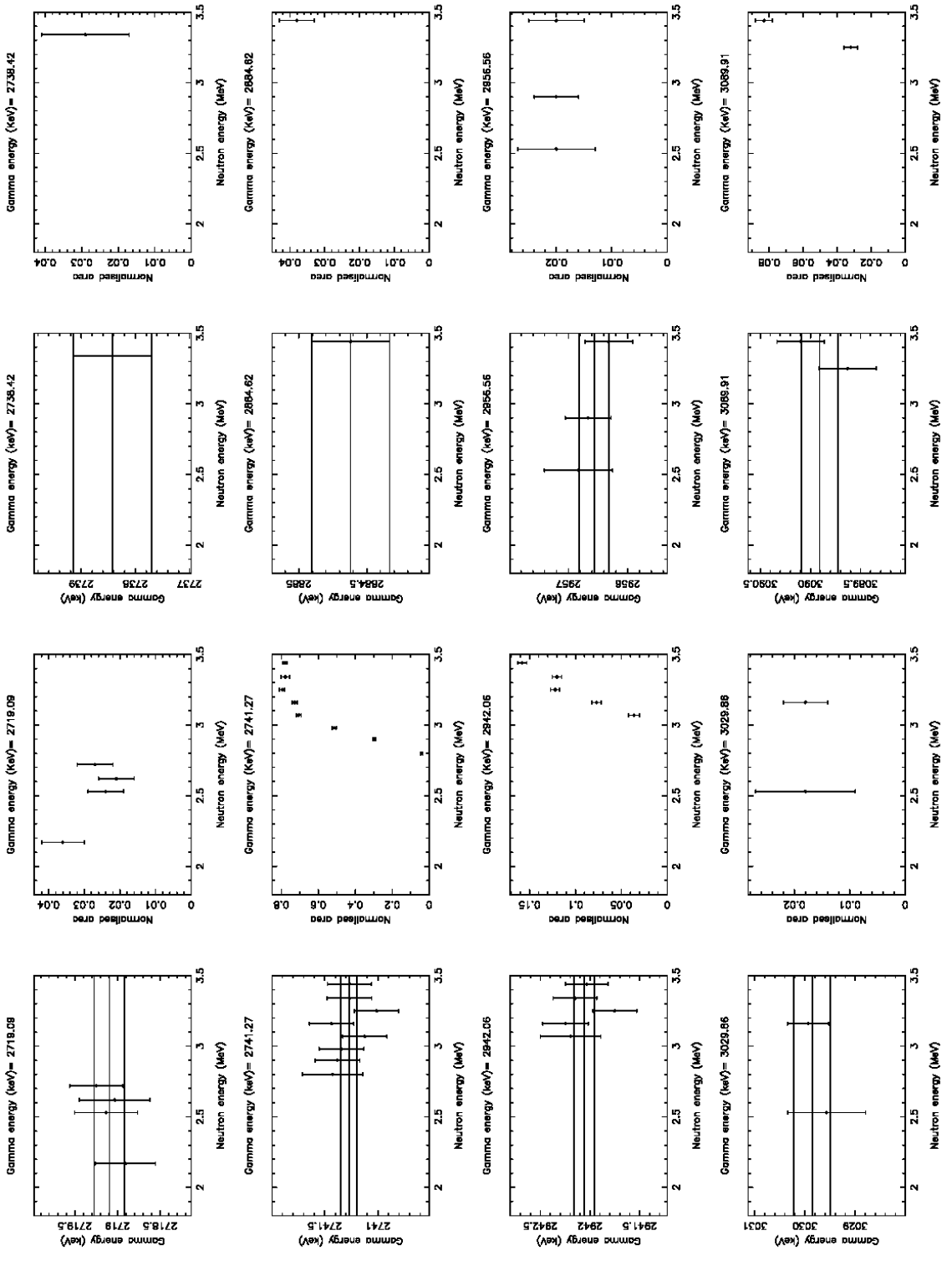
Gamma energy (keV)= 2718.09
Gamma energy (keV)= 2741.27
Gamma energy (keV)= 2942.06
Gamma energy (keV)= 3029.86
Gamma energy (keV)= 2738.42
Gamma energy (keV)= 2884.62
Gamma energy (keV)= 2956.56
Gamma energy (keV)= 3089.91
Neutron energy (MeV)
Normalised area
Gamma energy (keV)

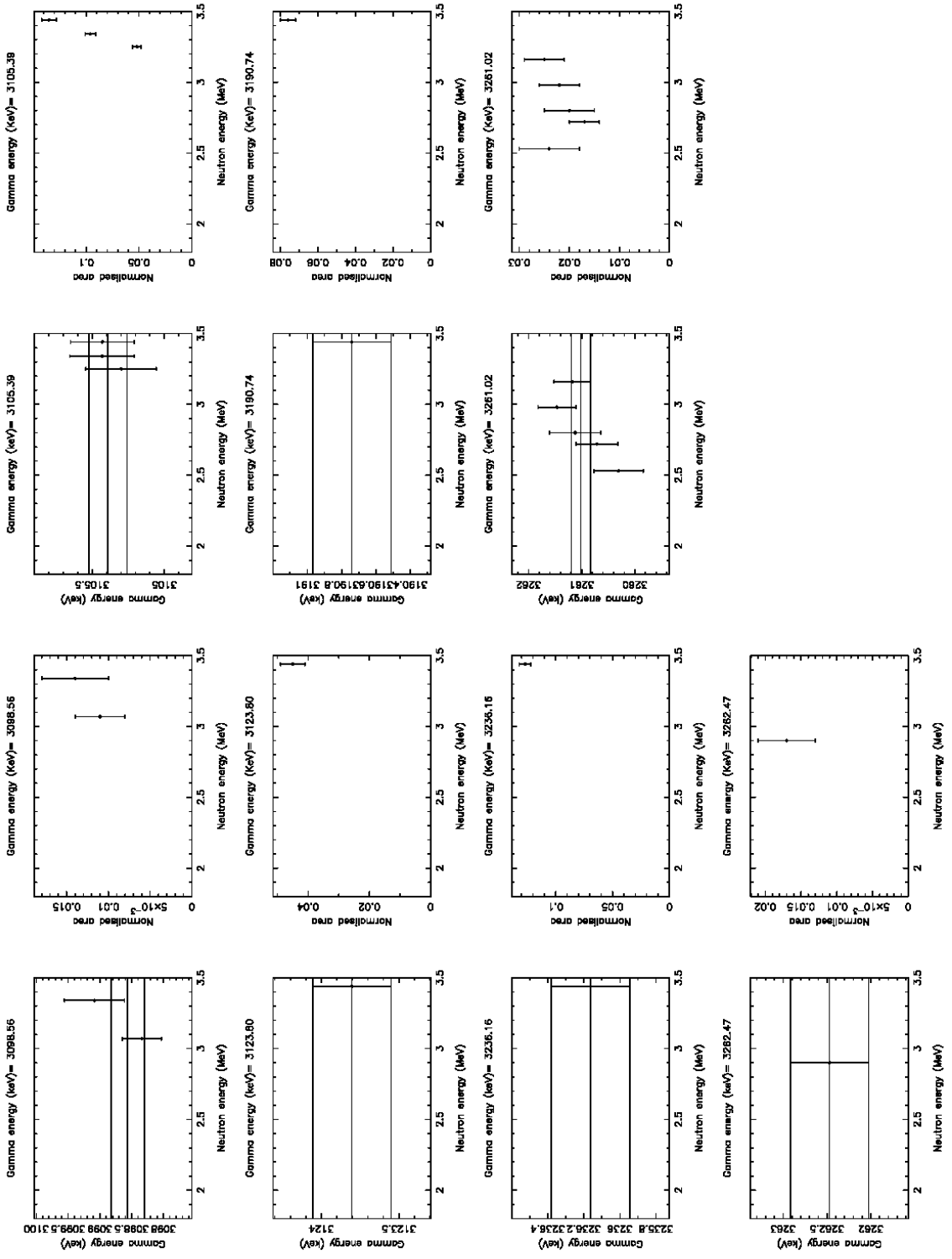
Gamma energy (keV)= 3088.56
Gamma energy (keV)= 3123.80
Gamma energy (keV)= 3236.16
Gamma energy (keV)= 3262.47
Gamma energy (keV)= 3105.39
Gamma energy (keV)= 3190.74
Gamma energy (keV)= 3261.02
Gamma energy (keV)= 3105.38
Neutron energy (MeV)
Normalised area
Gamma energy (keV)

Appendix B: Angular Distributions at 3.4 MeV

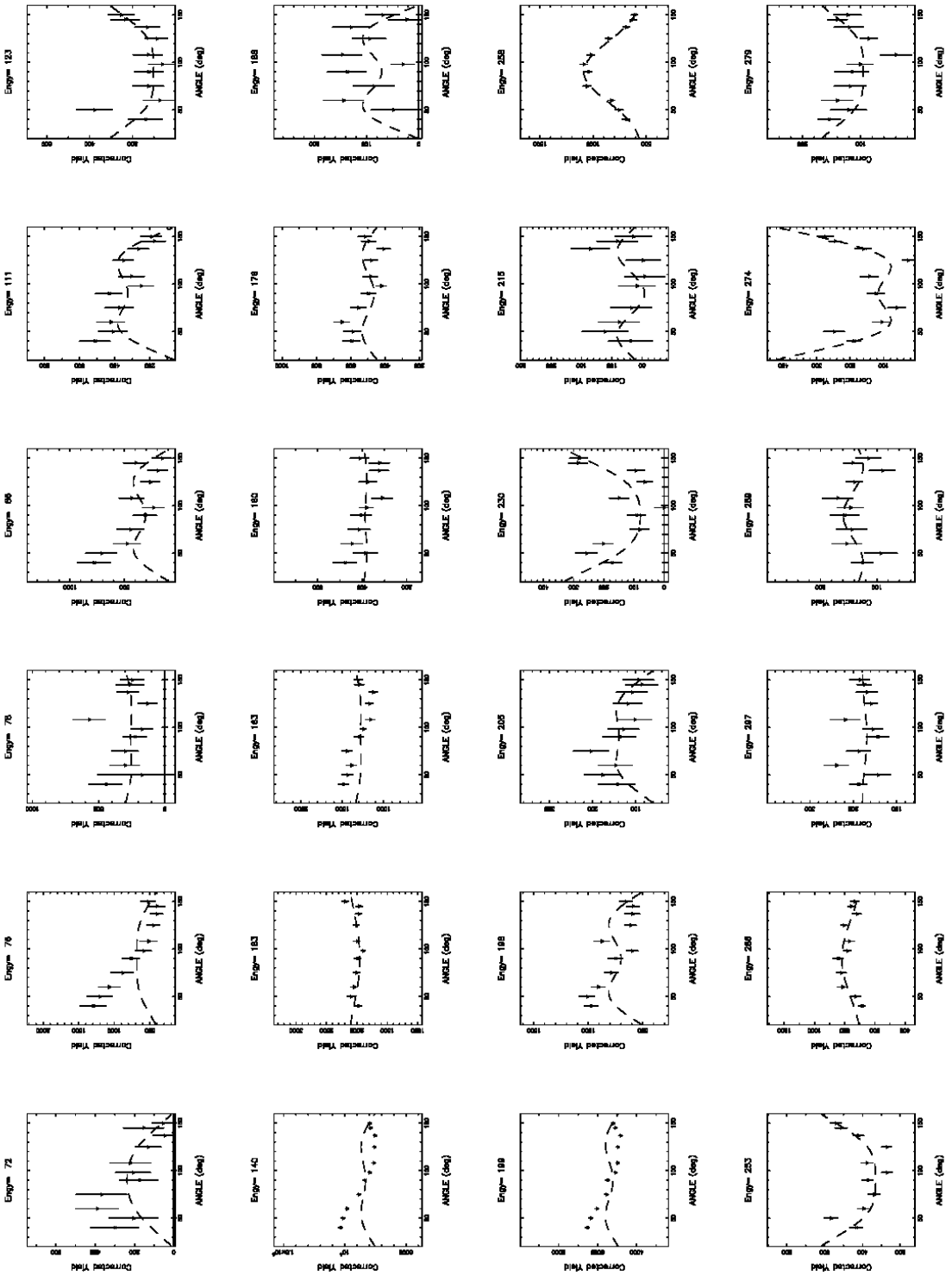
Energy= 72
Energy= 76
Energy= 78
Energy= 86
Energy= 111
Energy= 123
Energy= 140
Energy= 153
Energy= 163
Energy= 165
Energy= 178
Energy= 188
Energy= 199
Energy= 205
Energy= 230
Energy= 235
Energy= 258
Energy= 274
Energy= 253
Energy= 266
Energy= 267
Energy= 269
Energy= 279
Corrected Yield
ANGLE (deg)

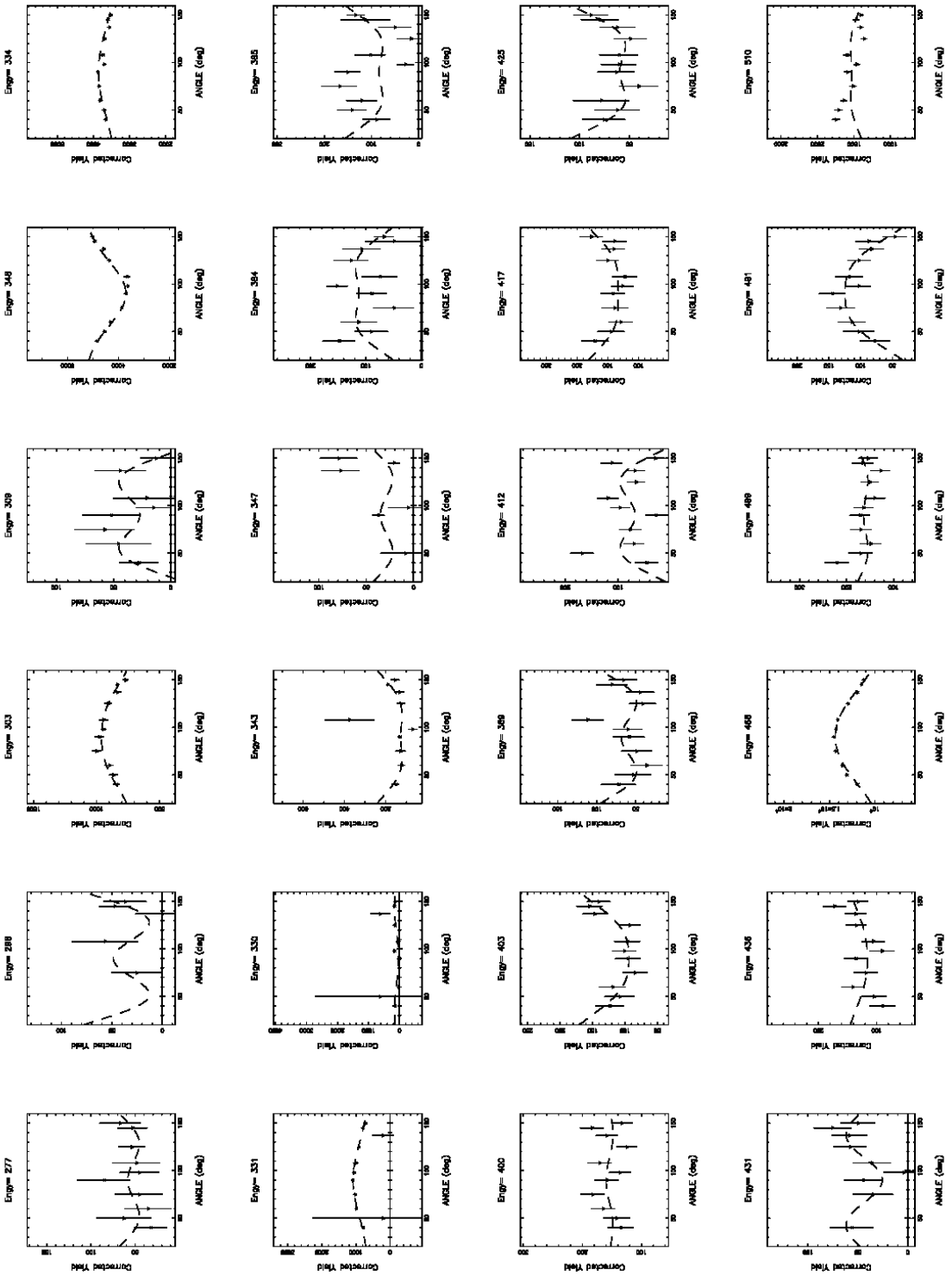
Energy= 277
Energy= 288
Energy= 303
Energy= 309
Energy= 334
Energy= 331
Energy= 330
Energy= 343
Energy= 347
Energy= 348
Energy= 400
Energy= 403
Energy= 359
Energy= 412
Energy= 417
Energy= 385
Energy= 431
Energy= 436
Energy= 466
Energy= 489
Energy= 481
Energy= 510
Corrected Yield
ANGLE (deg)

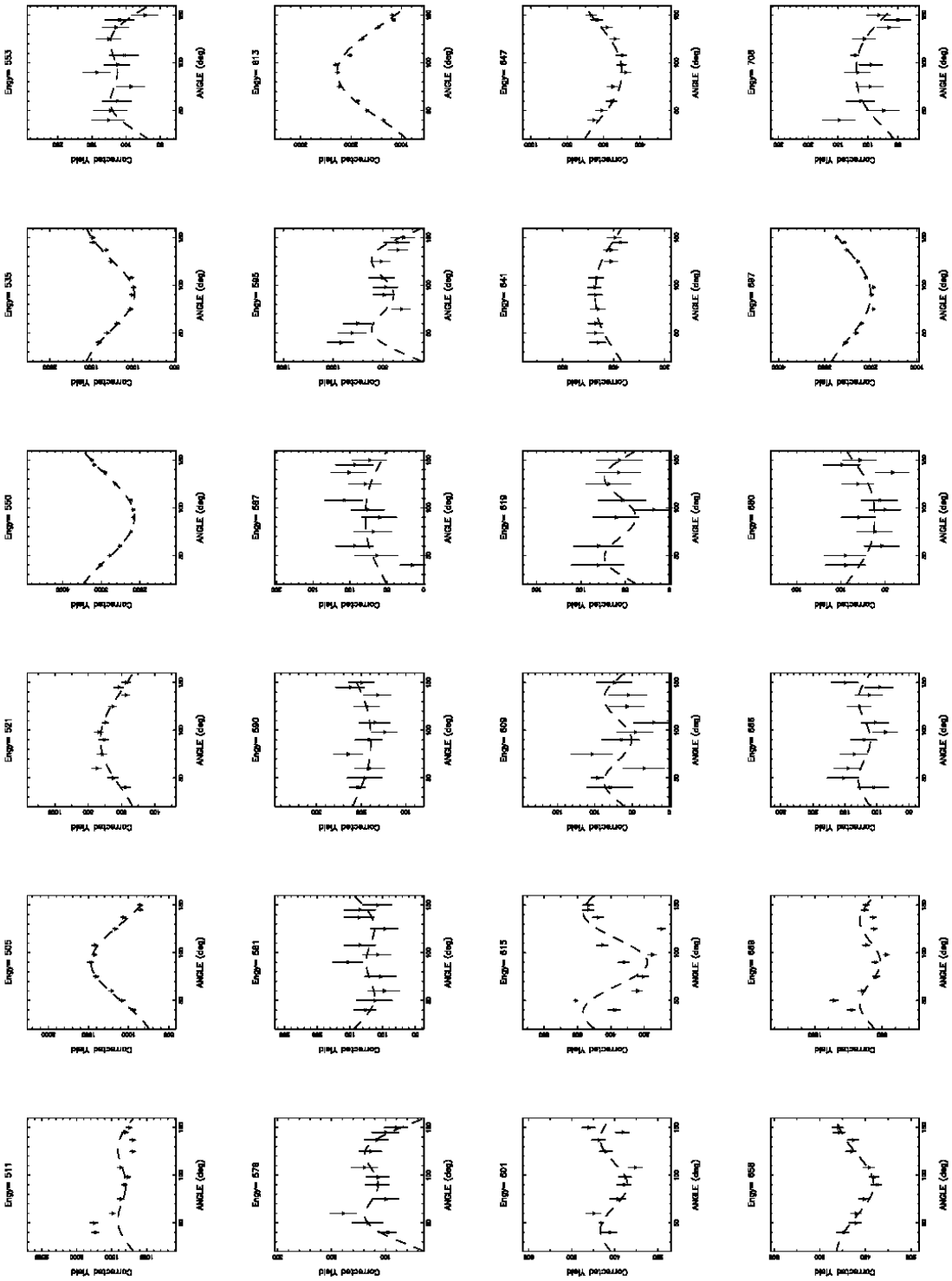
Engy= 511
Engy= 505
Engy= 521
Engy= 535
Engy= 553
Engy= 578
Engy= 561
Engy= 590
Engy= 587
Engy= 585
Engy= 613
Engy= 601
Engy= 615
Engy= 609
Engy= 619
Engy= 641
Engy= 647
Engy= 658
Engy= 669
Engy= 665
Engy= 680
Engy= 697
Engy= 708
Corrected Yield
ANGLE (deg)

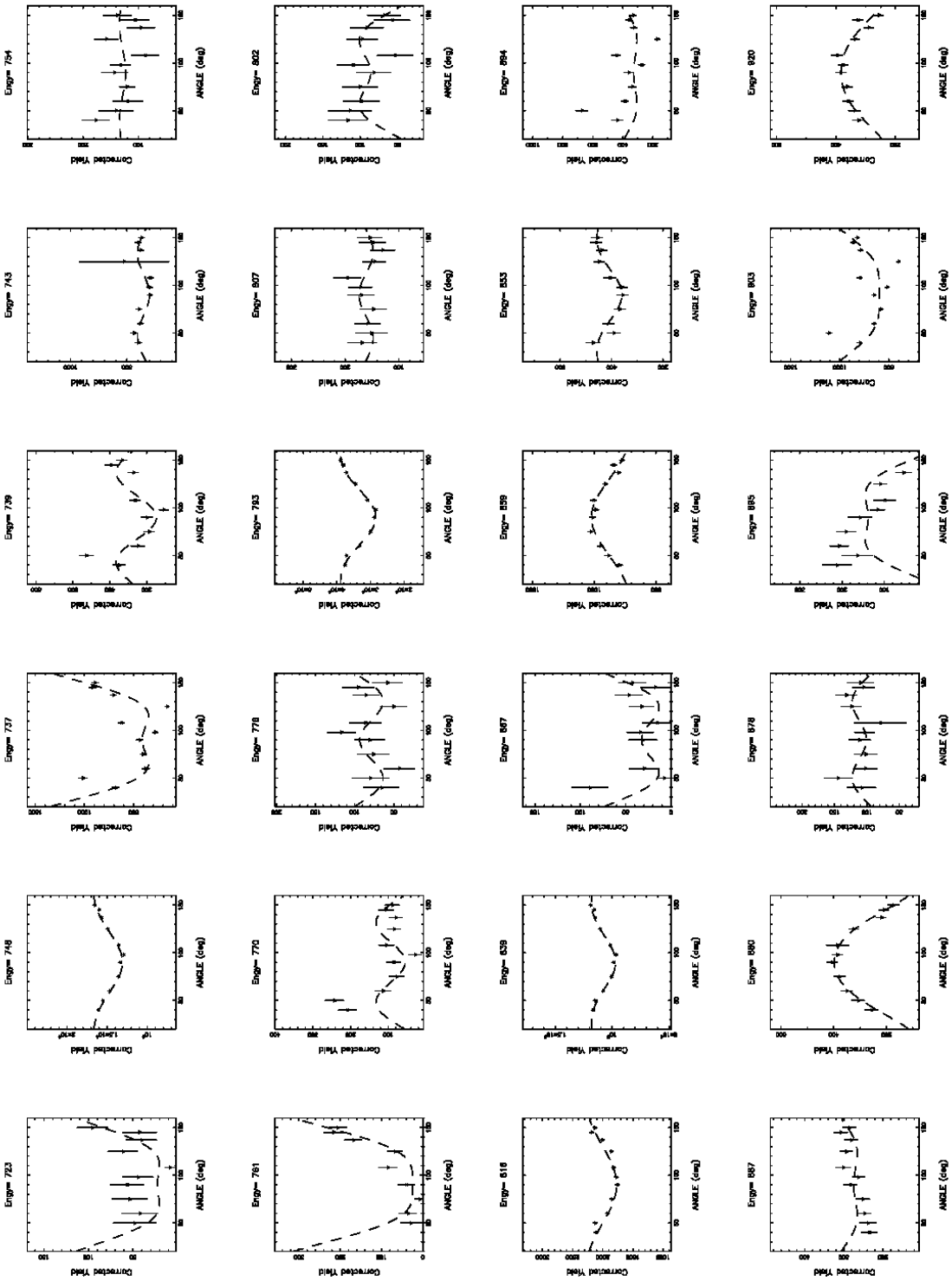
Engy= 754
Engy= 802
Engy= 854
Engy= 920
Engy= 743
Engy= 807
Engy= 853
Engy= 903
Engy= 739
Engy= 783
Engy= 839
Engy= 885
Engy= 737
Engy= 778
Engy= 847
Engy= 878
Engy= 748
Engy= 770
Engy= 839
Engy= 880
Engy= 723
Engy= 761
Engy= 818
Engy= 867
Corrected Yield
ANGLE (deg)

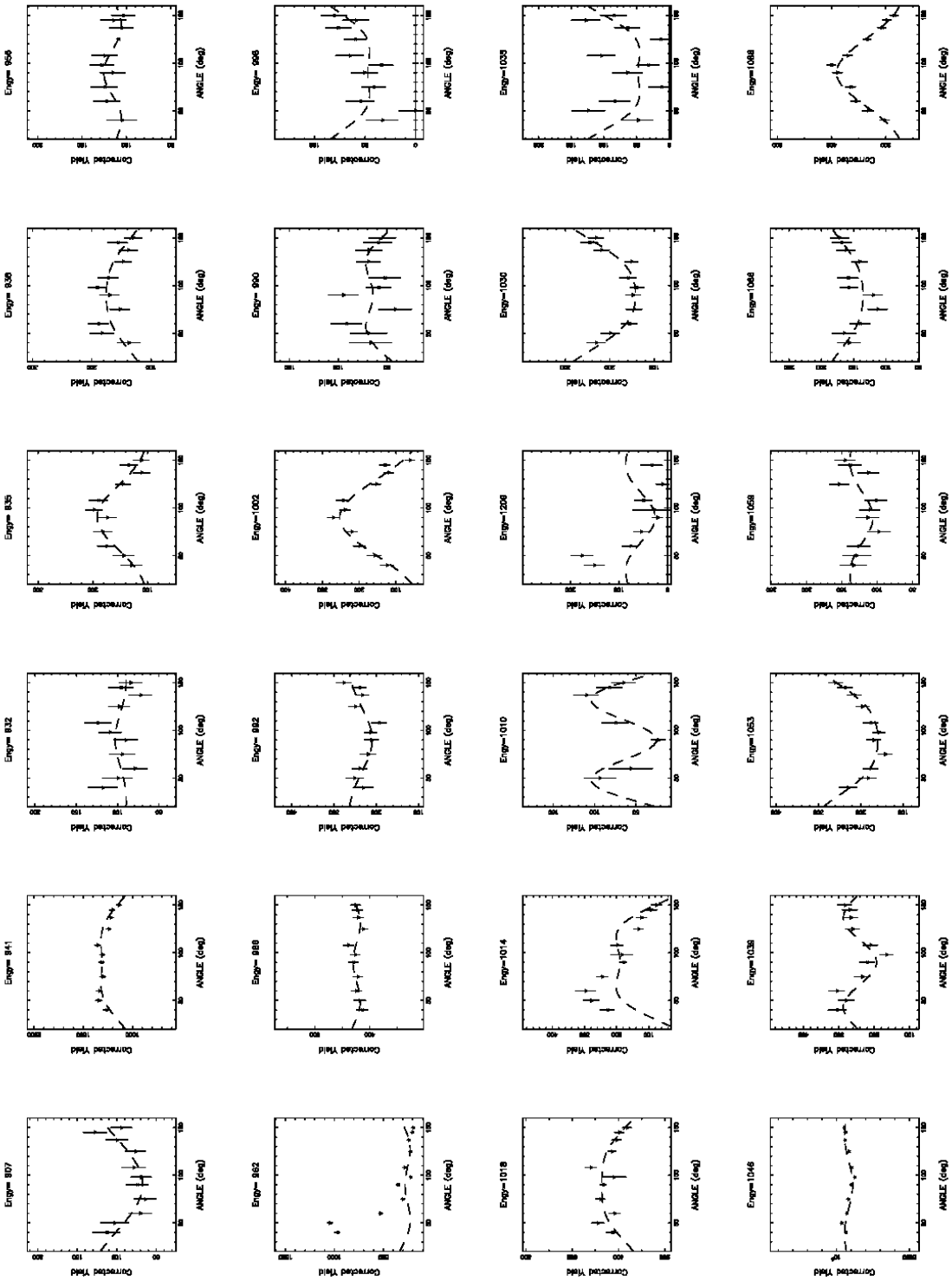
Engy= 907
Engy= 832
Engy= 835
Engy= 836
Engy= 956
Engy= 841
Engy= 862
Engy=1002
Engy= 990
Engy= 996
Engy=1014
Engy=1010
Engy=1206
Engy=1030
Engy=1033
Engy=1038
Engy=1053
Engy=1058
Engy=1066
Engy=1088
Engy=1346
Corrected Yield
ANGLE (deg)

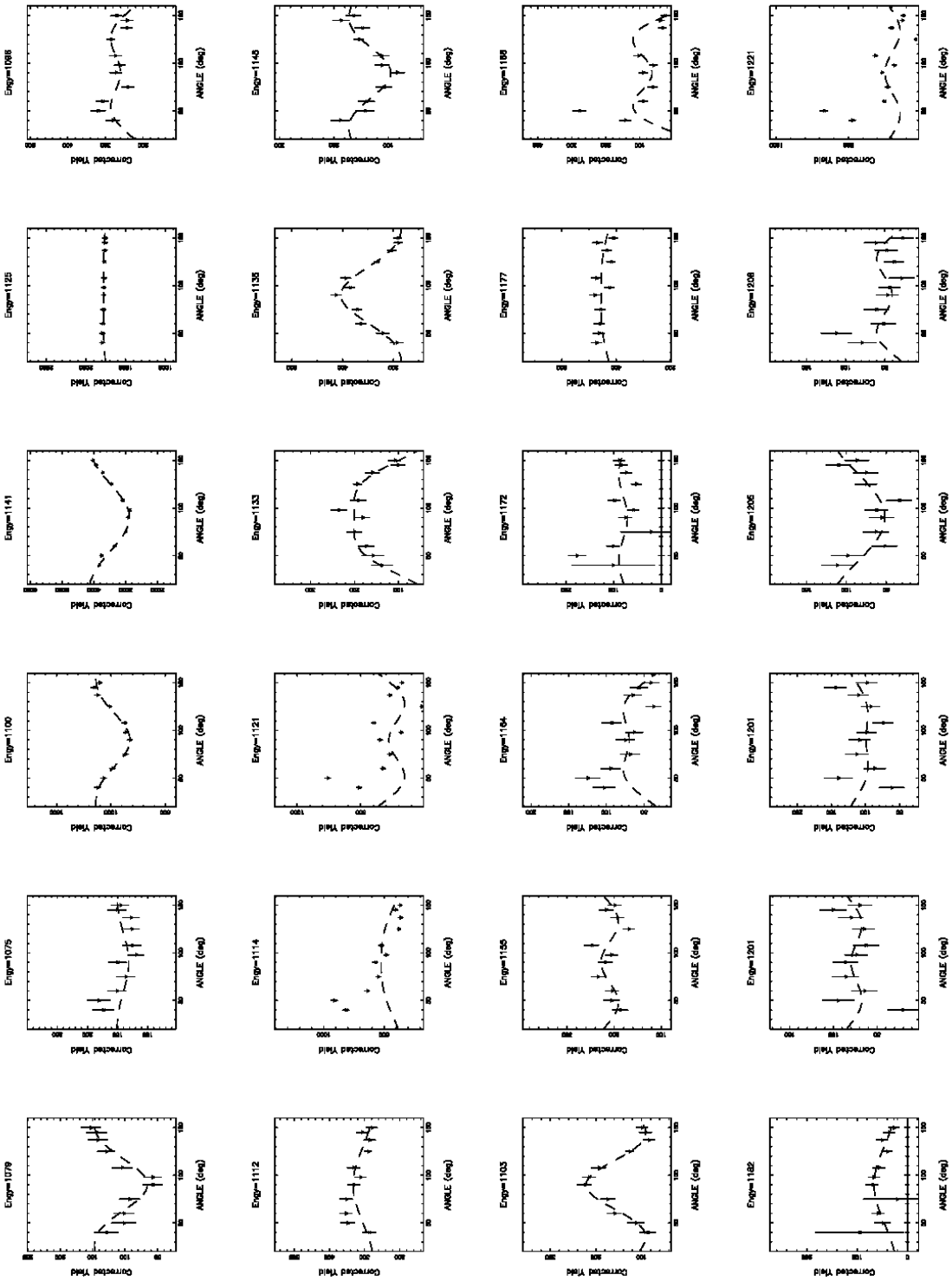
Engy=1088
Engy=1148
Engy=1188
Engy=1221
Engy=1125
Engy=1135
Engy=1177
Engy=1208
Engy=1141
Engy=1133
Engy=1172
Engy=1205
Engy=1100
Engy=1121
Engy=1164
Engy=1201
Engy=1079
Engy=1114
Engy=1155
Engy=1201
Engy=1078
Engy=1112
Engy=1103
Engy=1182
Corrected Yield
ANGLE (deg)

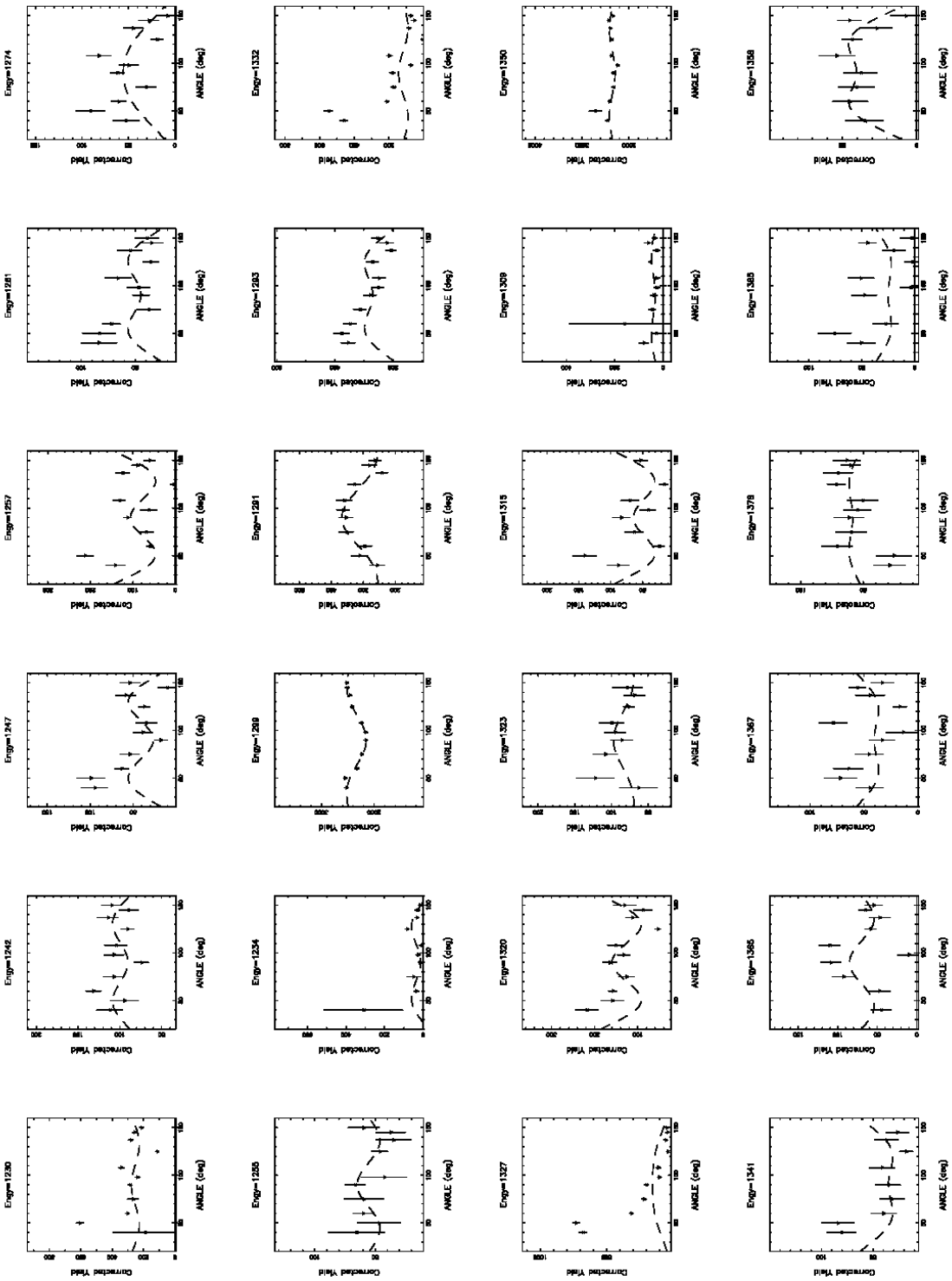
Engy=1230
Engy=1242
Engy=1247
Engy=1257
Engy=1261
Engy=1274
Engy=1255
Engy=1234
Engy=1269
Engy=1291
Engy=1283
Engy=1332
Engy=1327
Engy=1320
Engy=1315
Engy=1309
Engy=1350
Engy=1341
Engy=1365
Engy=1367
Engy=1378
Engy=1385
Engy=1358
Corrected Yield
ANGLE (deg)

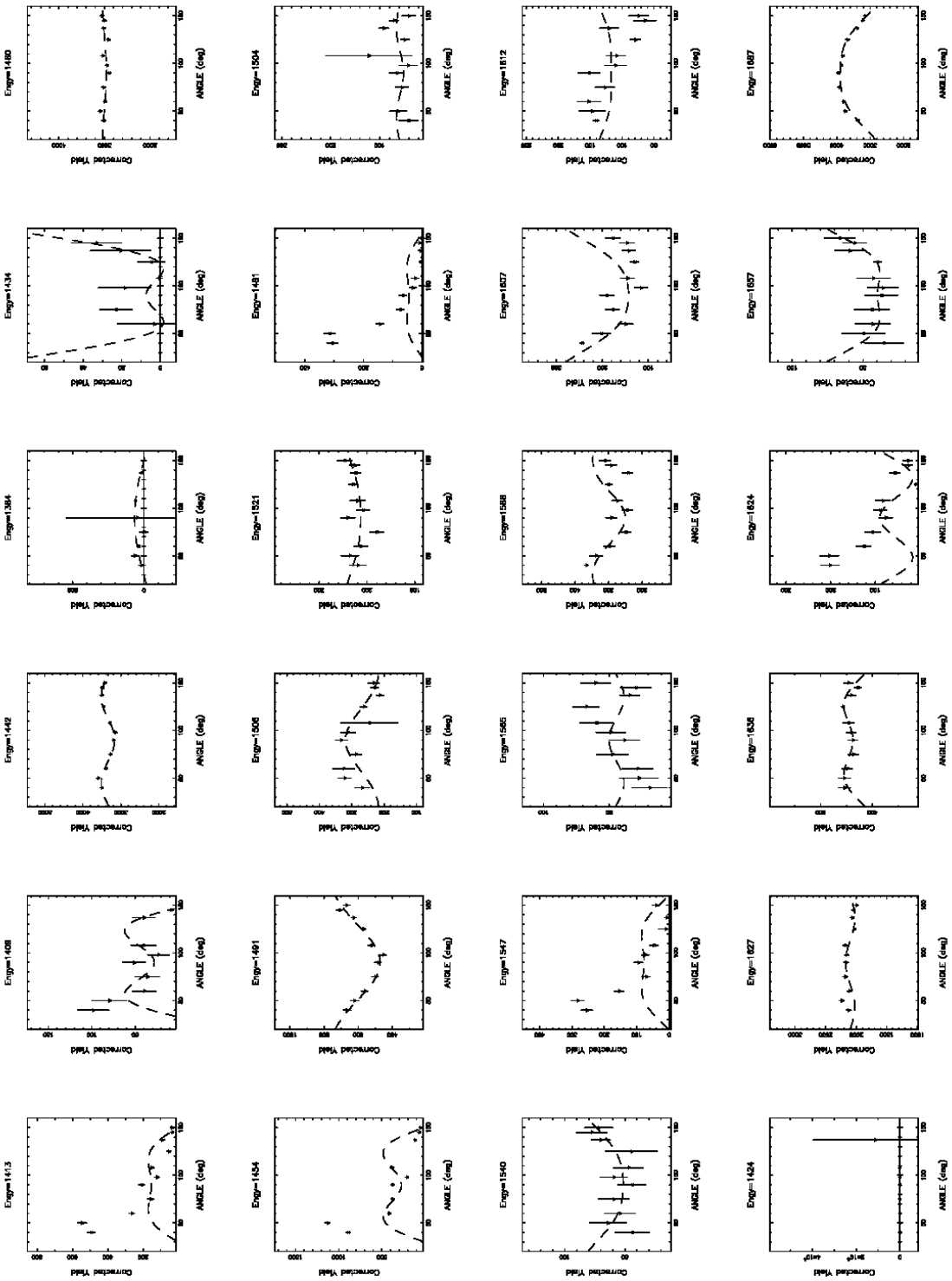
Engy=1413
Engy=1408
Engy=1402
Engy=1384
Engy=1434
Engy=1460
Engy=1454
Engy=1461
Engy=1506
Engy=1521
Engy=1481
Engy=1504
Engy=1540
Engy=1547
Engy=1565
Engy=1588
Engy=1577
Engy=1612
Engy=1624
Engy=1627
Engy=1638
Engy=1624
Engy=1657
Engy=1687
Corrected Yield
ANGLE (deg)

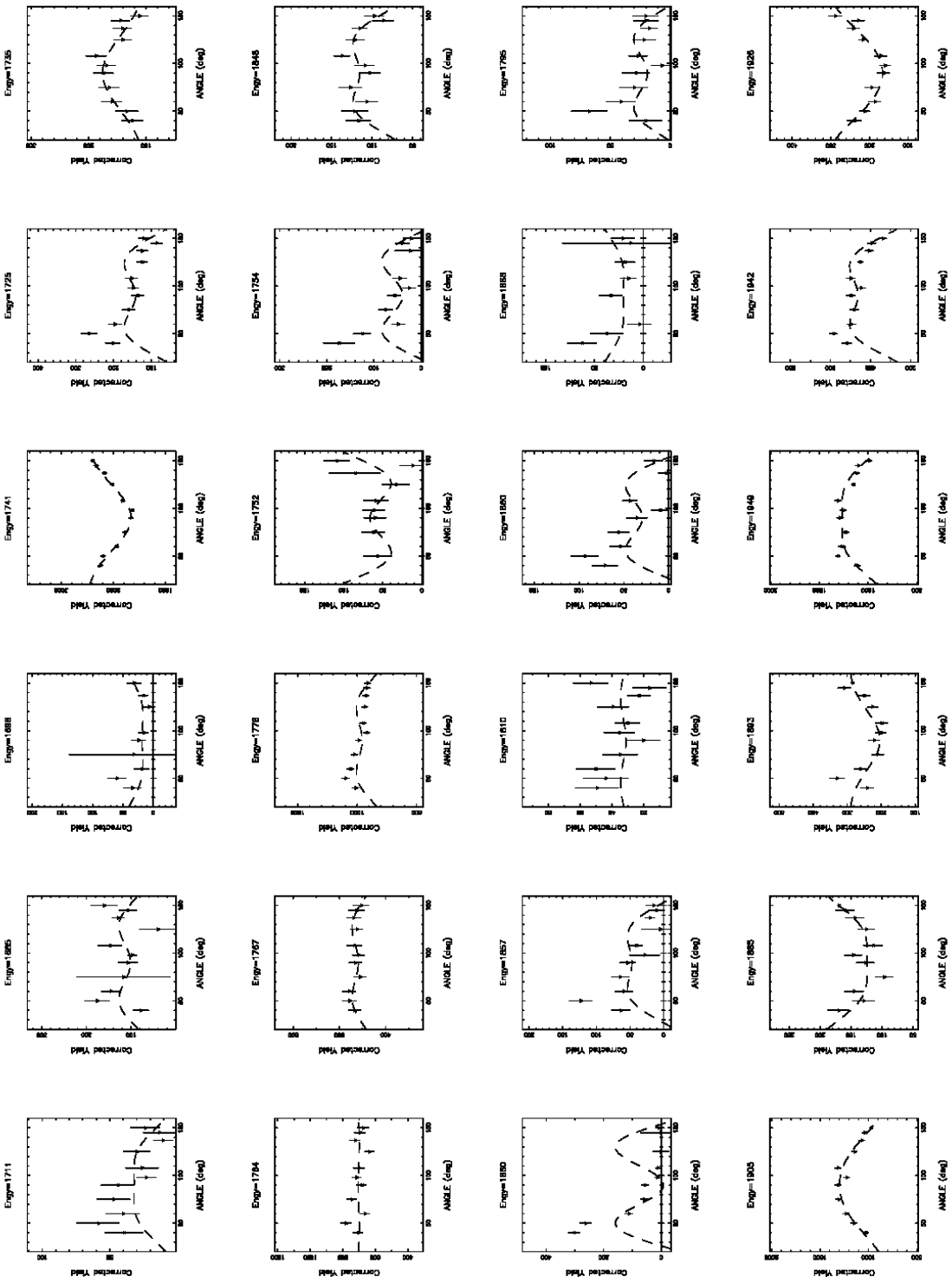
Engy=1711
Engy=1764
Engy=1817
Engy=1870
Engy=1923
Engy=1976
Engy=2029
Engy=1695
Engy=1747
Engy=1800
Engy=1853
Engy=1906
Engy=1959
Engy=2012
Engy=1678
Engy=1731
Engy=1784
Engy=1837
Engy=1890
Engy=1943
Engy=1996
Engy=1741
Engy=1794
Engy=1847
Engy=1900
Engy=1953
Engy=2006
Engy=2059
Engy=1725
Engy=1778
Engy=1831
Engy=1884
Engy=1937
Engy=1990
Engy=2043
Engy=1711
Engy=1764
Engy=1817
Engy=1870
Engy=1923
Engy=1976
Engy=2029
Corrected Yield
ANGLE (deg)

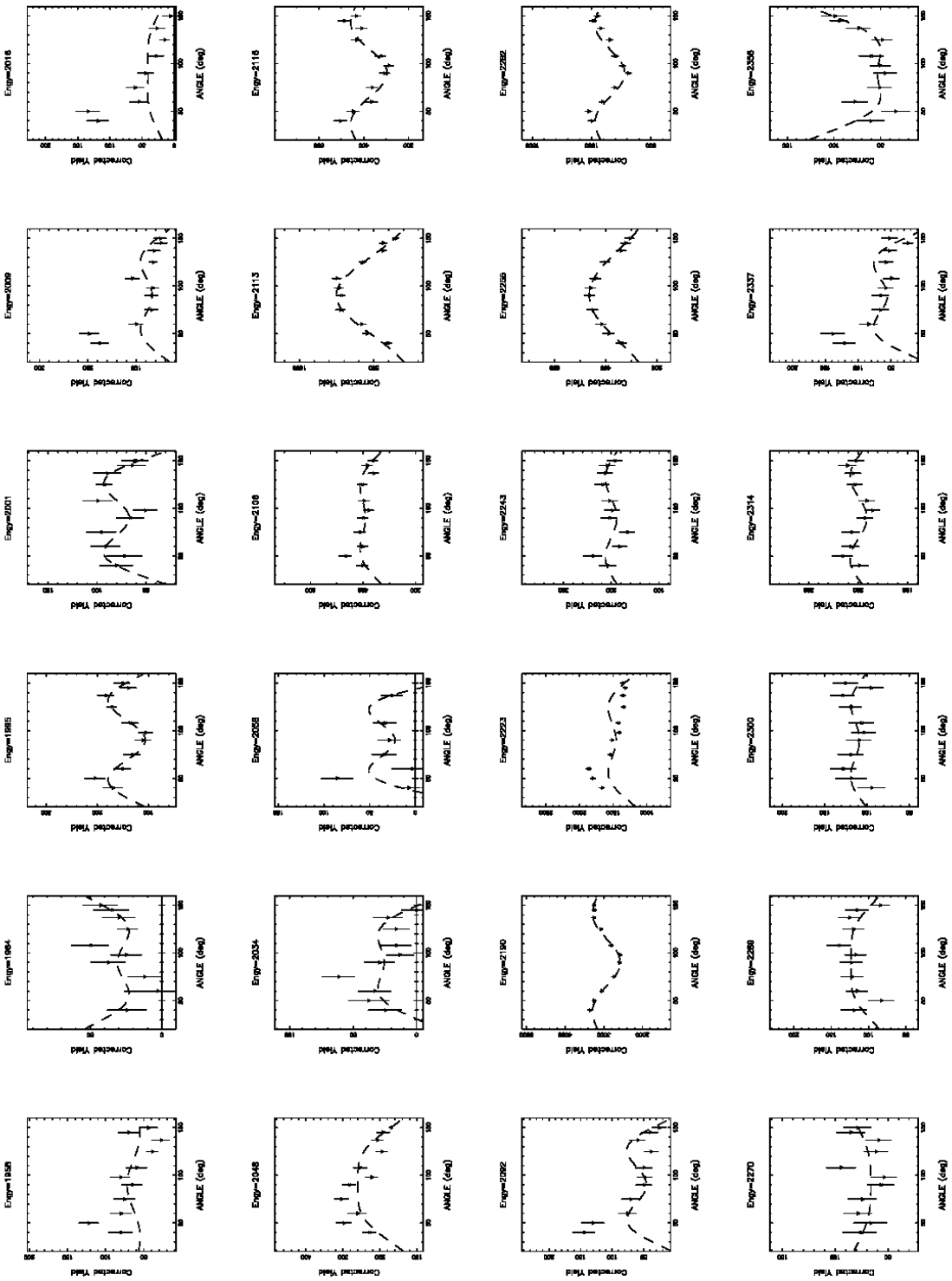
Engy=1838
Engy=1864
Engy=1885
Engy=2001
Engy=2009
Engy=2016
Engy=2034
Engy=2058
Engy=2108
Engy=2113
Engy=2116
Engy=2190
Engy=2223
Engy=2243
Engy=2255
Engy=2282
Engy=2292
Engy=2300
Engy=2314
Engy=2337
Engy=2355
Engy=2388
Engy=2270
Corrected Yield
ANGLE (deg)

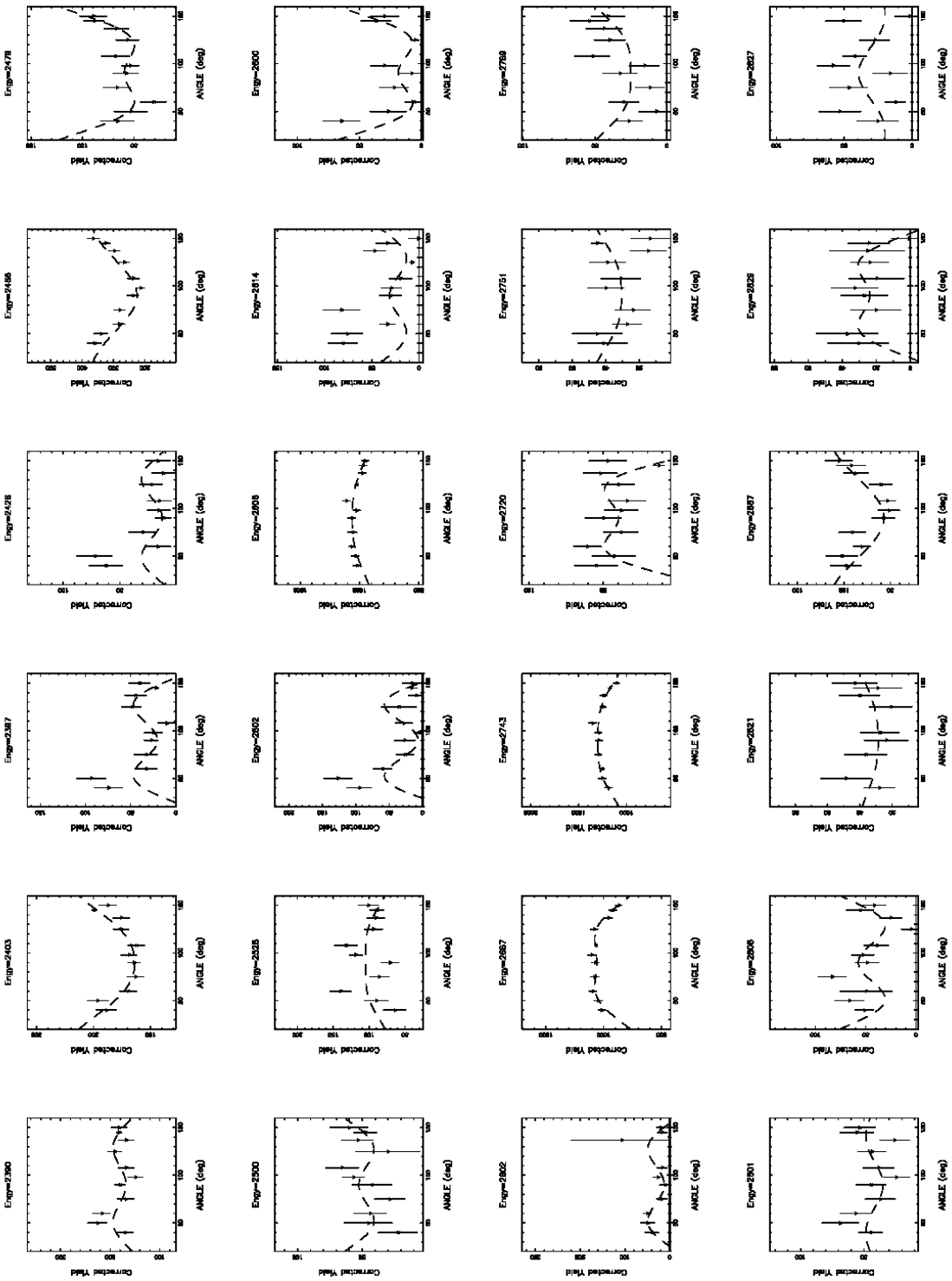
Engy=2478
Engy=2627
Engy=2769
Engy=2600
Engy=2495
Engy=2514
Engy=2751
Engy=2628
Engy=2426
Engy=2608
Engy=2720
Engy=2657
Engy=2387
Engy=2602
Engy=2743
Engy=2621
Engy=2403
Engy=2535
Engy=2667
Engy=2606
Engy=2380
Engy=2500
Engy=2602
Engy=2501
Corrected Yield
ANGLE (deg)

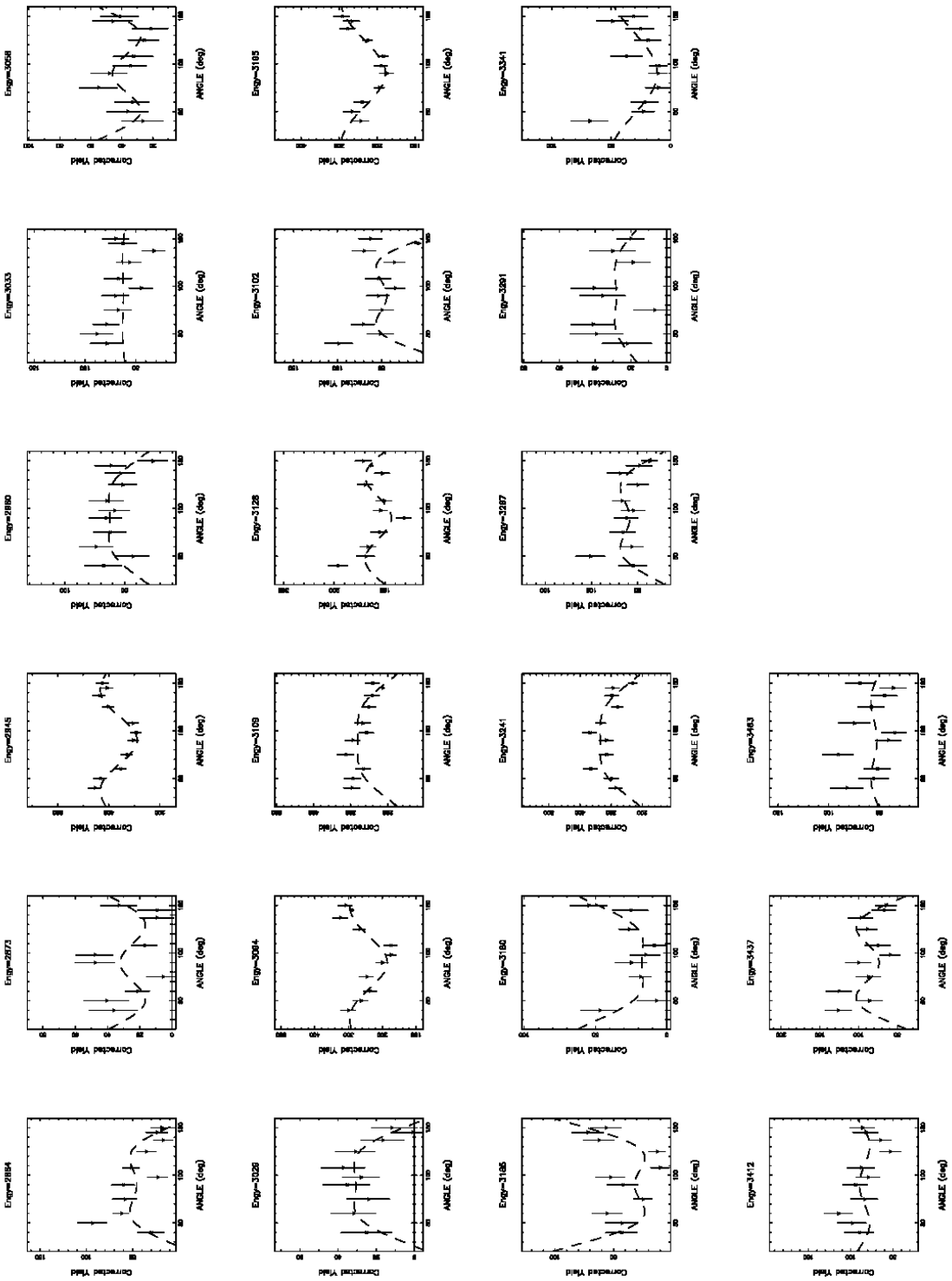
Engy=2824
Engy=2873
Engy=2845
Engy=2880
Engy=3033
Engy=3058
Engy=3026
Engy=3064
Engy=3109
Engy=3128
Engy=3102
Engy=3185
Engy=3185
Engy=3180
Engy=3241
Engy=3287
Engy=3291
Engy=3341
Engy=3412
Engy=3437
Engy=3463
Corrected Yield
ANGLE (deg)

Appendix C: Angular Distributions at 2.2 MeV

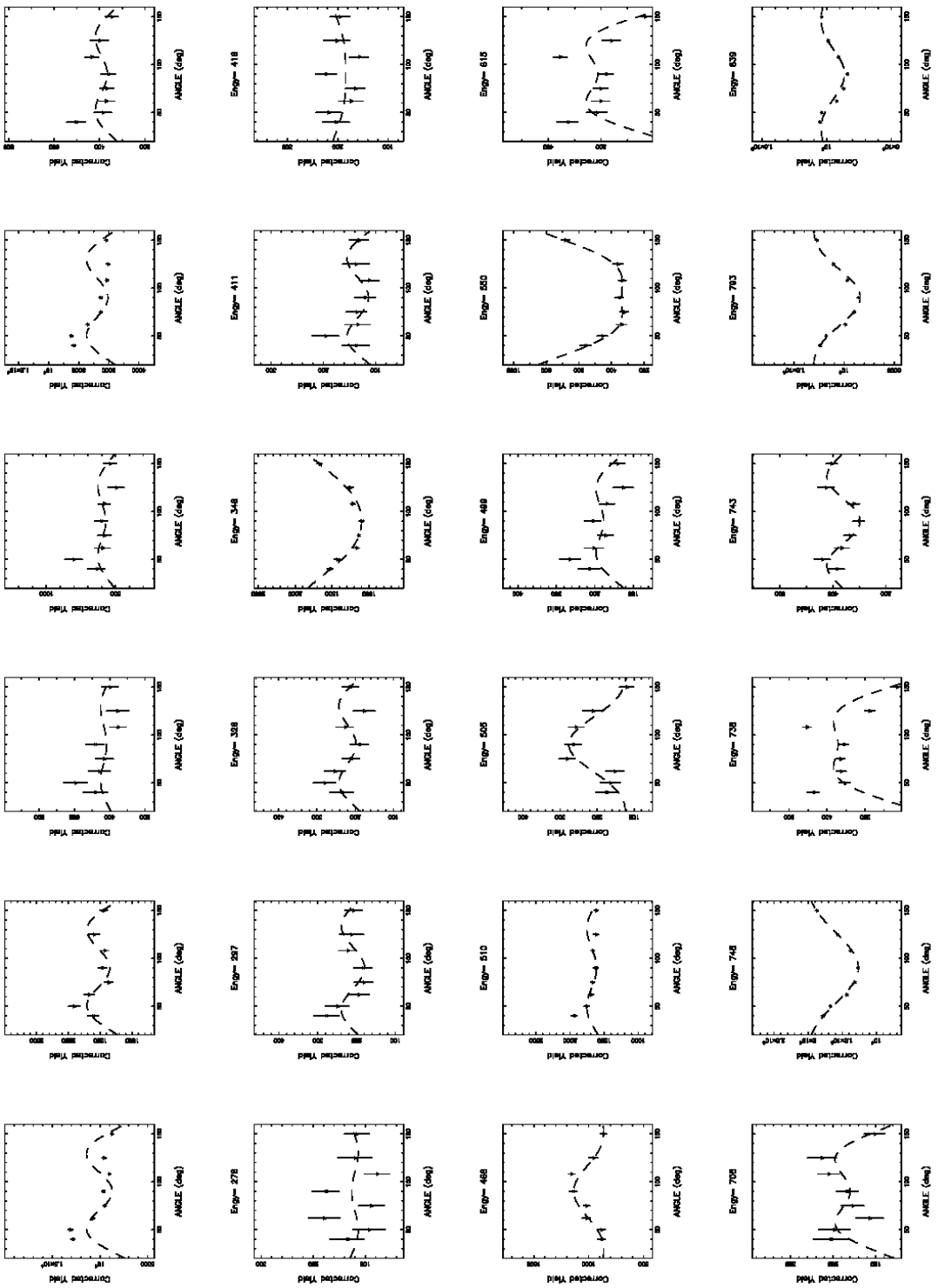
Engy= 140
Engy= 163
Engy= 190
Engy= 175
Engy= 188
Engy= 253
Engy= 278
Engy= 297
Engy= 328
Engy= 348
Engy= 411
Engy= 418
Engy= 468
Engy= 510
Engy= 505
Engy= 499
Engy= 550
Engy= 615
Engy= 708
Engy= 748
Engy= 735
Engy= 743
Engy= 783
Engy= 839
Corrected Yield
ANGLE (deg)

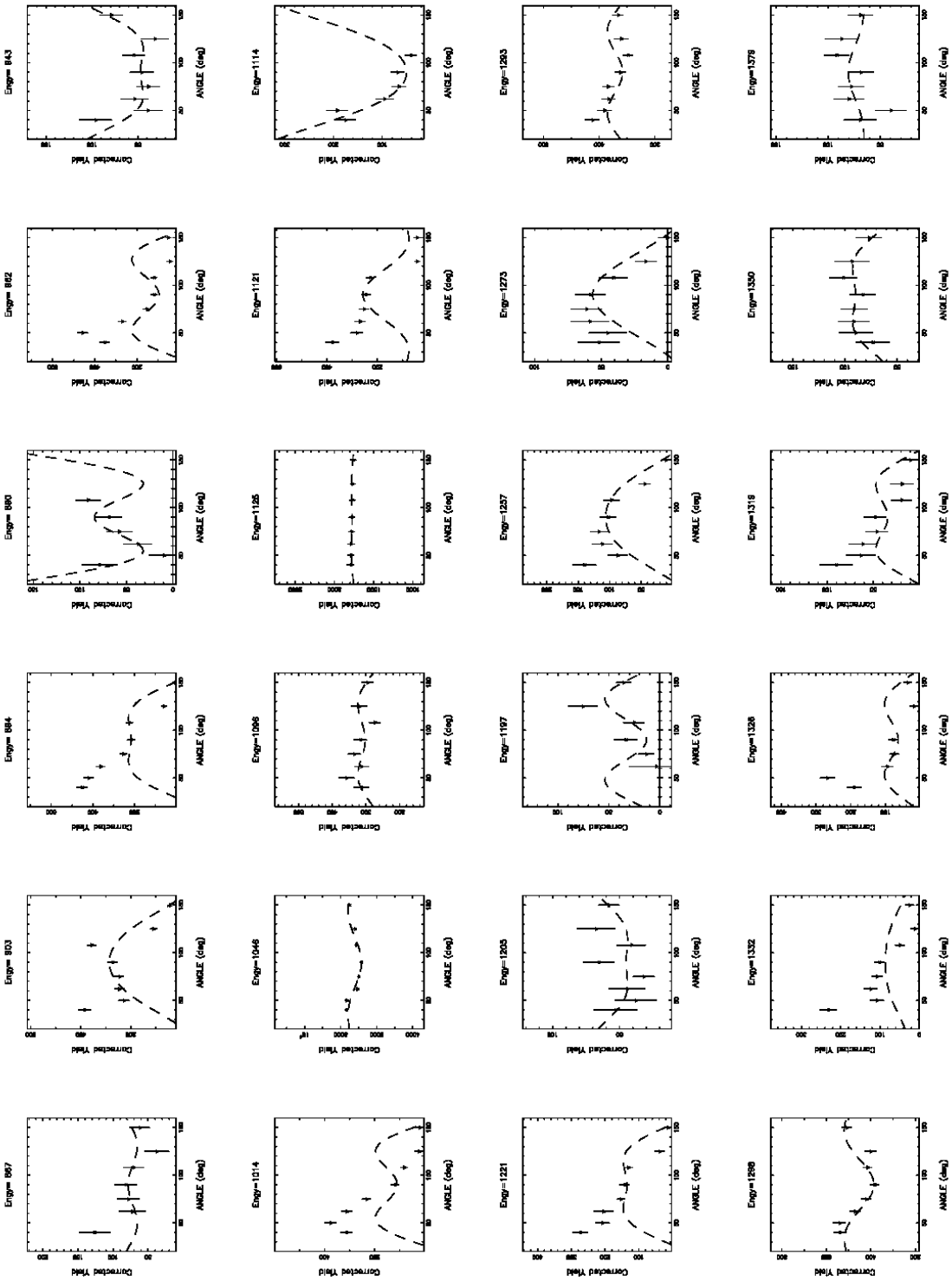
Engy= 843
Engy= 852
Engy= 880
Engy= 884
Engy= 903
Engy= 957
Engy=1114
Engy=1121
Engy=1125
Engy=1096
Engy=1046
Engy=1014
Engy=1293
Engy=1273
Engy=1257
Engy=1197
Engy=1205
Engy=1221
Engy=1579
Engy=1330
Engy=1319
Engy=1326
Engy=1332
Engy=1298
Corrected Yield
ANGLE (deg)

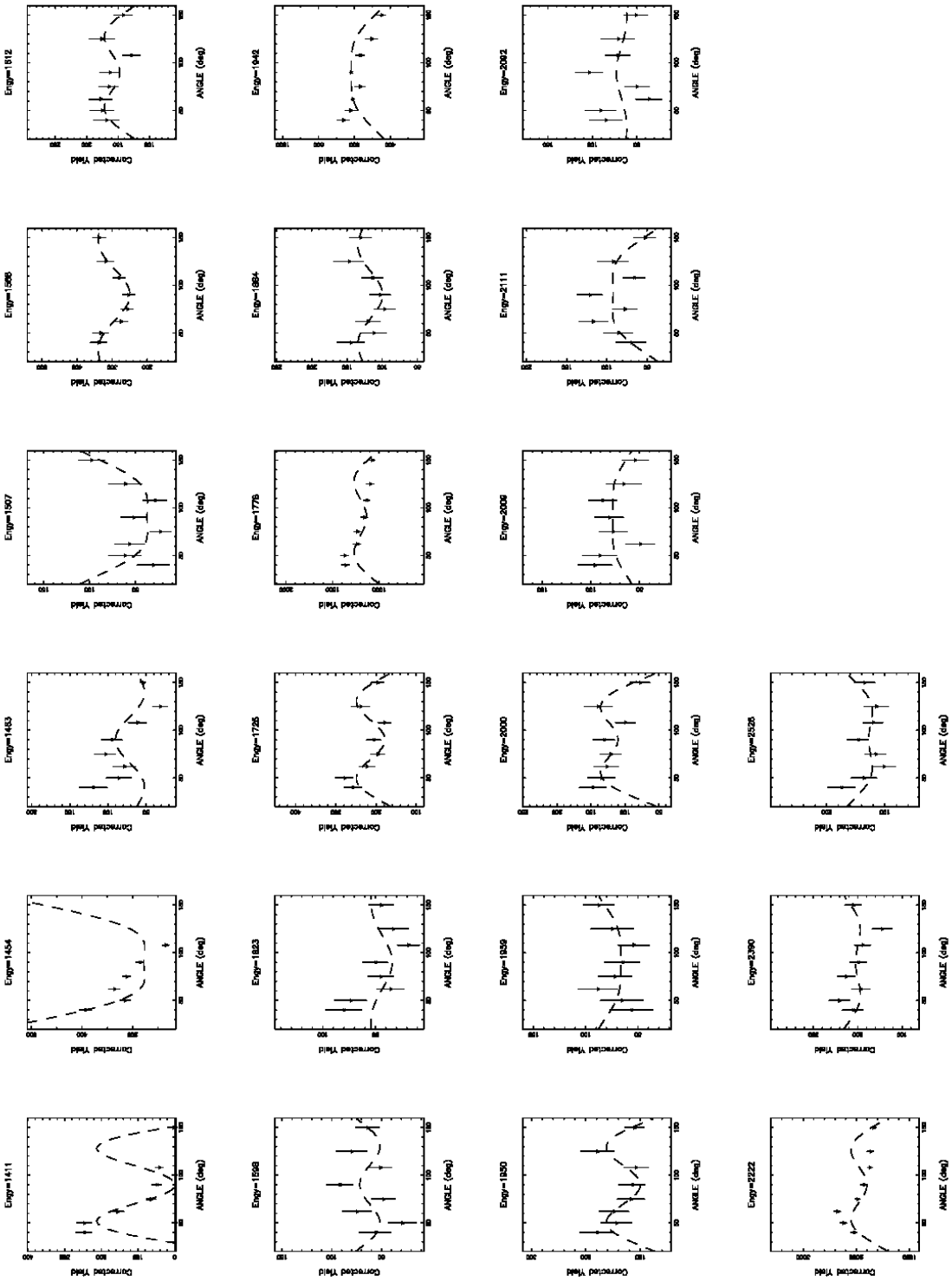
Engy=1411
Engy=1454
Engy=1463
Engy=1507
Engy=1595
Engy=1612
Engy=1598
Engy=1823
Engy=1725
Engy=1776
Engy=1884
Engy=1942
Engy=1850
Engy=1939
Engy=2000
Engy=2006
Engy=2111
Engy=2092
Engy=2222
Engy=2390
Engy=2535
Corrected Yield
ANGLE (deg)

Appendix D: Doppler Shifts at 3.4 MeV

As a preface to the collection of Doppler-shift figures, the reader is reminded that the energy shifts involved are tiny. In the centroid equation

$$E_\gamma(\theta)=E_\gamma^0 [\ 1 + F\beta \cos(\theta)\ ] , \qquad [1]$$

the maximum value for the product $F\beta$ is 0.00064, or, we are looking for differences in energy << 0.06%. The HPGe detector resolution is 2.2 keV. As a result, it is impossible to observe shifts for gamma rays with energies below ~ 900 keV and any scatter in those plots is meaningless.

Strong peaks in the spectrum generally provide the best information about the lifetime of the state. For weaker peaks, the point scatter in the plot is a result of poor statistics. Point scatter is also large when there are two close peaks in the spectrum.

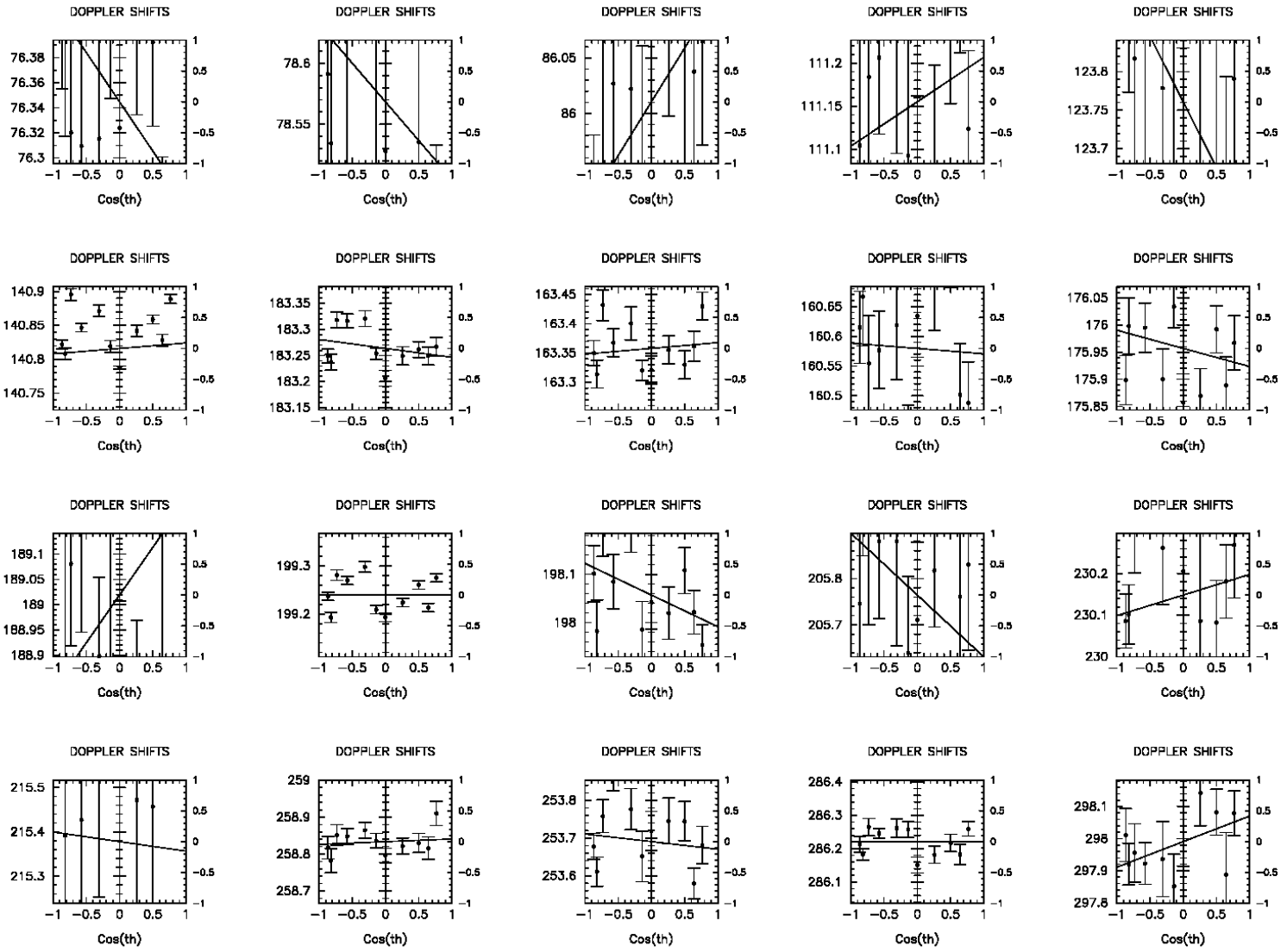
DOPPLER SHIFTS
76.38
76.36
76.34
76.32
76.3
78.6
78.55
86.05
86
111.2
111.15
111.1
123.8
123.75
123.7
140.9
140.85
140.8
140.75
183.35
183.3
183.25
183.2
183.15
163.45
163.4
163.35
163.3
160.65
160.6
160.55
160.5
176.05
176
175.95
175.9
175.85
189.1
189.05
189
188.95
188.9
199.3
199.2
198.1
198
205.8
205.7
230.2
230.1
230
215.5
215.4
215.3
259
258.9
258.8
258.7
253.8
253.7
253.6
286.4
286.3
286.2
286.1
298.1
298
297.9
297.8
−1 −0.5 0 0.5 1
1 0.5 0 −0.5 −1
Cos(th)

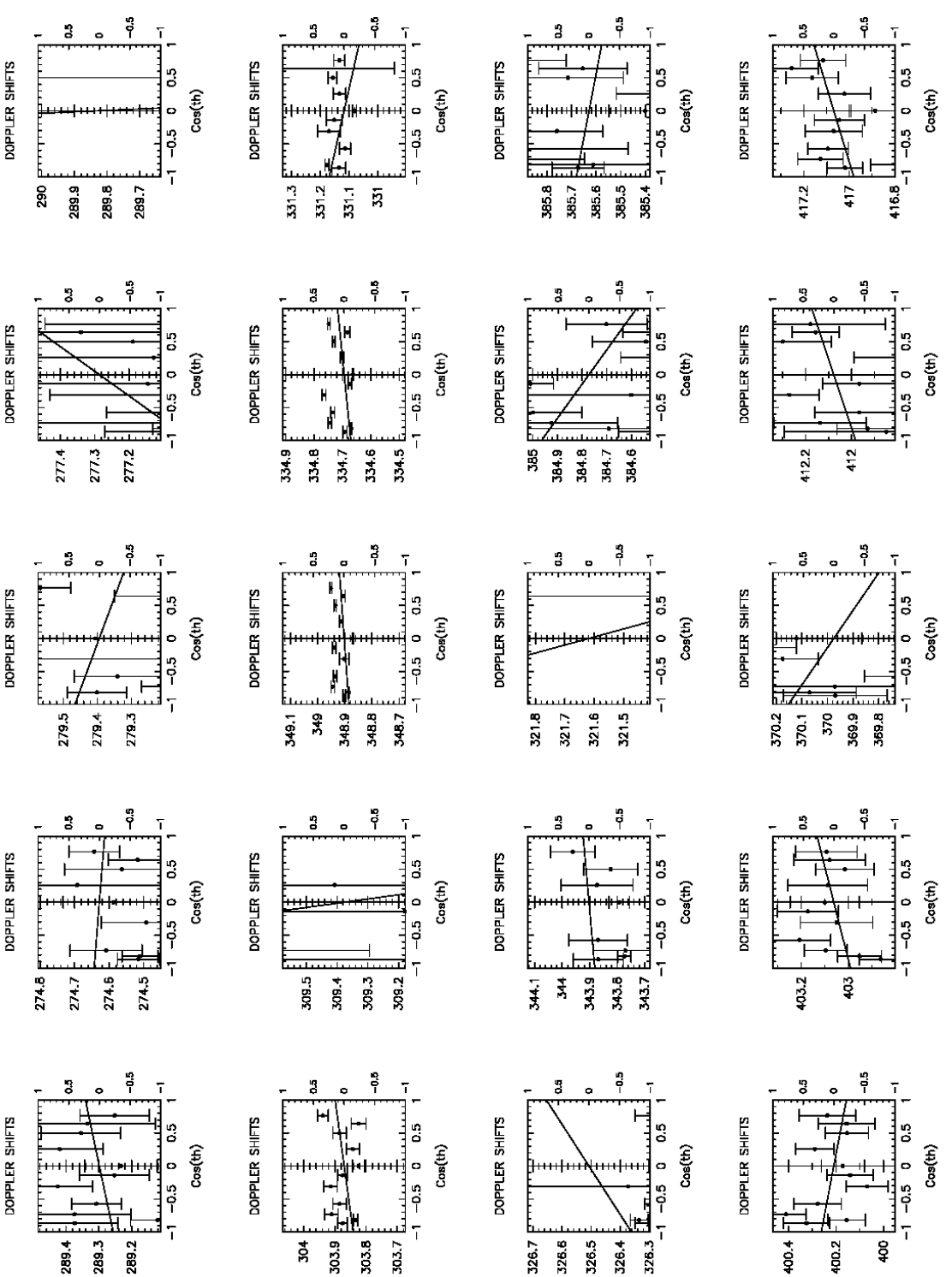
DOPPLER SHIFTS
Cos(th)

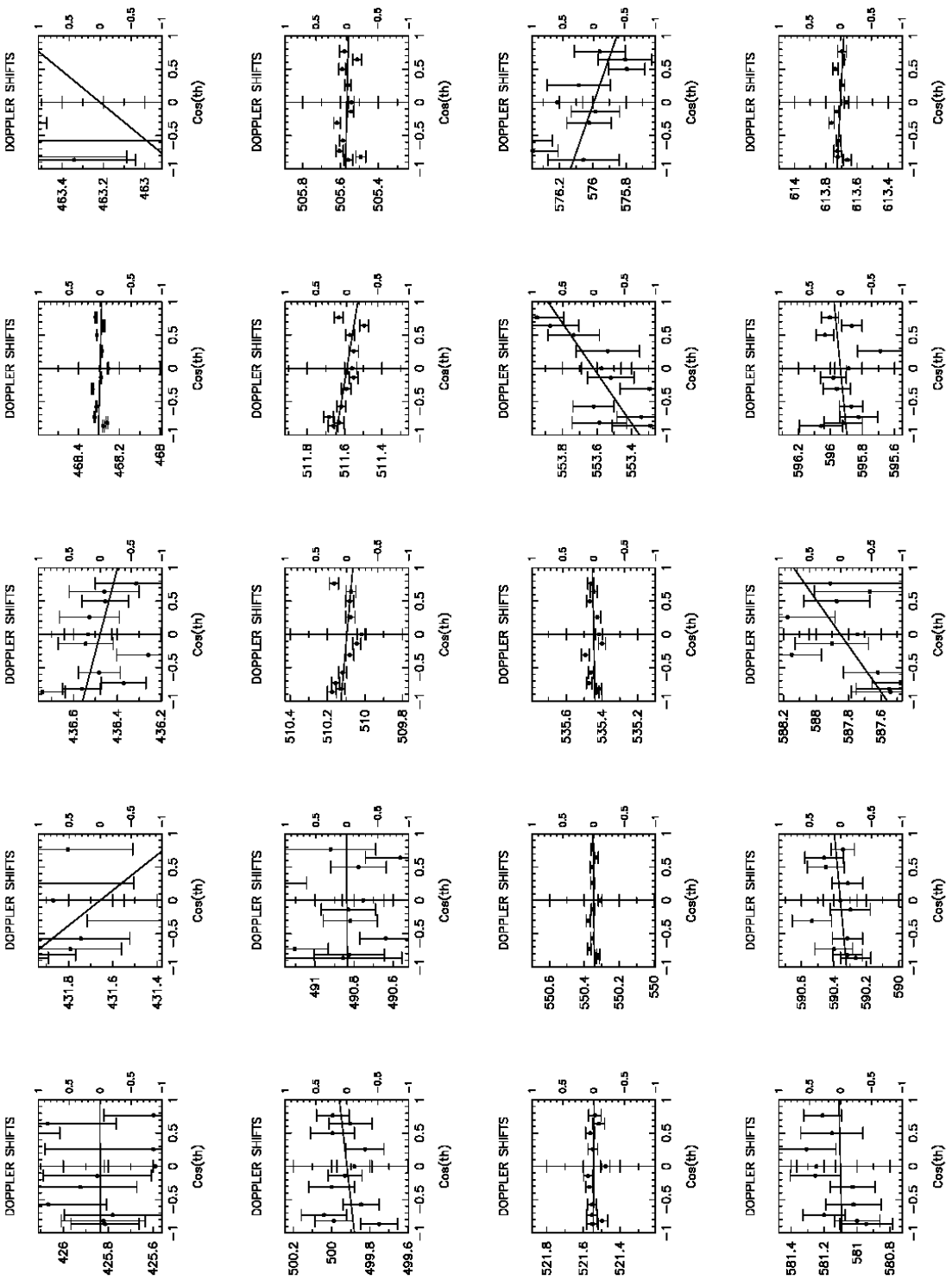
DOPPLER SHIFTS
Cos(th)

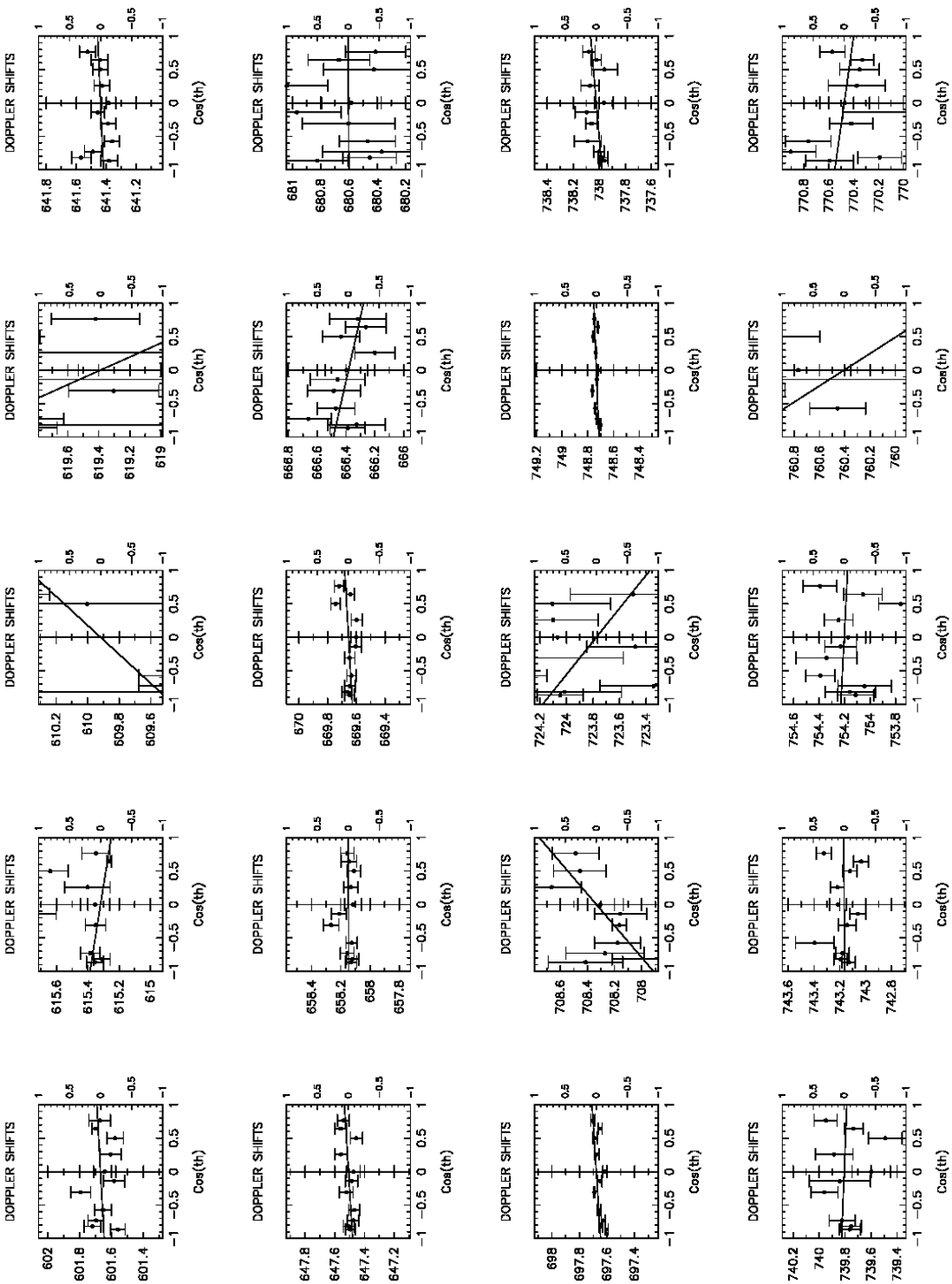
DOPPLER SHIFTS
Cos(th)

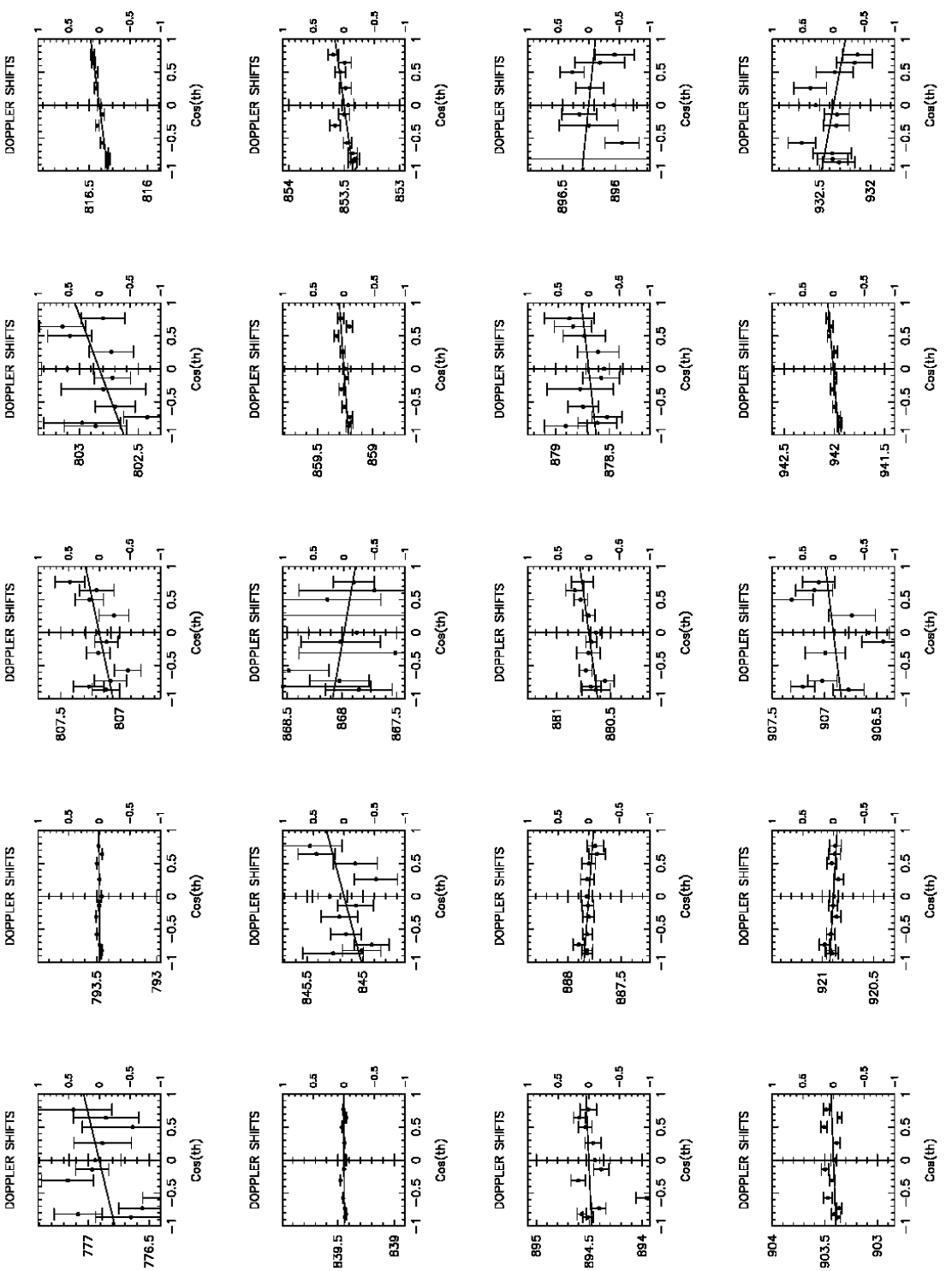
DOPPLER SHIFTS
Cos(th)

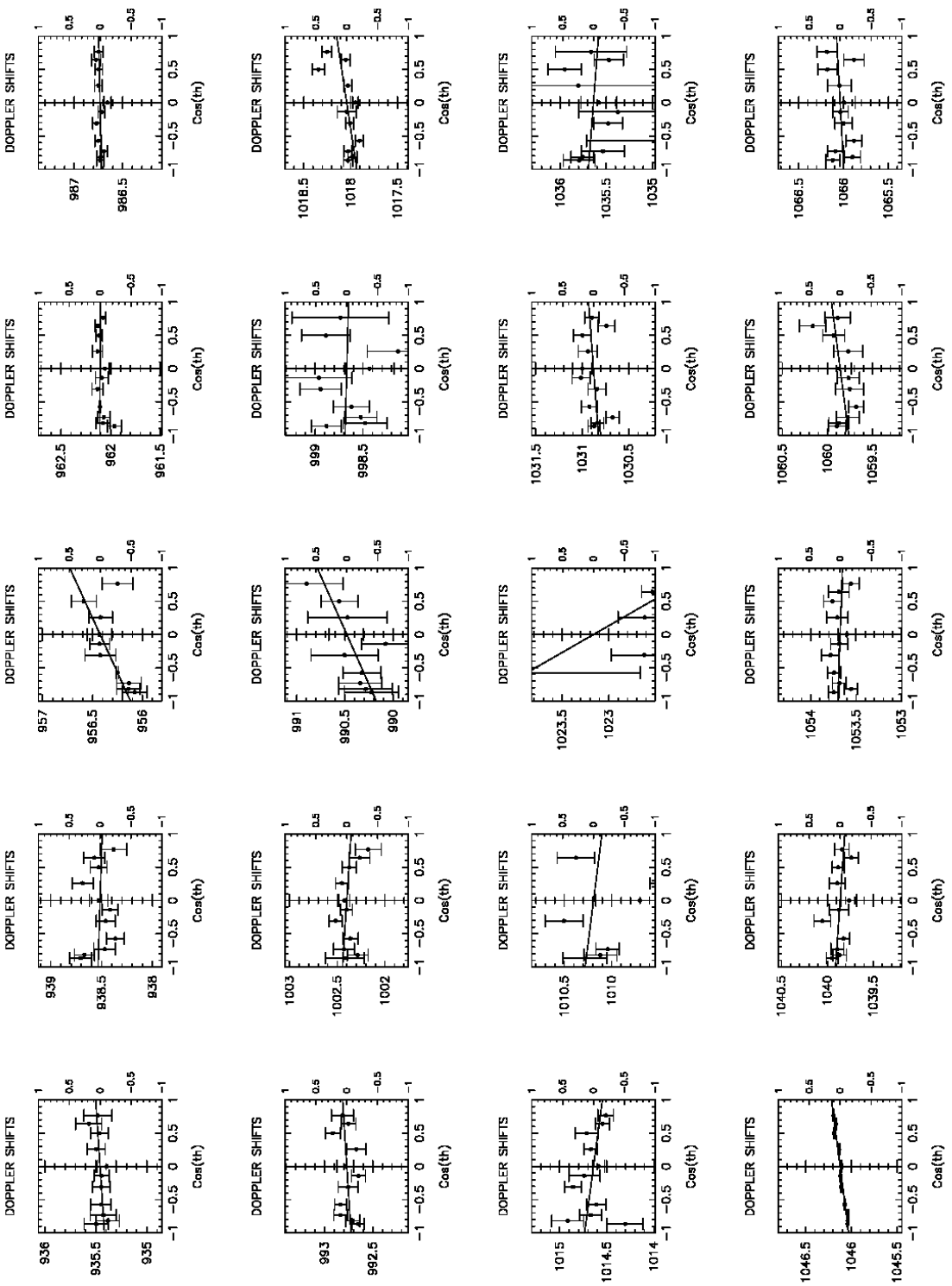
DOPPLER SHIFTS
Cos(th)

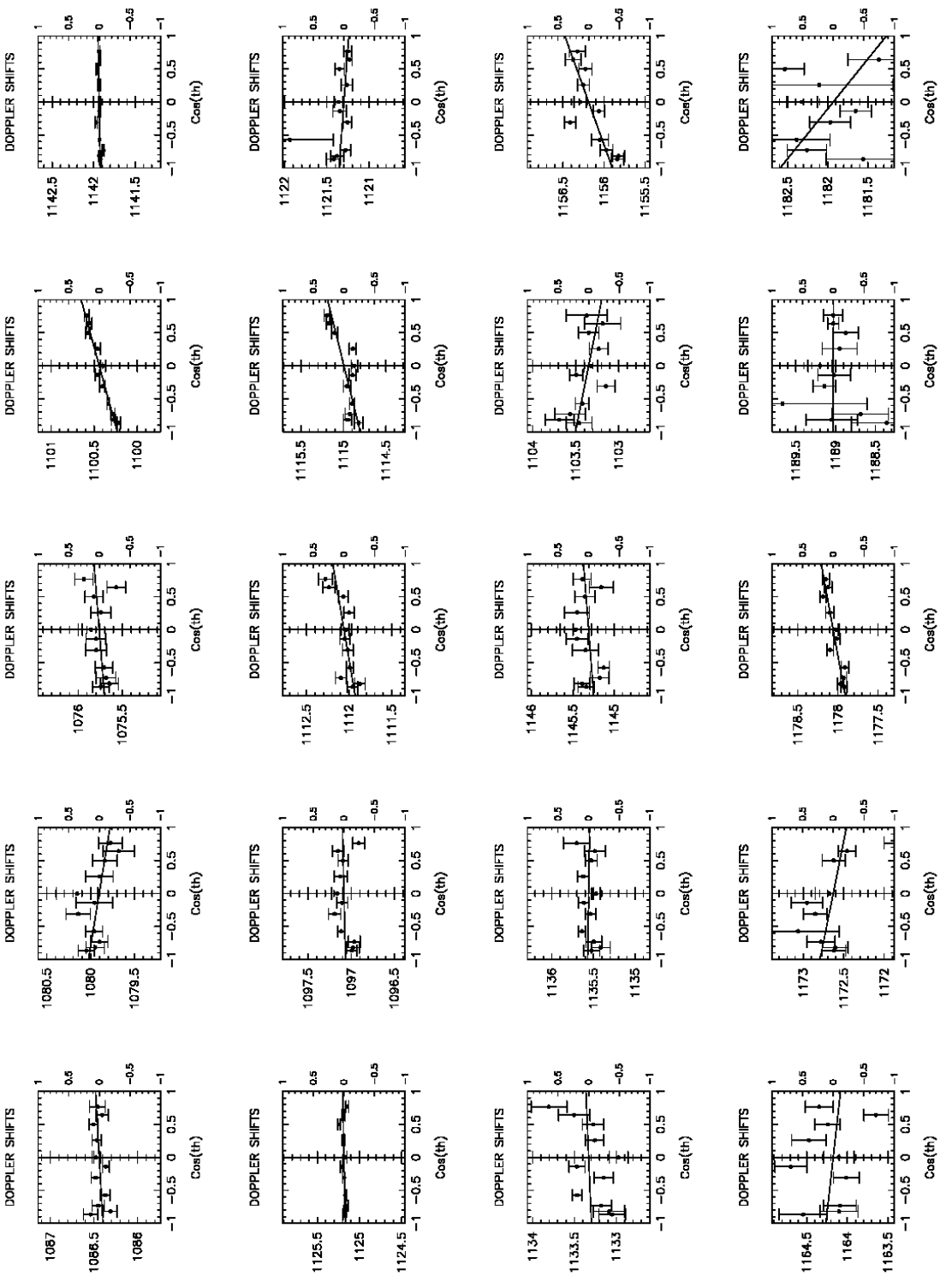
DOPPLER SHIFTS
Cos(th)

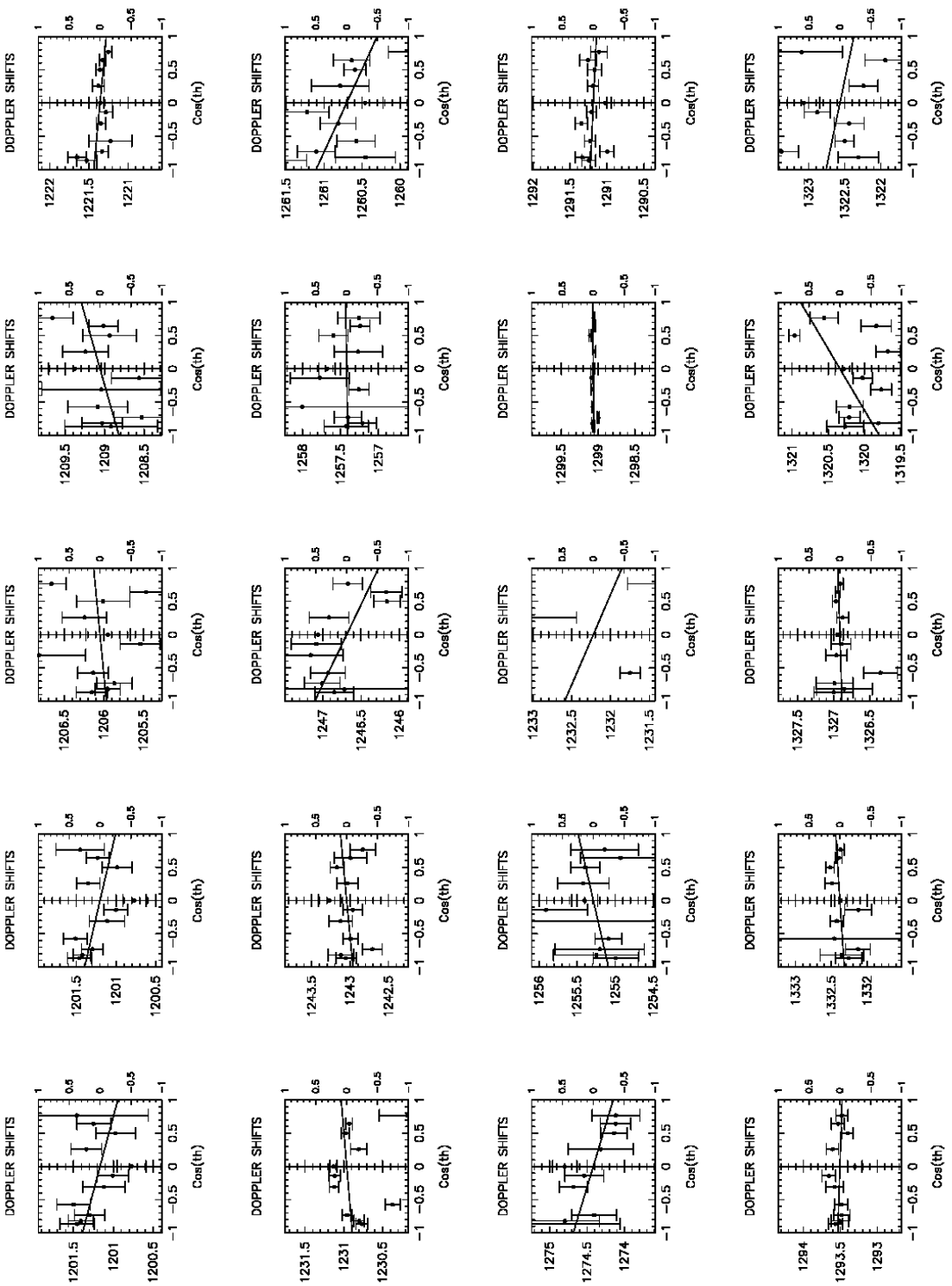
DOPPLER SHIFTS
Cos(th)

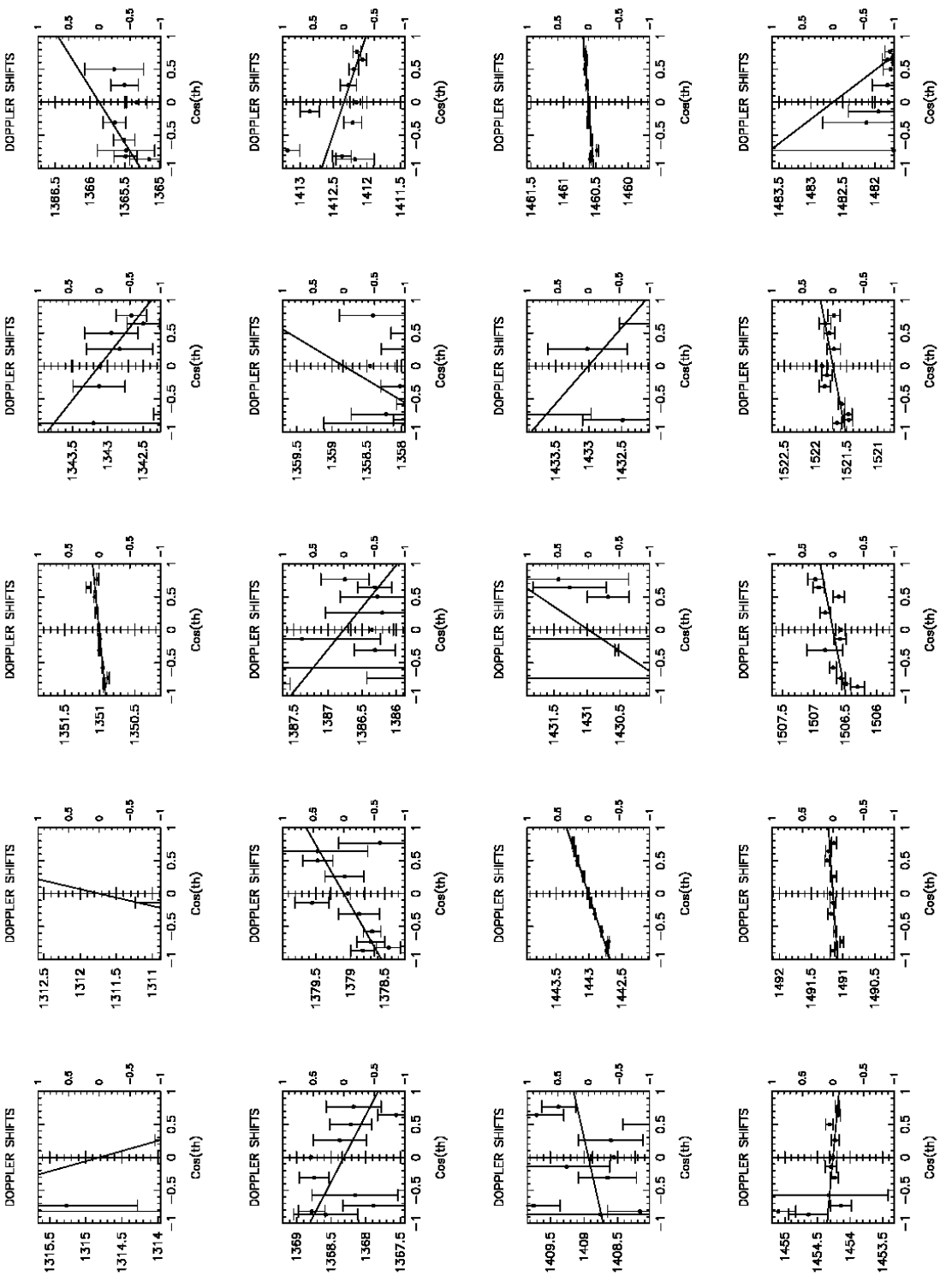
DOPPLER SHIFTS
Cos(th)

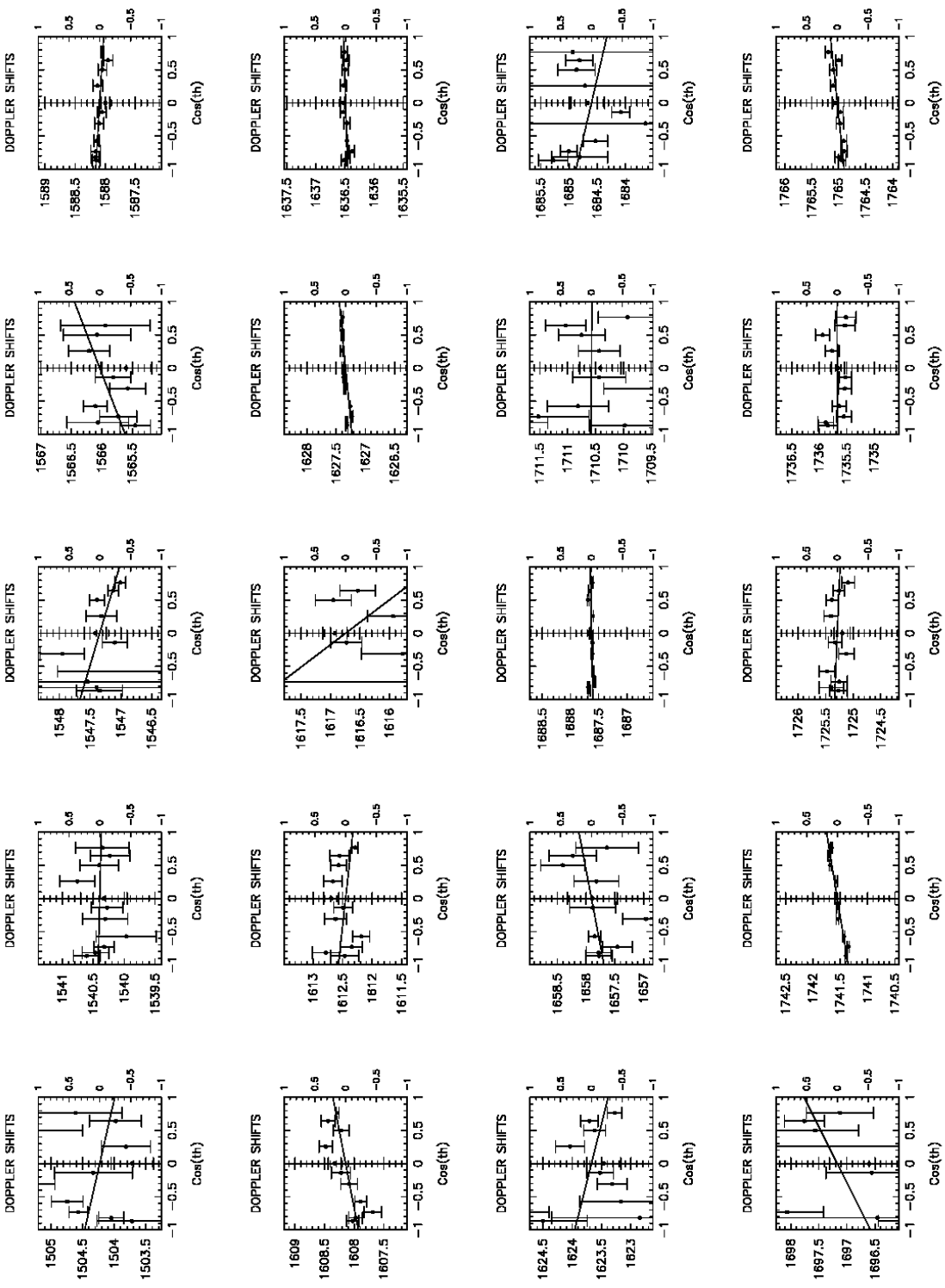
DOPPLER SHIFTS
Cos(th)

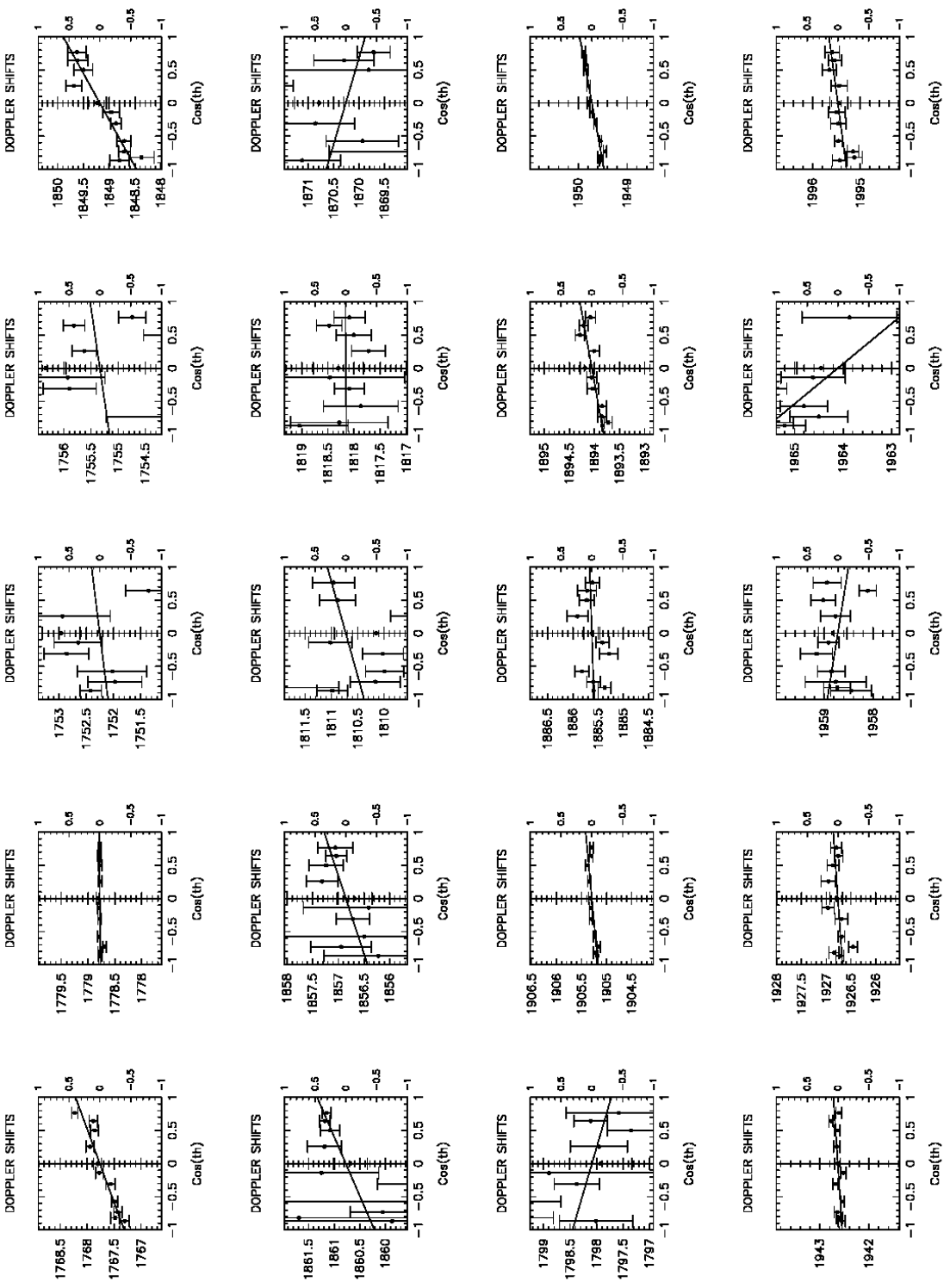
DOPPLER SHIFTS
Cos(th)

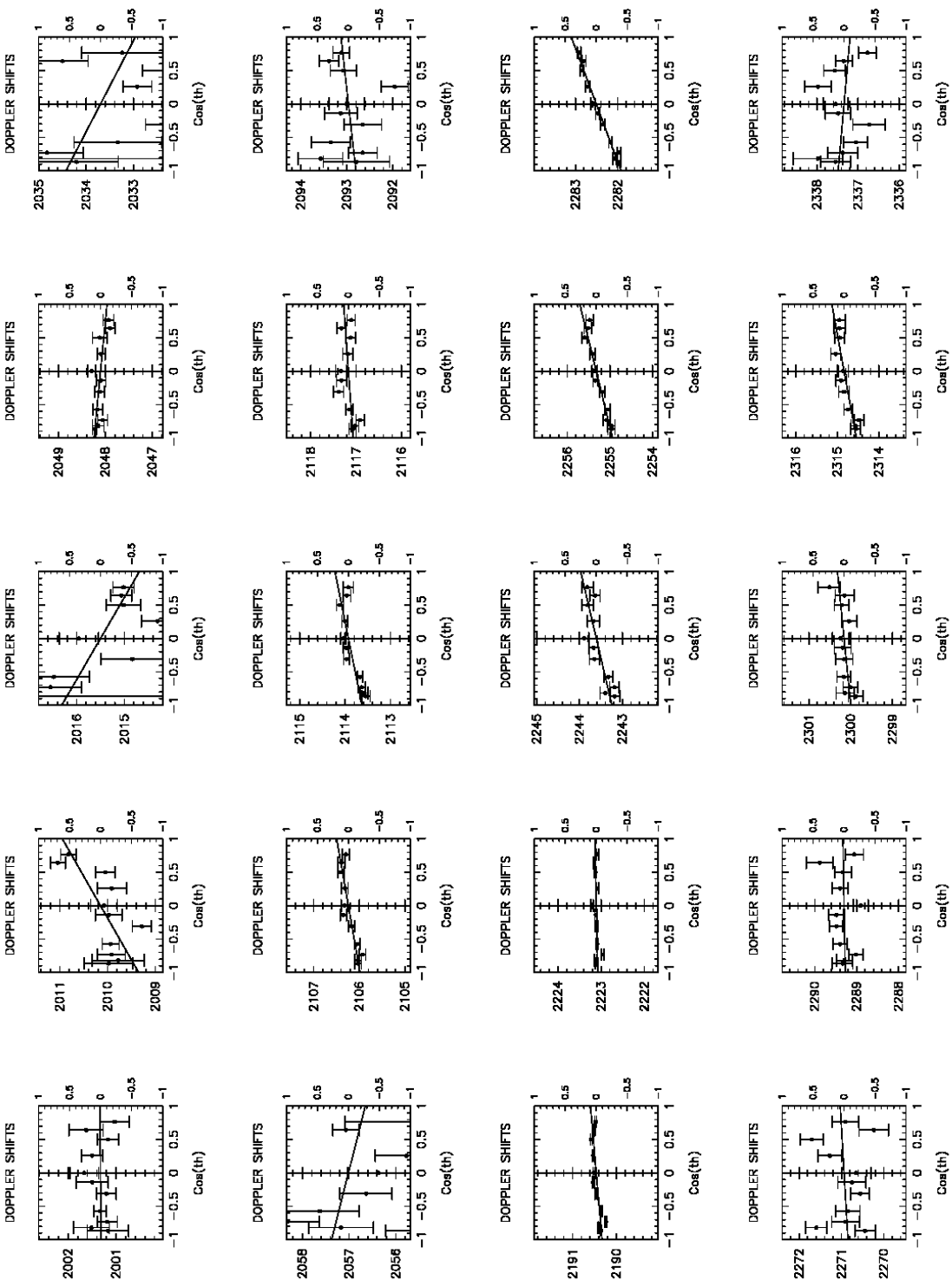
DOPPLER SHIFTS
Cos(th)

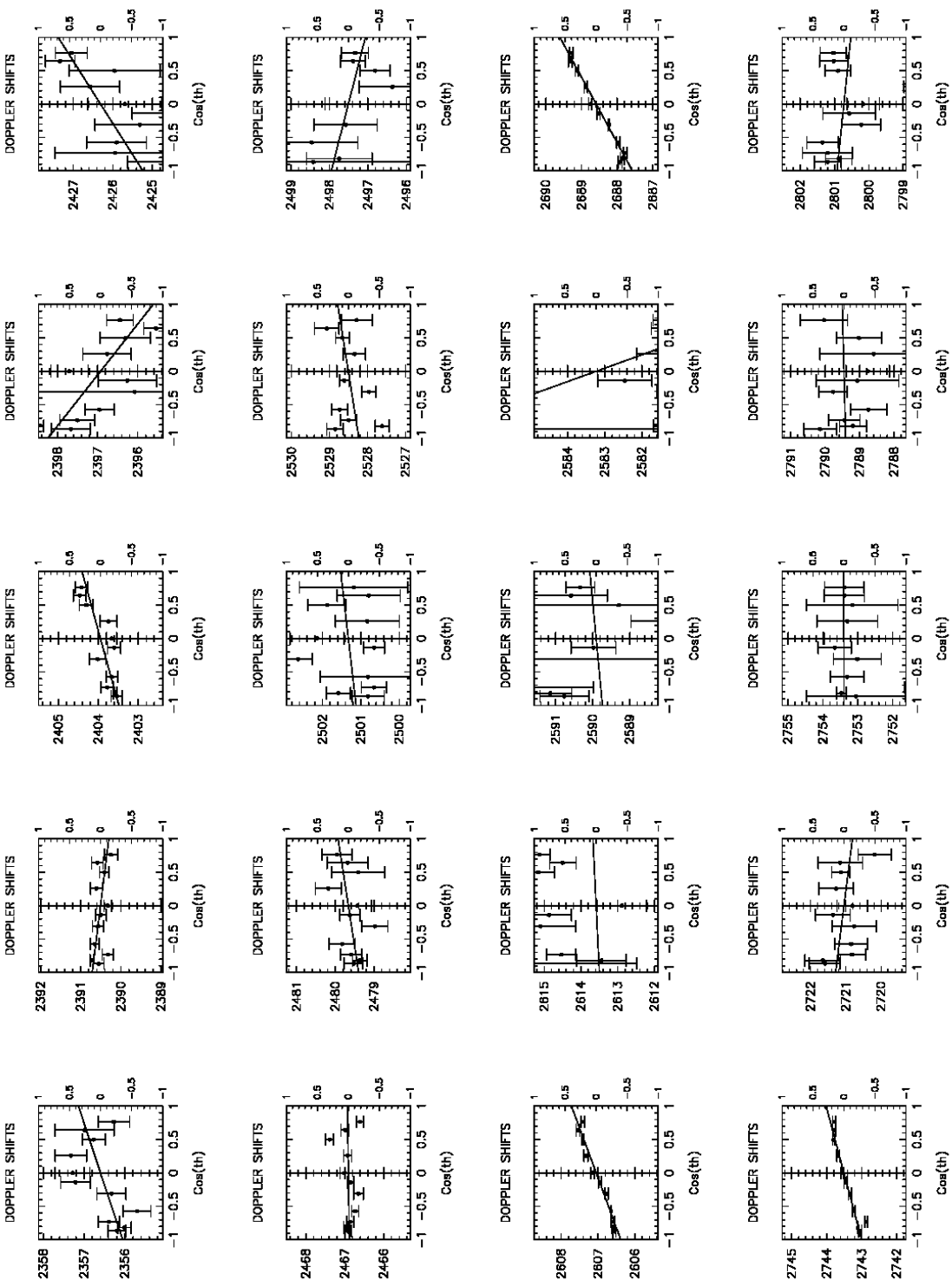
DOPPLER SHIFTS
Cos(th)

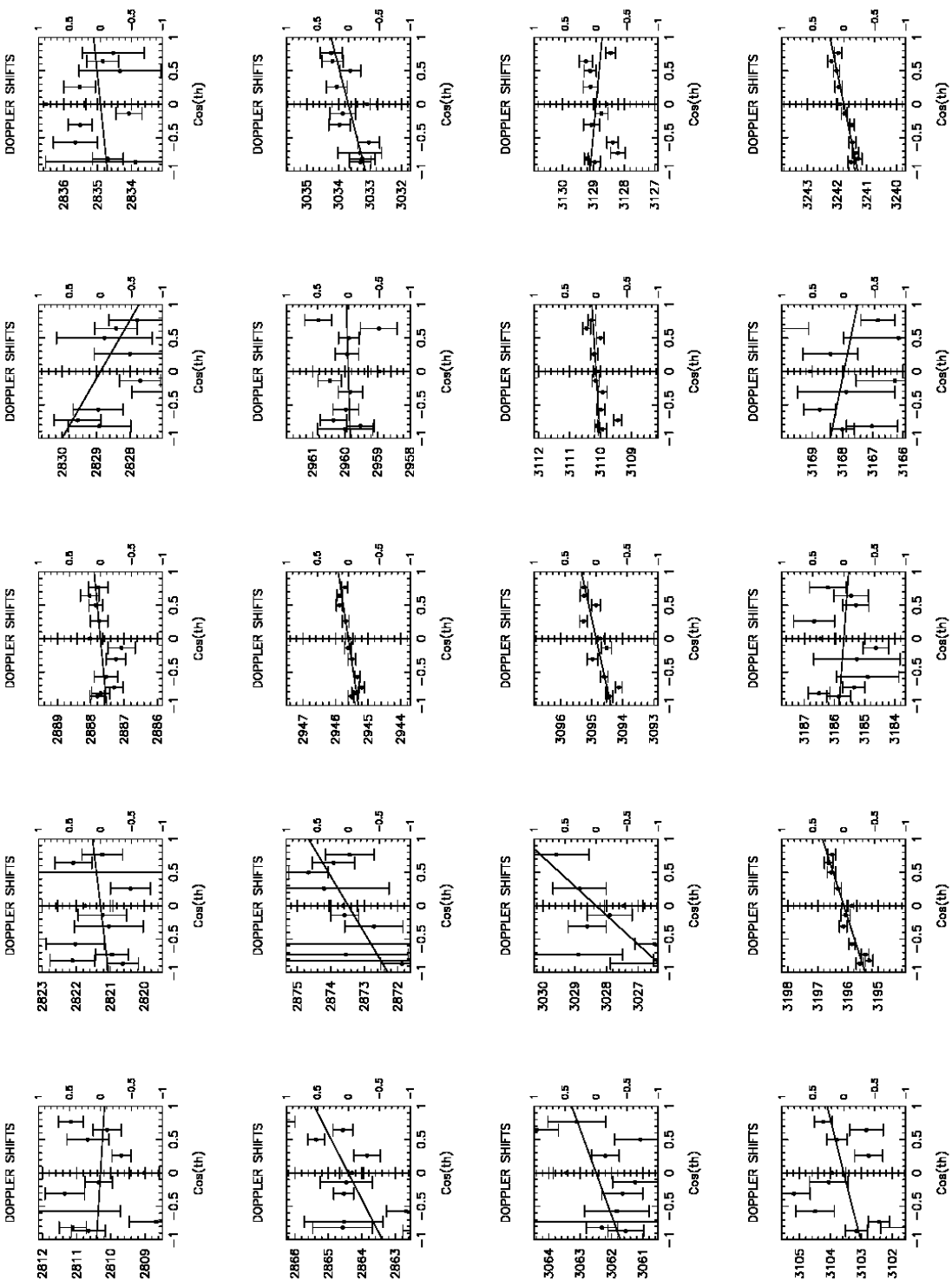
DOPPLER SHIFTS
Cos(th)

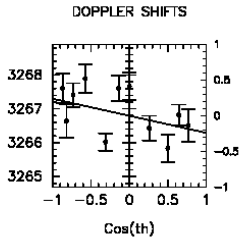
DOPPLER SHIFTS
3268
3267
3266
3265
1
0.5
0
−0.5
−1
−1 −0.5 0 0.5 1
Cos(th)

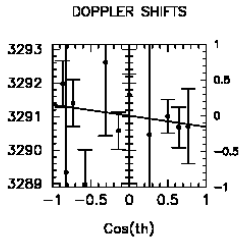
DOPPLER SHIFTS
3293
3292
3291
3290
3289
1
0.5
0
−0.5
−1
−1 −0.5 0 0.5 1
Cos(th)

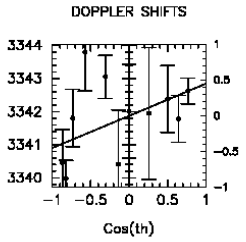
DOPPLER SHIFTS
3344
3343
3342
3341
3340
1
0.5
0
−0.5
−1
−1 −0.5 0 0.5 1
Cos(th)

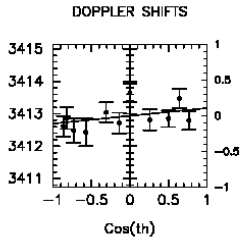
DOPPLER SHIFTS
3415
3414
3413
3412
3411
1
0.5
0
−0.5
−1
−1 −0.5 0 0.5 1
Cos(th)

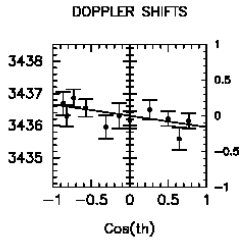
DOPPLER SHIFTS
3438
3437
3436
3435
1
0.5
0
−0.5
−1
−1 −0.5 0 0.5 1
Cos(th)

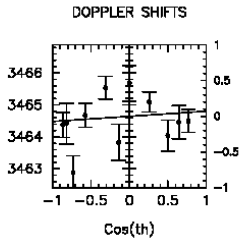
DOPPLER SHIFTS
3466
3465
3464
3463
1
0.5
0
−0.5
−1
−1 −0.5 0 0.5 1
Cos(th)

Appendix E: Doppler Shifts at 2.2 MeV

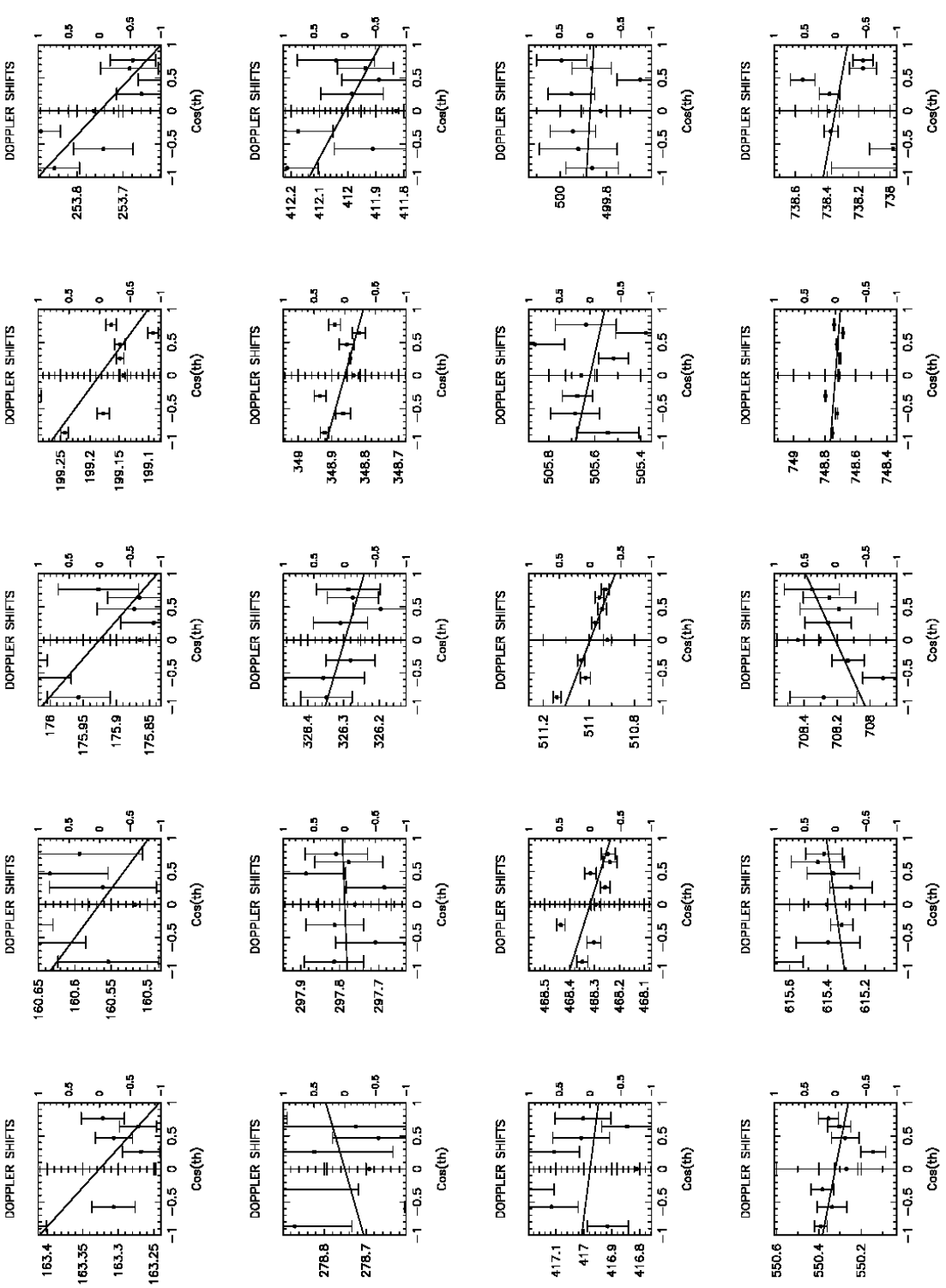
DOPPLER SHIFTS
Cos(th)

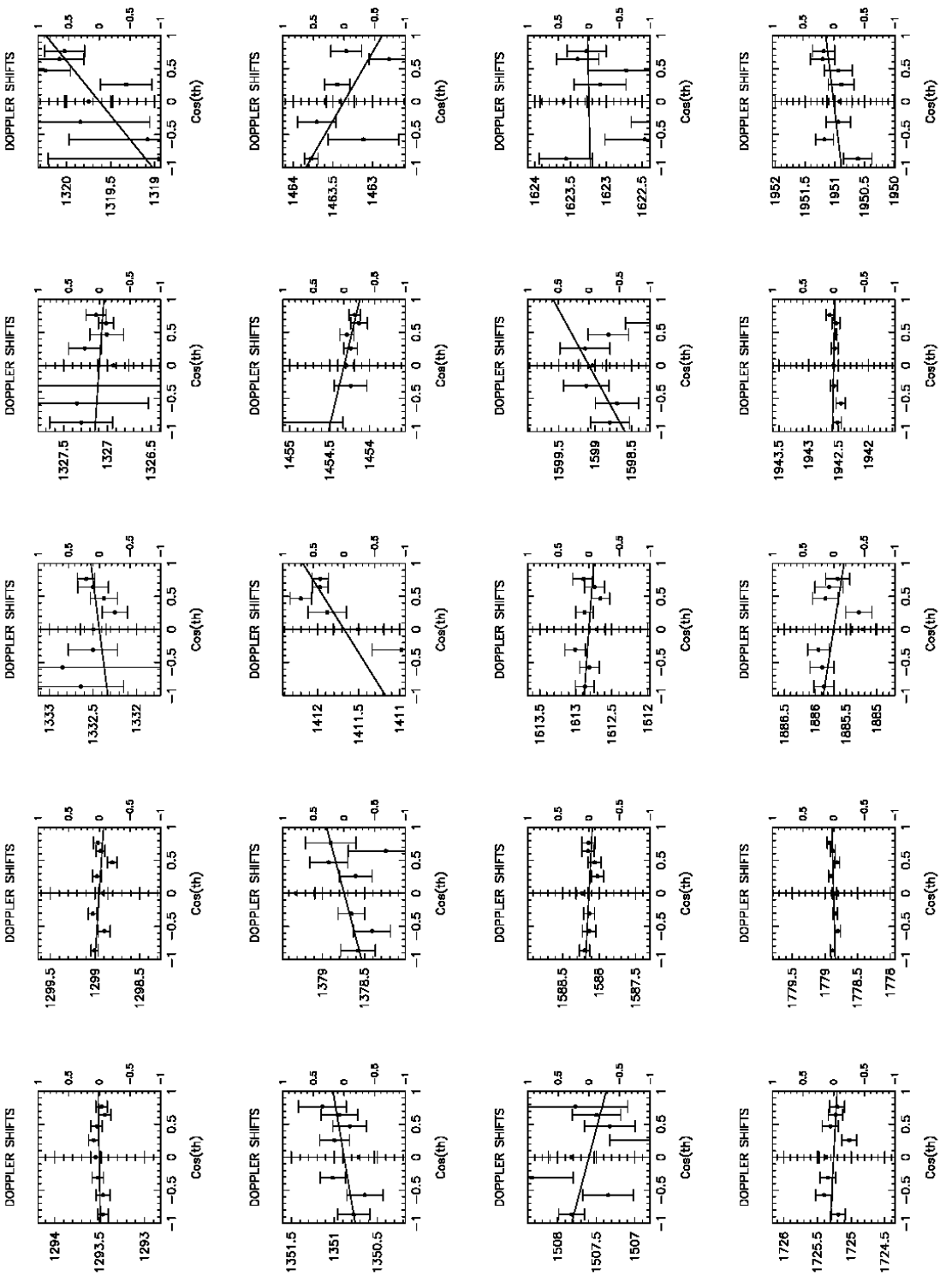
DOPPLER SHIFTS
Cos(th)

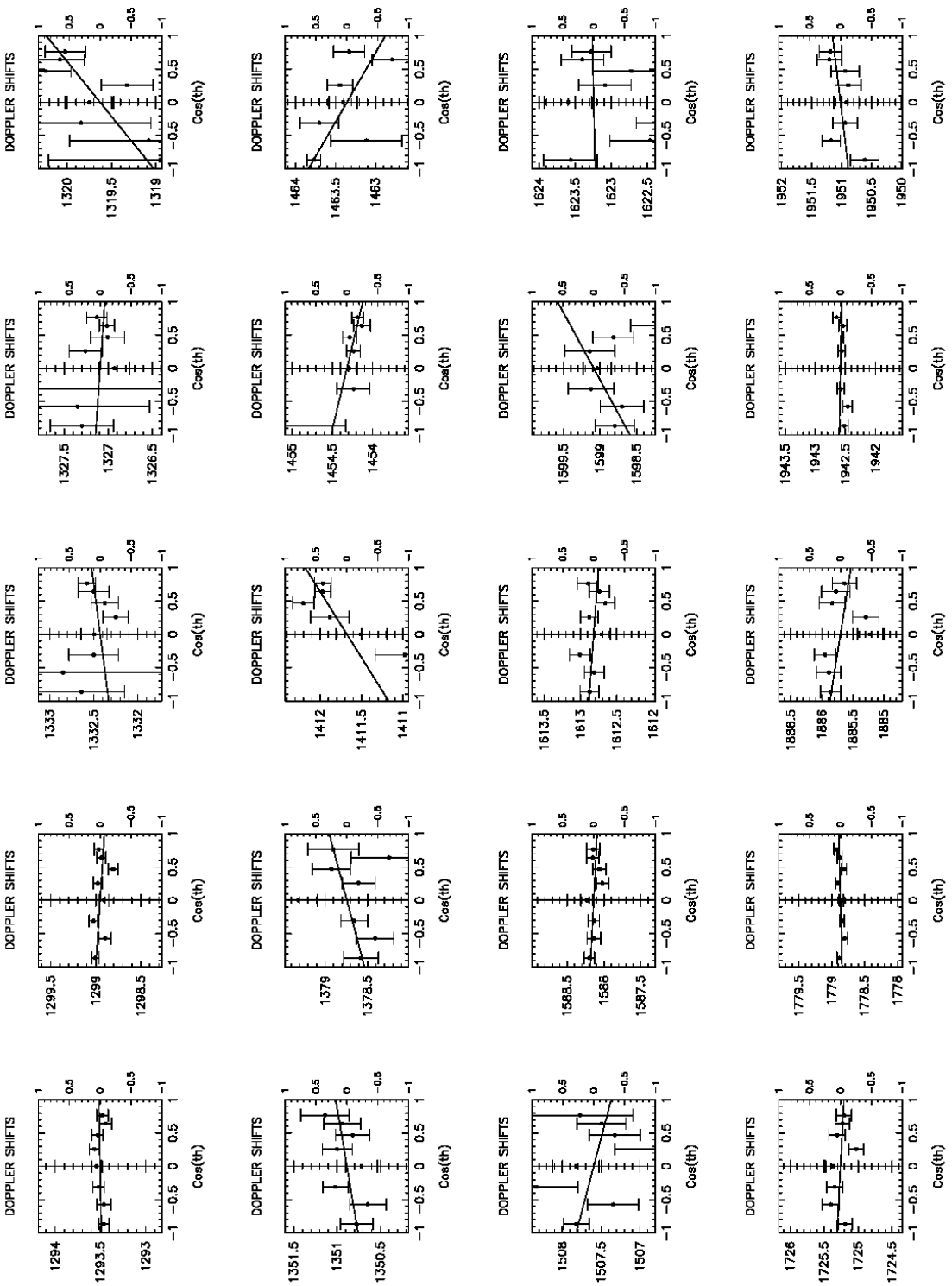
DOPPLER SHIFTS
Cos(th)

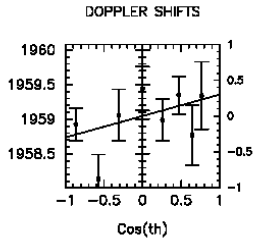
DOPPLER SHIFTS
1960
1959.5
1959
1958.5
1
0.5
0
−0.5
−1
−1 −0.5 0 0.5 1
Cos(th)

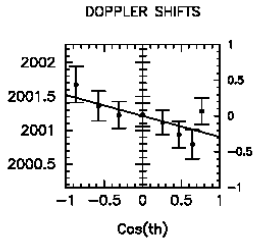
DOPPLER SHIFTS
2002
2001.5
2001
2000.5
1
0.5
0
−0.5
−1
−1 −0.5 0 0.5 1
Cos(th)

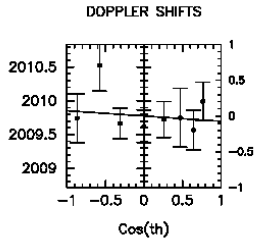
DOPPLER SHIFTS
2010.5
2010
2009.5
2009
1
0.5
0
−0.5
−1
−1 −0.5 0 0.5 1
Cos(th)

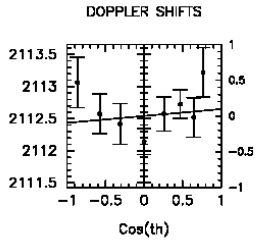
DOPPLER SHIFTS
2113.5
2113
2112.5
2112
2111.5
1
0.5
0
−0.5
−1
−1 −0.5 0 0.5 1
Cos(th)

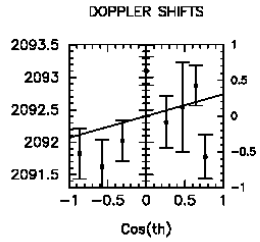
DOPPLER SHIFTS
2093.5
2093
2092.5
2092
2091.5
1
0.5
0
−0.5
−1
−1 −0.5 0 0.5 1
Cos(th)

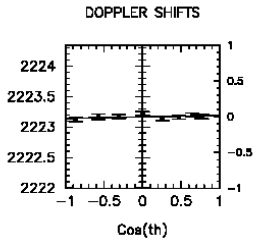
DOPPLER SHIFTS
2224
2223.5
2223
2222.5
2222
1
0.5
0
−0.5
−1
−1 −0.5 0 0.5 1
Cos(th)

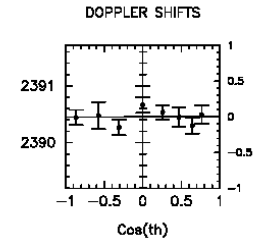
DOPPLER SHIFTS
2391
2390
1
0.5
0
−0.5
−1
−1 −0.5 0 0.5 1
Cos(th)

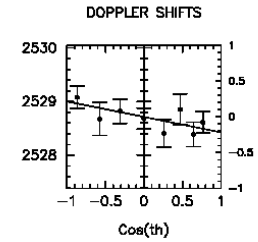
DOPPLER SHIFTS
2530
2529
2528
1
0.5
0
−0.5
−1
−1 −0.5 0 0.5 1
Cos(th)